

CONTENTS

	<u>Page</u>	
SUMMARY.	1	1/A6
INTRODUCTION	2	1/A7
DESCRIPTION OF EBF NOISE PREDICTION METHOD		
Development of Analysis Under This Contract	3	1/A8
Assumptions Within UTRC Method		
Basic Concepts	7	1/A12
UTW Slotted Wing	10	1/B1
UTW Mixer Nozzle	15	1/B6
Upper Surface Blowing.	15	1/B6
UTW Slotless Wing.	17	1/B8
Engine in Front of Wing.	17	1/B8
EVALUATION OF EBF NOISE PREDICTION METHODS		
Other EBF Noise Prediction Methods.	18	1/B9
Designated EBF Model Configurations	21	1/B12
Comparisons With Designated UTW Data		
Triple Slotted Flap, Approach.	22	1/B13
Triple Slotted Flap, Takeoff	24	1/C1
Slotless Version of Three-Flap Wing.	25	1/C2
Comparisons With Designated USB Data		
QCSEE USB, Takeoff	27	1/C4
QCSEE USB, Approach.	30	1/C7
TF-34 Scale Model.	31	1/C8
USB Vane Deflector	32	1/C9
Discussion of Error	34	1/C11
Comparisons for Additional EBF Configurations		
Additional UTW Slotless Wings.	36	1/C13
UTW Mixer Nozzle	39	1/D2
Engine in Front of Wing.	40	1/D3
Noise Predictions for Full-Scale QCSEE Configurations		
Zero Forward Speed	40	1/D3
Effects of Forward Flight.	42	1/D5
CONCLUSIONS.	43	1/D6
RECOMMENDATIONS FOR FUTURE RESEARCH.	44	1/D7
REFERENCES	44	1/D7

	<u>Page</u>
TABLE I: EXTERNALLY BLOWN FLAP MODELS FOR COMPARISON OF MEASURED AND PREDICTED NOISE.	5 1/A10
TABLE II: CAPABILITIES AND LIMITATIONS OF EBF NOISE PREDICTION METHOD	19 1/B10
TABLE III: OASPL AND PNL PREDICTION ERROR FOR 90° FLYOVER POSITION. .	35 1/C1
APPENDIX A: LIST OF SYMBOLS.	49 1/D12
APPENDIX B: LIST OF PUBLICATIONS PRODUCED.	50 1/D13
APPENDIX C: COMPUTER PROGRAM FOR CALCULATING EBF NOISE	
General Description.	52 1/E1
Input Variables.	54 1/E3
Test Case.	56 1/E5
Program Listing.	57 1/E6
Test Case Output	64 1/F7
APPENDIX D: NOISE SOURCE LOCATION FOR UPPER SURFACE BLOWING	
Purpose of Experiment.	68 1/F11
Apparatus and Procedure	
Test Apparatus.	69 1/F12
Procedure	70 1/F13
Presentation and Interpretation of Data	
Velocity and Turbulence Profiles.	71 1/F14
Crosscorrelation Traces	71 1/F14
Results of Crosscorrelation	74 1/G3

APR 25 1978

Item No.

830-H-14

NAS1.26:2954

NASA Contractor Report 2954

COMPLETED
ORIGINAL

A Method for Calculating Externally Blown Flap Noise

Martin R. Fink

CONTRACT NAS3-17863
MARCH 1978

NASA

NASA Contractor Report 2954

**A Method for Calculating
Externally Blown Flap Noise**

Martin R. Fink
United Technologies Research Center
East Hartford, Connecticut

Prepared for
Lewis Research Center
under Contract NAS3-17863



National Aeronautics
and Space Administration

**Scientific and Technical
Information Office**

1978

Blank Page

A METHOD FOR CALCULATING
EXTERNALLY BLOWN FLAP NOISE

Martin R. Fink
United Technologies Research Center

SUMMARY

A method is described for calculating externally blown flap noise as a sum of several simple basic noise components. These components are (1) compact lift dipoles associated with the wing and flaps, (2) trailing edge noise associated with the last trailing edge, and (3) quadrupole noise associated with the undeflected exhaust jet, deflection by a flap surface or nozzle deflecting surface, and the free jet located downstream of the trailing edge. These noise components are combined to allow prediction of directivity and spectra for under-the-wing (UTW) slotted flaps with conventional or mixer nozzles, UTW slotless flaps, upper-surface-blowing (USB) slotless flaps, and engine-in-front-of-the-wing slotted flaps. The development of this method as part of a four-year effort under this Contract is described. A digital computer program listing is given for this calculation method.

Directivities and spectra calculated by this method, the current NASA ANOP method, and a method developed by Lockheed-Georgia Co. are compared with free-field data for UTW and USB configurations recently tested by NASA Lewis Research Center. These data had not been part of the data base used in development of these three methods. The UTRC method best predicted the details of the measured noise emission, but the ANOP method best estimated the noise levels directly below these configurations.

INTRODUCTION

Noise generated by stationary solid bodies in the presence of the turbulent airflow in fan ducts is a major part of the noise of installed turbofan aircraft engines. For example, acoustically treated splitters within the engine inlet and exhaust ducts can attenuate turbomachinery noise but produce noise at their edges. Internal struts, necessary for structural support of the engine and splitters, are likely to be immersed in high-velocity turbulent engine airflows. Turbofan stator blades are subjected to fluctuating wakes produced by the fan rotor blade. For STOL aircraft, externally blown flaps deflect engine exit airflow in order to generate additional wing lift force at low flight speeds. In all these cases, a solid surface of finite extent is scrubbed by airflow containing velocity and pressure fluctuations. The same basic aeroacoustic mechanisms should be present for all of these examples.

The subject of this report is prediction of noise caused by externally blown flaps. This comprised the major portion of the investigation conducted under this four-year contract. Experiments with simple configurations were utilized to develop simple analytical models of several noninteracting noise components. Some components could, in concept, be calculated by rigorous methods. Such a theory would be extremely complex and is not presently available for externally blown flaps. Therefore a semi-empirical noise component method for externally blown flap (EBF) noise was developed instead. This UTRC method can be applied to under-the-wing slotless or slotted flaps and conventional or mixer nozzles, upper-surface-blowing configurations with uniform exhaust flow, and engine-in-front-of-the-wing installations. Other prediction methods also exist for some of these types of EBF configurations. All of these methods are described and are evaluated herein by comparing their predictions with NASA-designated free field data for a range of EBF configurations. These recent data had not been used in development of these methods, so that the comparison would not be biased. Crosscorrelation measurements to identify noise source locations are reported in Appendix D herein.

A companion final report describes the remainder of the contract effort, devoted toward the development of a method for predicting and reducing noise radiation from gas turbine engine struts and splitters.

Editorial review of this Contractor Report was performed at NASA Lewis Research Center and by colleagues within UTRC in order to assure clarity of ideas expressed. Drafts of this report were also reviewed by persons at NASA Lewis Research Center and at Lockheed-Georgia Co. who have developed competing methods, in order to assure correct evaluation of their EBF noise prediction methods.

DESCRIPTION OF THE UTRC EBF NOISE PREDICTION METHOD

Development of Analysis Under This Contract

The work conducted under this Contract was based on an earlier noise component method developed at UTRC and first presented in reference 1. That method had regarded under-the-wing (UTW) externaly flown flap (EBF) noise as a sum of three types of noise components. Scrubbing noise as described therein was taken to be a lift dipole noise acting on the wing and flap panels scrubbed by the exhaust jet. The noise generating process was taken as that described by Sharland (reference 2) for noise produced by a turbulent boundary layer on an airfoil surface. Such noise was assumed proportional to velocity raised to the sixth power, surface area scrubbed by the jet, and surface pressure fluctuation squared. Pressure fluctuations on the flap surfaces were assumed equal to those for the free-jet mixing region, an order of magnitude larger than those for an attached boundary layer. It was shown that equation (10) of reference 2 predicted lobes of flap-generated lift dipole noise that generally matched the available EBF noise data at low exhaust velocities for directions above and below the flaps. Another noise component was quadrupole noise generated by deflection of the exhaust jet. This noise contribution was evaluated from the data of reference 3 for a jet deflected by a large flat surface. Slotted and slotless UTW configurations were noted to have approximately equal peaks of quadrupole-like noise at shallow angles above and below the deflected jet. Measured deflected jet noise radiation was therefore assumed to apply at both these directions despite lack of an explanation for the upward-radiated noise. The sum of these quadrupole and lift dipole components generally matched the available data except for underprediction of noise measured in the upper forward quadrant. The only noise generating process that is strongest at directions opposite to the deflected flap trailing edge would be trailing edge noise. This additional noise component therefore had been assumed in order to match measured UTW directivity shapes in all quadrants.

The first fiscal year's work under this Contract, reported in references 4, 5, and 6, consisted of experiments directed toward evaluating the several available theories for incidence fluctuation noise, trailing edge noise, and scrubbing noise. Results for incidence fluctuation noise were presented in reference 5. That portion of the Contract effort, and additional Contract effort directed to predicting noise generated by struts and splitter rings within turbofan exit ducts, is summarized in reference 7. The study of trailing edge noise was also presented in reference 5. Those data, and 2/3 of the summary data given by Hayden in reference 8, were found to substantiate the functional dependence of trailing edge noise developed by















Pfowcs Williams and Hall (reference 9) and by Chase (reference 10). They did not agree with the dependence stated by Hayden in references 8 and 11. (Hayden has published a rebuttal in reference 12 which presents his data for the characteristic decay flow regime, which agrees with his equation and was not shown in reference 4. That comparison did not contain his data of reference 8 for a large range of velocities in the potential core or radial decay regimes, shown in figures 19 and 20 of reference 4 and in figure 6 of reference 5.)

The study of scrubbing noise, published in references 4 and 6, had a major effect on the EBF noise calculation method developed under this Contract. It was shown by crosscorrelation experiments that regions of the flap surface which experienced large fluctuations of static pressure were not strong generators of noise. This result is frequently found in crosscorrelation experiments, as noted in Siddon's basic studies (reference 13) of surface-radiated noise. It contradicted the major noise process assumed in reference 1. Variation of maximum normalized crosscorrelation coefficient with chordwise position and variation, with chordwise position, of the times at which maximum first derivative of crosscorrelation coefficient occurred, were utilized to develop a different description of this noise process during the second fiscal year. This concept also utilized the then-recent concepts of large-scale vortex structure in a UTW exhaust jet as influenced by feedback from the downstream solid surface (reference 14). These vortexes, convected past the wing and flap surfaces, were assumed to induce lift force fluctuations on those surfaces. Strength of the lift force fluctuation and therefore the noise radiation depended on distance between the vortex trajectory and the surface. The first year's study of incidence fluctuation noise provided analytical justification of the empirically assumed asymptotic spectrum slopes at large and small Strouhal numbers for this noise concept. The explanation developed at NASA (reference 15) to explain the measured variation of UTW noise with exhaust velocity to the 6.7 power rather than sixth power was also included for this component. That is, local exhaust velocity as calculated for the nozzle exit Mach number and flap trailing edge location was taken as the relevant flow velocity.

During this second fiscal year, a method was developed for predicting the increased quadrupole noise caused by an exhaust jet impinging against a flap surface. This calculation procedure used the NASA-developed method of reference 16 for noise radiated by an isolated jet. It was shown that if this noise was increased by an amount proportional to sine squared of deflection angle, and the directivity pattern was rotated through that angle, the data of reference 3 could be closely matched. OASPL directivities and $1/3$ octave spectrum shapes were then calculated for most of the small-scale EBF configurations tested at NASA Lewis Research Center. A detailed description of the calculation method, and comparisons between predictions and data, were

given in reference 17. Sketches of the twelve small-scale EBF configurations, which form the data base from which this UTRC method was developed, are shown in Table I.

TABLE I
EXTERNALLY BLOWN FLAP MODELS FOR COMPARISON
OF MEASURED AND PREDICTED NOISE

<u>Sketch</u>	<u>Descrip.</u>	<u>Sketch</u>	<u>Descrip.</u>
	UTW, 20° flap		USB, 20° flap circular nozzle
	UTW, 60° flap		USB, 60° flap circular nozzle
	UTW, 60° flap slotless wing		USB, 20° flap D nozzle
	UTW, 60° flap mixer nozzle		USB, 60° flap D nozzle
	UTW, 60° flap vary diameter		USB, 20° flap canted 5:1 slot
	UTW, 60° flap vary position		USB, 20° flap canted 10:1 slot
	Front of wing 20° and 60° flap		USB, long 20° flap, 10:1 slot

During the third fiscal year, the calculation method was modified to account for the fact that all the reference data base had been obtained under nonfree-field test conditions. Crosscorrelations among surface pressures on flap upper and lower surfaces, and far field acoustic pressures, were conducted for both UTW and upper surface blowing (USB) configurations. These results generally validated the assumed conceptual model. Noise calculations were conducted for large-scale UTW and USB EBF configurations tested at NASA Lewis Research Center and corrected to free field. Comparisons with these UTW and USB data, for which the exhaust jet was either a nominally half-scale cold jet or a TF-34 engine, were given in reference 18. The UTRC method for calculating EBF noise was frozen at this time, except for two changes. Forward flight effects were included later this third year. Prediction of noise radiation from UTW slotless wings was modified during the fourth year because of poor agreement found during the third year. At this time the calculation procedure consisted of two separate time-sharing digital computer programs, one for OASPL directivity of each noise component and of their sum, and one for spectrum. Considerable manual effort was needed in preparing inputs for each program. Forward flight effects on local flow properties, surface pressure fluctuations, and far field acoustic pressures were measured in an acoustic wind tunnel for a range of exhaust velocities at different ratios of flight velocity to exhaust velocity. A method was developed for calculating the resulting effects of forward flight on various noise components. One unexpected result was that the spectrum of USB surface-radiated noise is decreased in amplitude and shifted to higher frequency. Full scale spectra, at high-annoyance frequencies, also decrease in amplitude as frequency is increased. The result is a large predicted noise reduction at low frequencies, where the contribution to annoyance is small, and negligible forward flight effect on high-annoyance noise. This predicted behavior is substantiated by data. The UTRC method for predicting EBF noise was modified to include these predicted effects of forward flight. Results obtained during the third fiscal year were presented in reference 18. Papers containing portions of the results were given in references 19 and 20.

Activities conducted on EBF noise during the fourth (final) fiscal year included a test program to examine USB noise source locations by crosscorrelation of local velocity fluctuations and far-field acoustic pressures. The noise calculation method developed by Tam and Reddy in reference 21 had assumed that one of the dominant components of USB noise is the flow mixing process in the highly sheared region downstream of the trailing edge and below the deflected exhaust jet. Instead, the crosscorrelation results presented in APPENDIX B herein indicated that the noise was associated with large-scale structure of the exhaust jet that existed in the wing upper-surface boundary layer. These convected eddies produced noise only as they moved past the trailing edge. As another task, the several parts of the computer

programs for EBF noise as used in late 1975 were combined into one FORTRAN program, and a geometric error in calculating the effect of azimuth angle was corrected. This program calculates OASPL and 1/3 octave spectrum for ranges of polar angle and azimuth angle specified by the input, for UTW configurations that can have conventional or mixer nozzles and slotted or slotless wings, USB configurations, or engine-in-front-of-wing configurations. Calculations were compared with free-field data obtained by NASA Lewis Research Center and with limited additional data. Results for this fourth year are presented herein; portions of the results were presented in references 19 and 22.

Assumptions Within UTRC Method

Basic Concepts

The noise component method described in this report calculates the total noise as a sum of several components which are acoustically but not aerodynamically independent. In its initial development, each component had the analytically predicted functional properties of noise radiation from a simplified physical situation. If a fundamental analysis existed for noise radiation from surfaces in nonuniform flow, and if spatial distributions of mean velocity and turbulence spectrum were known for each EBF configuration, then the noise radiated by each component could be calculated rigorously. This information is not presently available. Empirical constants therefore have been developed in the analytical description of each noise component. These constants represent a combination of both the unknown local exhaust properties of the deflected jet (mean velocities, turbulence rms amplitudes, and turbulence integral scale lengths) and the unknown interactions between adjacent flap segments. From this viewpoint, the same basic simple noise components are assumed to occur for UTW slotted or slotless EBF configurations with conventional or mixer nozzles and for USB configurations. Amplitude of each noise component is calculated for the specific geometry of each case, and the resulting OASPL's and spectra for all components are summed as statistically independent quantities.

Noise radiation from surfaces in turbulent flow can have different behavior depending on the relative sizes of the chord, turbulence, and acoustic wavelength. One convenient approximation used in reference 25 was to compare measured noise radiation patterns with those predicted for two limiting cases: very small and very large chord relative to turbulence scale length and acoustic wavelength. The EBF noise prediction method given herein, denoted as the UTRC method, approximates the actual noise directivity pattern of surface-radiated noise as a sum of those two limiting cases. The limit of

very small chord is called fluctuating lift noise, and that of very large chord is called trailing edge noise. Functional dependence of noise amplitude is taken from theory; absolute level had been picked to match selected EBF data. The empirical agreement with data was improved if another component, having the directivity shape and general behavior of jet mixing noise rotated through the exhaust deflection angle, was also included.

Typical directivity patterns and relative amplitudes are sketched in figure 1 for each of these assumed noise mechanisms as it occurs for UTW and USB configurations. Fluctuating lift noise, also called scrubbing noise or inflow noise, is sketched in the upper part of this figure. It is defined as an acoustically compact lift dipole noise oriented perpendicular to each chordwise segment of the wing. As shown experimentally in references 4 and 6, local fluctuations of airfoil loading occurred which were coherent along the width of the region scrubbed by the exhaust jet. They moved downstream along the surface at the eddy convection velocity of about 80% of local maximum velocity. Local pressure fluctuations induced by this process resemble those caused by discrete vortices convected past an isolated airfoil. Amplitudes of these pressure fluctuations are small compared with pressure fluctuations generated by the shear-layer mixing process and impressed onto the adjacent surface. Thus the regions having strongest surface pressure fluctuations generally do not have strongest local noise source strength. This result that local dipole noise radiation is not necessarily proportional to local surface pressure fluctuation has been found in other studies (e.g., reference 13) of noise generation processes investigated by crosscorrelation techniques.

As sketched in the upper part of this figure, far-field lift fluctuation noise from the undeflected portion of a wing and from each separately deflected chordwise flap segment was represented by a separate dipole. Because an UTW flap (upper left sketch) is deflected into the jet exhaust and therefore closer to the hypothetical outer edge of the jet, the dipole associated with the aft flap segment is relatively strong. In contrast, an USB flap (upper right sketch) is deflected away from the jet exhaust. Its strongest assumed dipole tends to be that from the undeflected part of the wing.

Trailing edge noise, sketched in the second row from the top, has a directivity pattern that is strongest directly upstream from the deflected trailing edge. Other properties of trailing edge noise are discussed in references 4 and 5. Noise generated at intermediate trailing edges such as that of the undeflected forward part of the wing was neglected. Thus the calculation method developed here does not predict more trailing edge noise for multiple slotted flaps than for single slotted or unslotted flaps. The trailing edge noise component was included because its directivity pattern tends to fill the gap in the upper forward quadrant between lobes of fluctuating lift noise, and thus produce better agreement between predictions and data.

Quadrupole noise, sketched in the third row, is represented as a sum of three components for both UTW and USB installations. One component is the jet mixing noise from undistorted, undeflected parts of the exhaust jet. This noise is calculated for the isolated exhaust nozzle and increased 2 dB to account for reflection of noise by the wing surface. Such noise is radiated beneath the UTW and above an USB configuration. UTW installations also generate a quadrupole noise from the region where the jet is deflected by the flap. This noise was called impact noise in references 24 and 25. For conventional UTW installations, this quadrupole noise generated by deflection of the jet is stronger than that from the undeflected jet. This noise is radiated both above and below slotted flaps. USB configurations generate a similar increase of noise, radiated only above the wing and flap, caused by deflection of the exhaust jet through the nozzle roof angle or cant angle. Both types of configurations produce additional quadrupole noise from the shear layer that forms beneath the deflected exhaust jet downstream of the trailing edge. Finally, as sketched in the lower right portion of the figure, external flow deflection devices which produce attached flow of the USB exhaust jet to the deflected flap can radiate noise. Flow deflectors can generate high-frequency dipole noise which is usually shielded by the wing, but some of this noise can be radiated below the wing.

This empirical analysis models the exhaust jet as a line of discrete vortices at the jet edge. Discrete vortices convected along an airfoil are known to induce local loadings concentrated near the vortex. The loading strength is a function of vortex chordwise position and varies approximately inversely with distance between the vortex and surface at constant chord. Too close a spacing will cause viscous dissipation of the vortex, reducing the scrubbing noise. If the spectrum of vortex strength is that for jet turbulence and the lift force response is that for a discrete vortex in subsonic compressible flow, power spectral density of an acoustically compact source should vary as frequency squared at low reduced frequencies and frequency to the $-7/3$ power at high reduced frequencies. The resulting $1/3$ octave slopes of 9 dB/octave and -4 dB/octave for low and high reduced frequencies, along with dipole directivity and dependence on local velocity to the sixth power, are typical properties of observed fluctuating lift noise.

The concept of fluctuating lift noise as a lift dipole noise radiated on both sides of a wing and deflected flap, but generated by hypothetical coherent vortices in the exhaust jet on one side of the wing and flap, is fundamental to the prediction method. This explanation was validated by tests described in reference 4 in which far-field spectra measured on both sides of a wing were compared. If this concept is correct, spectra measured on the side opposite from the jet should have a sum of trailing-edge noise and lift-dipole noise. Spectra measured at the same angle from the wing chord plane,

but on the side adjacent to the exhaust jet, should be the sum of those two noise processes plus jet mixing noise radiated directly to the far field and jet mixing noise reflected from the wing to the far field. To test this assumption, spectra measured both above and below an undeflected wing tangent to an exhaust jet were compared in figure 34 of reference 4. Spectra for the isolated nozzle at the same direction angles and pressure ratios also were shown. Part of this figure for 250 m/sec exhaust velocity is reproduced as figure 2 herein. At directions 60° and 90° from upstream, spectra measured on the side adjacent to the jet (dotted line) were closely predicted (circles) by taking the spectra for the nozzle alone (dash line), adding 3 dB for reflection of jet noise from the wing, and adding that sum to the spectrum measured on the shielded side (solid line). Further comparisons of spectra measured on the shielded side at different directions and exhaust velocities, described in reference 4, substantiated that those spectra were a sum of two simpler spectra. One of these components had maximum amplitude at a relatively low frequency, decayed rapidly in amplitude at higher frequencies, and had the fifth-power velocity dependence and cardioid direction-angle dependence of trailing edge noise. The other component had a broader spectrum shape with less rapid high-frequency decay. Its amplitude varied with velocity to the sixth power, and its directivity was that of a lift dipole. This latter noise component is what has been described herein as fluctuating lift noise.

UTW Slotted Wing

Geometric properties of a UTW slotted wing are given (figure 43) by the number of flap slots, leading edge ordinates for the wing and each flap panel relative to the center of the nozzle exit, deflection of the wing chord line relative to the nozzle centerline and of each flap relative to the wing chord line, and chord of the last flap segment. If aerodynamic data are available for the effective turning angle of the flap segment, deflection angle of the last flap segment is taken as this aerodynamic angle rather than the geometric angle. Chord of the wing, and of all but the last flap segment, is taken as the distance from its leading edge to the next leading edge. However, trailing edge location is calculated from chord and the input deflection angle. The computer program can accept up to four chordwise flap segments (quadrupole slotted flaps). UTW wings with retracted flaps are discussed in the following section entitled "UTW Slotless Wings".

A hypothetical line of vortices is assumed to induce lift force fluctuations on the wing and flap segments. Vortex trajectory is taken as a straight line, parallel to the nozzle centerline, extending downstream from the nozzle lower lip until it gets within half a diameter of the flap surface. If the wing or flap extends below the nozzle centerline, the vortex

trajectory becomes parallel to the flap chord line and displaced half a diameter away from it.

Lift force fluctuation caused by a vortex convected past an airfoil is known to vary inversely with distance of closest approach. Noise radiation is assumed to vary with force fluctuation squared and therefore directly with the product of nozzle diameter and total chord and inversely with average distance squared. For each chordwise segment, the average value of inverse distance squared, h^{-2} , is taken as the average of this quantity evaluated at the segment leading and trailing edge. Spreading of the exhaust jet by the deflected flaps was neglected, so the mean square acoustic pressure from each segment is assumed proportional to the product of segment chord and nozzle diameter divided by far field distance squared. Noise amplitude caused by a vortex distance of one diameter was selected to match data from reference 4 for a wing with retracted flaps. By varying the assumed trajectory, the vortex minimum displacement of half a nozzle diameter was inferred as that value which would predict the measured noise increase reported in reference 26 in changing the flaps-retracted to the approach configuration for a double slotted flap. (Absolute amplitudes for noise radiation were later decreased because the data given in reference 26 are not free-field.) Thus for the wing and for each of n flap segments

$$K_n = 1 \times 10^{-7} (c_n/c) (h_n/c)^{-2} \quad (1)$$

and the total overall fluctuating lift noise is given by

$$OASPL_L = 10 \log \left(\rho U_i^3 / \rho P_{ref} \right)^2 (cD/r^2) (U_i/V)^2 \sum K_n \sin^2 \theta_n \quad (2)$$

As with the basic concepts of the NASA ANOP method of reference 27 for EBF, fluctuating lift noise was assumed to vary with impingement velocity raised to the sixth power. Impingement velocity was defined as the maximum velocity in an isolated axisymmetric exhaust jet at the axial distance of the impingement point. For a flap configuration that extends below the nozzle centerline, the impingement point is the position where the centerline intersects the flap. For flaps that are not deflected that far into the exhaust jet, the impingement point is taken as the trailing edge of the last flap segment. The ratios of impingement velocity and trailing edge velocity to nozzle exhaust velocity were calculated from the NASA-developed equation (3) of reference 15.

$$U_i/V = \left\{ 1 + \left[0.14 (x/D) (1 + M_N)^{-1/2} \right]^4 \right\}^{-1/4} \quad (3)$$

Large ratios of flap length to nozzle diameter have been found to generate less noise than this procedure would predict. Lift fluctuation noise therefore was arbitrarily multiplied by the ratio of trailing edge velocity to impingement velocity squared. Equivalent nozzle velocity for an unmixed coaxial jet was calculated from equation (5) of reference 27, the NASA ANOP method for EBF.

Trailing edge noise is proportional to the product of turbulence integral scale length and spanwise distance along the edge. Both of these dimensions are proportional to nozzle diameter. Amplitude of trailing edge noise is proportional to the ratio of diameter squared to far-field radius squared, and to trailing edge velocity raised to the fifth power. Directivity is given by cosine squared of half the angle from the last flap segment's upstream direction.

$$\text{OASPL}_T = 10 \log 0.5 \times 10^{-5} (\rho^2 U_1^5 / \rho_{\text{ref}}^2) (D/r)^2 \cos^2 \phi \cos^2[(\theta + \delta_F / 2)] \quad (4)$$

Normalized 1/3 octave spectra taken from equations (11) and (12) of reference 17 are used for fluctuating lift noise and trailing edge noise. These spectra have analytically justified asymptotic slopes at small and large Strouhal numbers, but nevertheless they are empirical curves based on published normalized spectra. The sole justification for use of these equations is the good agreement with measured normalized EBF spectra given in reference 1.

$$(\text{SPL}_{1/3} - \text{OASPL})_L = 10 \log 0.037 \text{St}^4 (\text{St}^{8/3} + 0.008)^{-2} \quad (5)$$

$$(\text{SPL}_{1/3} - \text{OASPL})_T = 10 \log 0.029 \text{St}^4 (\text{St}^{3/2} + 0.5)^{-4} \quad (6)$$

Calculation of the several kinds of quadrupole noise is based on the NASA ANOP method of reference 16 for quadrupole noise of an isolated axisymmetric subsonic exhaust jet. OASPL is calculated by an explicit equation, with an empirical correction for refraction at direction angles close to the downstream centerline. Normal to the jet,

$$\begin{aligned} \text{OASPL}_{90} = & 141 + 10 \log [M_J^{7.5} (1 + 0.010 M_J^{4.5})^{-1}] + 10 \log [(A_J/r^2) (\rho_0/\rho_{\text{ISA}})^2 (a_0/a_{\text{ISA}})^4] + \\ & 10 [3M_J^{3.5} (0.60 + M_J^{3.5})^{-1}] \log (\rho_J/\rho_0) \end{aligned} \quad (7)$$

For direction angles, relative to the deflected jet upstream direction, smaller than $M_J \times 150^\circ$,

$$\text{OASPL}_J = \text{OASPL}_{90} - 30 \log [1 + M_c (1 + M_c^5)^{-1/5} \cos \theta] \quad (8)$$

where the convective Mach number M_c was taken as $0.62M_J$.

For relative direction angles between $M_J \times 150^\circ$ and 180° , the negative quantity

$$\Delta OASP_J = -18 \left[1 - (6 - M_J \theta / 30) \right] \quad (9)$$

is added to $OASPL_J$ calculated from equation (8) to account for refraction within the jet. Deflection of the exhaust jet by a flap segment is assumed to add a quadrupole noise term given by 6 sine squared of the effective turning angle (input as the last flap angle) multiplied by noise of the isolated jet. The sum of these two quadrupole terms

$$OASPL_Q = OASPL_J + 10 \log \left[(1 + 6 \sin^2 \delta_F)(1 + \cos^2 \phi) / 2 \right] \quad (10)$$

has its directivity defined relative to the deflected-flow centerline. Quadrupole noise is also assumed to be generated by the portion of the exhaust jet downstream of the last flap segment trailing edge. This noise is arbitrarily taken as that for an isolated jet having a diameter equal to the nozzle diameter and exhaust velocity equal to the calculated maximum velocity at the trailing edge. It is then multiplied by the same factor, $1 + 6 \sin^2$ (deflection angle), used with the jet deflection process. This quadrupole noise component is also referenced to the deflected-flow centerline. All of these quadrupole noise components radiate equal intensities above and below the deflected jet. This assumption was made because experimentally determined UTW directivity patterns contain equal-amplitude peaks of quadrupole noise above and below the deflected jet.

Quadrupole noise at directions below the jet, termed impact noise in reference 24, was taken in that study as equal to the noise measured at the same angle beneath a jet deflected by a large solid surface. Acoustic reflection from that simplified configuration raises the noise caused by the undistorted portion of the jet between the nozzle exit and the impingement region, and by jet distortion and deflection in the impingement region. Whether slotted flaps were assumed to transmit or reflect this noise, it was necessary to postulate an additional quadrupole noise process having approximately the same strength and orientation. Their sum would match UTW data at directions 20° to 40° above and below the deflected jet. The quadrupole noise arbitrarily attributed to the exhaust jet downstream of the trailing edge was hypothesized for this reason.

UTW quadrupole noise is important at direction angles greater than 90° from the upstream direction of the deflected jet. Within this region, normalized spectrum shape for an isolated jet changes greatly (figure 5 of reference 16) with direction angle. Spectrum shapes for directions near peak OASPL amplitude have a more rapid high-frequency decay than that for more upstream directions. It was found that spectrum shapes which were correct for an isolated jet at peak OASPL underpredicted the measured high-frequency

noise for UTW slotted flaps at approach flap position. Closer agreement was obtained by use of the normalized spectrum for an isolated jet at 140° direction angle for all angles between 140° and 180° .

$$(\text{SPL}_{1/3} - \text{OASPL})_0 = 10 \log 0.1 \text{St}^4 (\text{St}^{17/12} + 0.11)^{-4} \quad (11)$$

The contribution of quadrupole noise to total UTW noise below the wing decreases as direction angle is decreased from this range. Rather than include the complexity of a spectrum shape that varies with direction angle, over a direction range where this contribution becomes small, this one normalized spectrum for quadrupole noise is used at all directions.

As part of the development of the UTRC method, calculated variations of UTW noise with changes in configuration geometry were compared with available data. Measured effects of axial and vertical displacement of a double slotted flap approach configuration (reference 26) were shown in reference 17 to be closely predicted. Measured effects of doubling and halving the nozzle diameter of that model, at constant axial and vertical position of the nozzle upper edge, were also (reference 18) correctly given. Although based on data for that double slotted flap at 20° and 60° flap deflections, this UTW noise prediction method was shown in reference 18 to predict closely the measured noise from a 40° deflection triple slotted flap.

Forward flight effects on UTW fluctuating lift noise and trailing edge noise, taken from references 18 and 20, are represented as a decreased amplitude given by the ratio of relative velocity to exhaust velocity squared. Forward flight effects on quadrupole noise from the undeflected portion of the exhaust are assumed to vary with relative velocity ratio to the sixth power as with the NASA ANOP method of reference 16 for noise of an isolated jet. However, the increases of quadrupole noise attributed to impingement against the flap lower surface and to the jet downstream of the trailing edge are assumed to vary with relative velocity ratio squared. This reduced exponent was based on the data of reference 18. Relative velocity between the exhaust jet and the surface against which it impinges is not affected by forward flight. These calculations provide the predicted effect of forward flight on EBF noise source strength in a coordinate system fixed to the airframe. They do not include the effect of airframe motion relative to a ground-fixed observer. Corrections for this difference between an aircraft flyover and an acoustic wind tunnel test are given in reference 27.

UTW Mixer Nozzle

Some UTW slotted flaps have been operated with mixer nozzles to decrease the peak velocity and temperature at the deflected flaps. For this type of configuration, ratio of local velocity at the impingement point to exhaust velocity must be supplied as input. This quantity is arbitrarily defined as the average of the two largest local peak values of velocity ratio measured in the exhaust of the isolated mixer nozzle at the impingement-point axial location. The same velocity ratio is assumed to apply at the trailing edge. Nozzle diameter is taken as the hydraulic diameter of the mixer nozzle total exit area. Calculation of fluctuating lift noise and trailing edge noise then follows the method for UTW slotted flaps having conventional axisymmetric nozzles, except that the resulting levels are arbitrarily increased 3 dB. This increased amplitude, possibly caused by higher turbulence levels or larger-diameter core of high-velocity exhaust flow, was shown in references 17 and 18 to be necessary for obtaining good agreement with data.

This computer program does not calculate quadrupole noise for UTW mixer nozzles. Although OASPL amplitudes for a mixer nozzle generally match those for the unmixed exhaust jet, spectrum levels depend strongly on the mixer nozzle geometry. It is assumed that measured noise spectra and OASPL amplitudes are available for the isolated mixer nozzle at takeoff and approach flight speeds. This measured noise must be increased by $10 \log (1 + 6 (\text{velocity ratio})^8 \sin^2 (\text{flow deflection angle}))$ to account for deflection of the mixed exhaust jet. The resulting quadrupole noise should be rotated through the flow deflection angle, and all amplitudes at directions below the wing and flaps should be increased 3 dB. This increase had been stated in reference 17 and 18 to be caused by reflection of quadrupole noise from the wing and flap. However, improved agreement with data measured above the wing is obtained if upward-radiated noise is assumed to be transmitted through the flap slots. The resulting quadrupole noise component (increased 3 dB below the wing and flap, not increased above them) should be added to surface-radiated noise given by the computer program.

Upper Surface Blowing

Geometry of a USB (figure 43) is idealized as two straight lines, one for the wing and one for the last flap. The wing is described by the upper surface coordinate at the nozzle exit plane and by the wing incidence relative to the nozzle centerline. The flap is given by its trailing edge coordinates and by the aerodynamic turning relative to the wing chord line. Coordinates at the intersection of those two lines are computed as part of the solution. Effects of nozzle exit shape are neglected, and the nozzle is specified by its hydraulic diameter and its roof angle, cant angle, or external vane deflection angle relative to the nozzle centerline. Details of the

nozzle and deflector shape have been found empirically to have significant effects on noise amplitudes; these can be estimated using the data given in reference 28.

Trailing edge noise and fluctuating lift noise OASPL's are calculated in the same manner as for UTW slotted wings. However, amplitude of trailing edge noise was taken as twice as large for USB as for UTW. The vortex trajectory is assumed to be one hydraulic diameter above the wing. Lift fluctuation noise from the flap is arbitrarily taken as 1.5 times that for a hypothetical vortex trajectory one hydraulic diameter above the flap. Velocity ratio at the trailing edge is calculated for a distance equal to the path length along the wing and flap. It was found that spectra calculated in this manner decayed less rapidly than the data for large Strouhal numbers and low exhaust velocities. Therefore the normalized spectrum shape for trailing edge noise was arbitrarily used with OASPL calculated from the sum of lift fluctuation noise and trailing edge noise.

Quadrupole noise caused by impingement of the exhaust jet against a deflecting surface is assumed to increase the quadrupole noise of an isolated exhaust jet. This increase caused by roof angle, cant angle, or vane angle is given by the same factor as that for impingement of a UTW exhaust jet against a deflected flap. The resulting quadrupole noise is assumed to be shielded by the wing and flap upper surface. It is rotated through the aerodynamic turning angle and is calculated only for direction angles above the wing and deflected flap. Quadrupole noise from the portion of the exhaust jet downstream of the trailing edge is increased by the same factor and rotated through the same angle, but it radiates to all directions. As with UTW, one normalized spectrum shape is used at all directions. It is likely that for direction angles at which USB quadrupole noise is important, improved agreement with data would be obtained if the normalized spectrum was assumed to vary with angle relative to the deflected jet centerline as with an isolated jet. Measured noise of each isolated nozzle and deflector, without the wing and flap, should be compared with quadrupole noise calculated for the deflected jet. Any increment of measured dipole noise associated with the presence of the deflector should be added to the predicted USB noise for directions above the wing.

Forward flight effects on the sum of trailing edge noise and fluctuating lift noise was taken as a decrease of amplitude combined with an increase of frequency. As with UTW, the OASPL amplitude is taken proportional to relative velocity ratio squared. However, normalized $1/3$ octave SPL is calculated for Strouhal numbers that were multiplied by the quantity $(1 + \text{flight velocity/exhaust velocity})$. This adjustment had been developed in references 18 and 20. Forward flight effects on quadrupole noise are taken equal to

those for UTW. One reasonable validation of these predicted forward flight effects on USB noise would be comparisons with flyover data for the Boeing YC-14 Advanced Medium STOL Transport, the only full-scale USB airplane, if noise from the installed engine proves to be sufficiently low.

UTW Slotless Wing

Geometry of a UTW slotless wing is specified and calculated in the same manner as that for USB. Quadrupole noise and trailing edge noise are computed in the same manner as for a UTW slotted wing. To obtain closer agreement between measured and predicted noise directivity, it was found necessary to add a noise component having the general shape and velocity dependence of a lift dipole oriented perpendicular to the deflected aft flap. However, increasing the flap chord was experimentally found not to increase this OASPL. This noise component was arbitrarily modeled as fluctuating lift noise with an amplitude three times that which would be calculated for the wing segment, rotated through the flap deflection angle.

This special calculation of fluctuating lift noise is applied only if the slotless wing extends below the nozzle centerline. Any slotless UTW which does not meet this condition is regarded as a wing with retracted flaps. Geometry of a wing with retracted flaps is specified as that for a USB configuration having zero flap deflection. It could also be specified as a UTW single slotted flap having a flap with zero deflection and zero chord, located at the wing trailing edge. Both calculations will give the same result.

Engine in Front of Wing

This type of configuration has the wing chord line coincident with the exhaust nozzle centerline. The wing is completely immersed in the turbulent exhaust jet. For the one configuration tested, maximum wing thickness was about half the nozzle exit diameter. Therefore the exhaust jet was substantially altered by the presence of the wing. Maximum local velocities at the trailing edge flaps probably were reduced by viscous decay along the wing. Spectra radiated by this model were characterized by a high-frequency decay rate larger than that for other EBF configurations. This rate of about 12 dB per octave for 1/3 octave band spectra agreed with data for isolated airfoils in turbulent flow.

A calculation method developed in references 4 and 5 for predicting noise radiated by isolated airfoils in three-dimensional compressible flow was applied to the undeflected wing panel and each flap segment. Each lift

dipole was assumed to act normal to the local chord. Calculated jet mixing noise for an isolated undeflected exhaust jet was added to the lift fluctuation noise. Width of the turbulent flow was taken equal to the nozzle diameter, and flow velocity was taken as the nozzle exit velocity. It was found that free-field spectrum could be matched if turbulence intensity was arbitrarily set equal to 7 percent and turbulence integral scale length was taken as one-eighth the nozzle radius. (The data had been measured with a reflecting ground surface, and a 10 percent turbulence level was cited in reference 17 to match those data.) Resulting calculated OASPL directivity tended to overpredict the data for the first and third quadrant at approach flap deflection. Closer agreement was obtained by neglecting the acoustic contribution of the last flap panel. It is possible that local flow velocity at that location was decreased by the presence of the wing within the jet, causing a decrease of local noise radiation.

Calculated noise radiation for this type of configuration should be applicable to interference noise of a wing-mounted propfan. Slipstream velocities for highly loaded propfans designed for cruise at Mach numbers near 0.8 would be comparable to exhaust velocities of lightly loaded high bypass ratio turbofan engines.

EVALUATION OF EBF NOISE PREDICTION METHODS

Other EBF Noise Prediction Methods

The method developed under this contract is evaluated in this section by comparing its predictions, and those from other openly published methods, with NASA-supplied data. These new data had not been part of the data base used in development of the EBF noise prediction methods compared herein. Capabilities and limitations of these methods are compared in Table II.

TABLE II - CAPABILITIES AND LIMITATIONS OF
EBF NOISE PREDICTION METHODS

Method	UTW Slotted	UTW Slotless	UTW Mixer	USB, Slot Nozzle	USB, Deflector	Front of Wing	Limitations of These Comparisons
UTRC (1976)	Yes	Yes	Yes	Yes	Yes	Yes	
ANOP (1975)	Yes	No	No	Yes	Yes	No	
GELAC (1973)	Yes	Yes	No	Yes	Yes	No	Used for UTW only.
GELAC (1975)	Yes	Yes	No	Yes	Yes	No	Used for USB only.
NASA Lewis (1975)	Yes	Yes	No	No	No	No	Spectra not given.

Note that the UTRC method is the only one which can be applied to UTW configurations with mixer nozzles. The recent NASA Lewis method for UTW configurations having a uniform exhaust jet is currently limited to prediction of OASPL directivity; it does not predict spectra. One widely used method is the NASA ANOP (Aircraft Noise Prediction Program) method of reference 27. This method is based on empirical curves drawn through data available in 1975; these data were corrected for ground reflection. Application to USB configurations having noncircular exhaust nozzles was not specifically described. However, noise from such configurations has been calculated by NASA using the ANOP method by replacing the actual nozzle with a circular nozzle of equal exit area. This same usage is made herein.

Another method used for this evaluation is the GELAC (Lockheed-Georgia Co.) method developed for the FAA. It is a noise component method which contains separate calculations of surface-radiated noise and quadrupole noise from several geometric regions. The early version of this procedure (reference 29) included the effects of many UTW geometric variables (flap vertical and axial position, nozzle pitch angle, and number of flap slots) not represented in the ANOP method. A more recent version (reference 30) has much less dependence on flap geometry and is more strongly directed toward USB configurations. Both versions exist as digital computer programs and as

hand calculation procedures. Predictions given herein were obtained by the hand calculation method of reference 29 for UTW and that of reference 30 for USB. Because the data base for the method of reference 29 consisted of measurements that were affected by ground reflection, predicted levels were decreased 3 dB for closer agreement with NASA free field data. The earlier method of reference 29 represents all UTW noise as varying with exhaust velocity to the sixth power. This method was utilized because OASPL's and directivity patterns calculated from reference 30 were in very poor agreement with UTW data. It was later recognized that all quadrupole noise terms given in reference 30 were of the order of 10 dB below expected levels. Quadrupole noise calculations developed in the GELAC method of reference 30 were scaled from levels predicted by the NASA ANOP method for jet exhaust noise (reference 16). Jet exhaust noise for an isolated circular exhaust nozzle is given by equation (5) of reference 30, which agrees with the corresponding equation (6) of reference 16 except for one item. The numerical value for the constant K used in reference 16 was 141 dB. However, this constant as specified on p. A-86 of reference 30 for hand calculations by the GELAC method was 134 dB. This same constant, 7 dB less than that specified for the NASA ANOP method for jet noise also appears within the GELAC computer program listing (line 110 of subroutine JET, p. A-24 of reference 30). Comparisons between calculated and measured OASPL were not shown within the GELAC document. Although not explained in reference 30, this change from the constant used in reference 16 was included to provide closer agreement with unpublished GELAC USB data and its effect on UTW predictions was not examined.

A method was developed at NASA Lewis Research Center for calculating OASPL directivity of UTW configurations at directions under the wing in the flyover plane. Use of this method for slotless wings was first described in reference 24. The significant noise sources for slotless wings were assumed to be trailing edge noise and impact noise. Trailing edge noise was calculated from local maximum velocity, boundary layer thickness at the position of maximum velocity, and width of the exhaust jet (all measured at the trailing edge). Impact noise caused by a jet impinging against a very large deflecting surface was obtained from data such as that of reference 3. This method was extended in reference 25 to include application to UTW slotted wings. An additional noise mechanism, inflow noise (called fluctuating lift noise in the UTRC method), is included for those configurations. This noise is assumed to result from the large-scale turbulence structure, present in jet exhausts, moving past the flaps to cause fluctuations of lift force. The noise was calculated using local flow properties estimated at midchord of each flap panel. This NASA Lewis method currently does not predict noise spectra. OASPL directivities calculated for slotless wings by this method were provided by Mr. D. J. McKinzie, Jr., of NASA Lewis Research Center.

Other calculation methods for USB had been developed by Hayden (reference 11), Filler (reference 31), and Reddy (reference 21). Noise levels measured directly beneath two USB models were compared in figures 10-12 of reference 32 with predictions by the methods of references 11 and 31, and by an early version (reference 17) of the method of this report. Upper surface length from the slot nozzle to the flap trailing edge differed by a factor of 2 for these models. QASPL of both models was overpredicted roughly 10 dB by the method of reference 11 and underpredicted the same amount by the method of reference 31. For both of those methods, the predicted spectrum shape was more sharply peaked than the measured shape. Good agreement on level and spectrum shape was obtained with the early UTRC method. Those two prediction methods were not evaluated herein because they gave such poor agreement with those data. The more recent method of reference 21 was not available in sufficient detail to be applied.

Designated EBF Model Configurations

The EBF model configurations shown in figures 3 and 4 were designated by NASA Lewis Research Center to be used for evaluation of noise prediction methods. These models were relatively small, with nozzle exit areas generally equal to that of a 5.2 cm (2 in.) diameter circular nozzle. All had been tested at NASA Lewis Research Center in an outdoor facility equipped with a mat of acoustic absorbing foam to give free-field data above 200 Hz. Data had been corrected for atmospheric attenuation. Comparisons were also made with nonfree-field data for specific unique configurations.

Two designated models were under-the-wing configurations. Sketches of these models are given in figure 3. These were a three-flap installation at both takeoff and approach flap deflection, for a range of sideline angles, and a slotless wing having the same lower surface contour as the three-flap approach flap shape, for only the flyover plane. Portions of these data had been presented in reference 19. They were compared therein with predictions by the UTRC, NASA ANOP, and GELAC methods.

The other three models, shown in figure 4, were upper-surface-blowing (over-the-wing) configurations. One was the QCSEE configuration having an aspect ratio 2 slot nozzle, tested at nominal 1/11.5 scale with 14 cm (5.5 in.) equivalent nozzle diameter. Data were supplied for a range of flap length and sideline angle at takeoff flap deflection and a range of sideline angle at approach flap deflection. These data had been presented in reference 22 where they were compared with predictions by the UTRC method. Another was a 1/18.5 scale model of the TF-34 over-the-wing aspect ratio 4 slot-nozzle short-flap configuration of reference 33 with takeoff flap deflection. The third

configuration (reference 3⁴) had a circular nozzle above the wing and an external jet-flow deflector to direct the exhaust jet toward the wing upper surface. This arrangement was expected to reduce adverse interference of the exhaust jet on the wing drag force during cruise.

Aerodynamic performance data (lift, thrust, and trailing edge velocity profile) at zero forward speed are available for all these configurations.

Comparisons With Designated UTW Data

Predicted and measured UTW noise radiation are compared in the following order: OASPL at the 90° polar angle 0° azimuth angle flyover position, general shape of OASPL directivity in the flyover plane, effect of azimuth angle on OASPL amplitudes, and normalized 1/3 octave spectra. The discussion is directed primarily toward evaluation of the UTRC method, the subject of this report.

Triple Slotted Flap, Approach

This configuration had been tested at nominal 1/28 scale. Data were presented, and were compared with predictions by several methods, in reference 19. The free-field spectra contained small peaks and valleys at non-uniformly spaced frequencies. These frequencies did not vary with exhaust velocity but were altered by changing the flap deflection.

Calculated and measured OASPL directivities in the flyover plane for approach flap deflection and four exhaust velocities are compared in figure 5. At low exhaust velocities the UTRC and ANOP methods underestimated the measured OASPL at 90° polar angle by 3 to 4 dB, and the GELAC method was about 2 dB high. At the two higher exhaust velocities the UTRC and GELAC methods were within 1 to 2 dB and 1 to 3 dB, respectively; the ANOP method remained 3 dB low.

Both the ANOP and GELAC methods use a constant directivity shape that generally matched the data. In contrast, directivity shape calculated by the UTRC method varied with exhaust velocity. Except at polar angles near the deflected exhaust, the measured directivity shape did not change greatly with exhaust velocity. Measured OASPL amplitudes varied approximately with the 6.5 power of exhaust velocity.

Effects of sideline angle on measured and calculated OASPL for this approach flap configuration are shown in figure 6. These effects are plotted as changes in OASPL relative to that for the flyover plane, at two exhaust velocities, as a function of polar angle (angle relative to the nozzle centerline). The GELAC predictions (defined only for 90° polar angle) essentially match the maximum noise reductions calculated by the ANOP method. In contrast, the UTRC predicted maximum reductions are about twice as large and generally agree with the data. These calculations differ from those given in reference 19, which contained a trigonometric error. Details of the predicted shape do not precisely match the data; maximum reduction is predicted near 90° polar angle but occurred about 10° further downstream. For 60° sideline angle the predicted and measured maximum reductions of about 6 dB generally agree with the analytically expected dependence of surface-radiated noise on sine squared of the sideline angle. For 85° sideline angle the measured and UTRC calculated sideline noise decrease roughly 10 dB to a floor set by quadrupole noise from the deflected jet. Measured and UTRC calculated noise was increased several dB at 120° polar angle. This angle is within the refraction valley of quadrupole noise from the deflected exhaust jet as viewed in the flyover plane, but is near peak amplitude of quadrupole noise when viewed from the side.

Calculated and measured 1/3 octave spectra normalized with respect to OASPL, for approach flap deflection, are compared in figure 7. Frequencies are normalized as Strouhal number based on nozzle diameter and exhaust velocity. Data are shown for 70° and 110° polar angle and 120 and 228 m/sec exhaust velocity, in the flyover plane and at 85° sideline angle. For the flyover plane and large Strouhal numbers, the data points for 70° polar angle were about 5 dB below those for 110° polar angle. OASPL was somewhat affected by irregular peaks in the spectra measured at forward polar angles; actual 1/3 octave band SPL's for the two directions differed by about 10 dB near peak amplitude but were within 2 dB for Strouhal numbers above 2. All three prediction methods generally matched the normalized spectra for 110° and (not shown) 90° polar angles. Normalized spectra for the 85° sideline plane had about 8 dB data spread at large Strouhal numbers. The ANOP and GELAC methods bracketed the data for small Strouhal numbers and generally matched the high-velocity spectra for large Strouhal numbers. Spectrum shapes calculated by the UTRC method varied because the relative amplitudes of different noise components vary with exhaust velocity and polar angle. The resulting calculated spectra lie within a narrow envelope. The UTRC method was closer to an average of the data for large Strouhal numbers. It gave a more rapid spectrum roll-off at high frequency than did the other two methods. This stronger decay was in closer agreement with the data.

Triple Slotted Flap, Takeoff

Calculated and measured OASPL directivities in the flyover plane for the takeoff configuration and four exhaust velocities are shown in figure 8. Calculation by the ANOP method used equation (16) of reference 27, rather than equation (11) of that reference, for predicting the variation of OASPL with flap deflection angle. Use of equation (16) was recommended for configurations in which the flaps extend relatively far into the high-velocity exhaust jet at small deflection angles. If the other equation had been used, calculated noise levels would have been 5.2 dB smaller. Measured amplitudes were underpredicted by all three methods. Near 90° polar angle the UTRC method and the ANOP method with the more favorable equation were about 5 dB low. The GELAC method of reference 29 was about 8 dB low. This ANOP equation had been developed specifically from data for triple-slotted flap configurations with this type of geometry. In contrast with this poor agreement, these three methods were known to predict closely (within 2 dB) the OASPL directivity data of reference 26 for an UTW double-slotted flap at takeoff deflection. All three methods had been developed to match those data. That double-slotted flap configuration had a smaller total flap chord than the model triple-slotted flap, and about the same wing leading edge position and wing chord. At takeoff deflection, the trailing edge of the double-slotted flap's last flap segment was located above the nozzle centerline. From the viewpoint of the UTRC method, the deflected flap panels did not greatly distort the exhaust jet so they did not produce much lift fluctuation noise. Nearly all the last panel of the triple-slotted flap extended below the nozzle centerline at takeoff deflection. None of these three methods correctly predicted the resulting increased noise levels. The GELAC method, which was the only method to overpredict measured levels near 90° polar angle for the approach configuration, gave the worst underprediction at takeoff.

A fourth set of predicted curves, labeled NASA LEWIS, shows OASPL directivities calculated by D. J. McKinzie, Jr. of NASA Lewis Research Center by the method of reference 25. These calculations require extensive knowledge of local turbulence and mean velocity. Such calculations were supplied by NASA only for this takeoff configuration, where other methods gave worst agreement with data. These calculated amplitudes were within 2 dB of data near 90° polar angle. They generally matched the data from there to the deflected jet and were up to 4 dB high in the forward quadrant. This good agreement with data was achieved by use of estimated local flow properties evaluated from data for isolated jets, and illustrates the need for such flow-field information. As previously noted, this method has not yet been extended to prediction of spectra or of sideline directivity.

The effect of sideline angle on calculated and measured OASPL directivity is shown in figure 9. Measured maximum reductions, relative to those in the flyover plane, were about 7 and 12 dB for 60° and 85° sideline angle, respectively. These reductions were more than twice those predicted by the ANOP method and were generally predicted by the UTRC method. The UTRC method also correctly predicted that the difference between OASPL in the sideline plane and the flyover plane would be positive at 150° polar angle. This polar angle is in the deflected exhaust jet's refraction valley for the flyover plane but not for the 60° or 85° sideline angles.

Calculated and measured normalized $1/3$ octave spectra at takeoff flap deflection are compared in figure 10 for two polar angles and two exhaust velocities in both the flyover and 85° sideline plane. The scatter among normalized data points near peak amplitude in the flyover plane was ± 2.5 dB for different polar angles at the same velocity and ± 4 dB for different velocities at the same angle. This scatter greatly exceeds the approximately $\pm 3/4$ dB day-to-day repeatability of these data. The scatter was caused by the previously mentioned spectrum irregularities. All of the noise prediction methods use a smooth normalized spectrum or a sum of smooth spectra. Therefore the existence of irregular spectra causes an inherent uncertainty in the predictions. There was no systematic effect of polar angle or exhaust velocity on normalized spectrum. All three predictions generally matched the flyover spectra for Strouhal numbers from 0.2 to 2 and overestimated the levels at higher Strouhal numbers.

A different situation occurred for the takeoff flap setting at 85° azimuth angle. As shown in the lower part of figure 10, the normalized levels at large Strouhal numbers were higher at the larger exhaust velocity. This difference occurred because levels for large Strouhal numbers varied with exhaust velocity to at least the eighth power while those near peak amplitude followed approximately a 6.5 power variation. At Strouhal numbers larger than 2, corresponding to highly weighted frequencies for perceived noise at full scale, the ANOP prediction matched the data for the higher exhaust velocity and rearward direction. The GELAC prediction was closer to data for the lower velocity, and the UTRC prediction generally was between the two.

Slotless Version of Three-Flap Wing

Measured directivity in the flyover plane for an UTW slotless wing having a lower surface contour tangent to that of the three-flap configuration at approach flap deflection is plotted in figure 11. The data are compared with predictions by the UTRC and GELAC methods and with the NASA Lewis method of references 24 and 25. This NASA method represents the OASPL noise radiation from slotless wings as a sum of two terms. One term is the noise measured for a jet impinging against a large flat surface at the same deflection angle

and impingement velocity, scaled from the data of reference 3. Because these data were influenced by ground reflection, they were decreased 2 dB for comparison with these free-field slotless wing data. The other term represents trailing edge noise. It uses measured variations of deflected-jet width, boundary layer thickness, and maximum velocity at the trailing edge within an equation having the correct functional dependence. The GELAC hand calculation method of reference 29 predicts that a slotless UTW configuration will be 3 dB quieter than the double or triple slotted equivalent shape. Additional comparisons of the NASA Lewis and UTRC methods are made in the section entitled "Additional Slotless Wings".

Measured directivity shapes changed from a broad lift-dipole sort of pattern at low exhaust velocities, with peak amplitude normal to the deflected flap region, to nearly constant amplitude below the wing and flap at large velocities. The UTRC method matches these shapes and levels, although it generally predicts too low a noise level for directions above the deflected aft surface. For directions below the wing and flap, agreement ranges from 2 dB underestimate at the lowest exhaust velocity to 2 dB overestimate at the highest. Levels calculated by the NASA Lewis method of references 24 and 25 agree with the UTRC predictions near 100° polar angle where both are dominated by deflected-jet noise. This NASA Lewis method matches the data within 2 to 3 dB over the range of polar angles from 20° to 120° for which the method applies. Note that because the test model is relatively small, it was necessary to use the flow-field data of reference 24 for the same model size rather than that of reference 25 for a geometrically larger model. The constant-shape GELAC curve tended to be about 5 dB above the data, and did not match measured shapes for the higher velocities.

Free-field spectra measured at 90° polar angle are compared in figure 12 with those calculated by the UTRC method. Irregularities, including a strong minimum in the $1/3$ octave band centered at 630 Hz, dominate the low-frequency portion of the measured spectra. These spectrum irregularities were especially strong near 40° polar angle, which is not an obvious angle for noise generation or reflection for this slotless wing. Above 1600 Hz these spectra at 90° angle contain mild oscillations of about 2 dB half-amplitude about the calculated smooth curves. Oscillations were shown in reference 19 to be larger for this slotless wing than for the three-flap slotted wing at either deflection. Possible causes of the nonsmooth spectra were discussed therein. Note that according to the data of reference 33, this slotless wing was too many nozzle diameters downstream to produce noise by acoustic feedback between the nozzle and deflected solid surface. The measured spectrum oscillations strongly affect the statistical accuracy of measured OASPL. Therefore the normalized $1/3$ octave spectra for this slotless wing are less reliable than those for the triple slotted flaps.

Calculated and measured normalized $1/3$ octave spectra for the slotless wing are shown in figure 13. The spectrum measured at the lower exhaust velocity and 70° polar angle contains the largest scatter. Measured normalized levels for this spectrum and Strouhal numbers larger than 2 are about 5 dB below those for the other spectra. All the calculated normalized spectra lie 2 to 3 dB above those other measured spectra for Strouhal numbers larger than one. As with all other normalized spectra shown except those for the flyover plane and takeoff flap deflection, the ANOP method markedly underpredicts measured levels for Strouhal numbers less than 0.2. This may be important for predictions of airframe structure acoustic fatigue.

Comparison With Designated USB Data

QCSEE USB, Takeoff

Acoustic and aerodynamic results for $1/11.5$ and $1/28$ scale models of the QCSEE USB configuration were presented by NASA in reference 22. Acoustic data were compared by NASA with predictions made at UTRC before the data were available. These comparisons are plotted herein. Calculated and measured OASPL directivities in the flyover plane are compared in figure 14 for the larger model. Measured directivities clearly changed shape with exhaust velocity. Amplitudes near 90° polar angle were predicted by the UTRC method within 2 dB, and the directivity shapes were closely matched. In contrast, the ANOP method matched the measured shapes only at low exhaust velocities (not used at takeoff) and was about 4 dB low near 90° polar angle. Amplitudes near 90° angle, as calculated by the GELAC method of reference 30, were no worse than those from the ANOP method, but directivity shapes were in poor agreement with data. This GELAC method contains several noise components which vary with nozzle velocity raised to the eighth power. For USB configurations they represent noise from the exhaust jet downstream of the trailing edge, the wall jet on the wing and flap upper surface, and the canted nozzle exhaust impinging against the wing upper surface. However, the sum of these calculated terms is 5 to 10 dB below what would be needed to achieve reasonable agreement with the data. As mentioned in the preceding section entitled "EBF Noise Prediction Methods", even the noise from an isolated exhaust nozzle would be calculated as 7 dB less than that given by the NASA ANOP method of reference 16.

Effects of polar angle on calculated and measured sideline directivity are given in figure 15 for 63° and 85° sideline angles. Results are shown for the nominal flap length and for two other flap lengths to be discussed later. Measured reductions between 75° and 105° polar angle were about 6 dB and 9 dB for 63° and 85° sideline angle, respectively. These reductions were predicted by the UTRC method and greatly underpredicted by the ANOP and GELAC. Measured reductions between 75° and 105° polar angle were about 6 dB and 9 dB for 63° and 85° sideline angle, respectively. These reductions were predicted by the UTRC method and greatly underpredicted by the ANOP and GELAC methods. The ANOP prediction for USB is defined only for 90° polar angle. Details of the measured sideline effect in the aft quadrant were poorly predicted by the UTRC method. As with the comparison for UTW configurations, maximum noise reduction occurred behind 90° polar angle but was predicted to occur at or ahead of that angle. Increased OASPL at 63° sideline angle, at a polar angle within the deflected jet exhaust refraction valley in the fly-over plane, was larger than predicted and occurred at 20° larger polar angle. This good qualitative agreement, but poor agreement in details, probably results from the incorrect assumption that quadrupole noise radiation from a USB slot nozzle is axisymmetric about the deflected jet centerline.

Effects of polar angle and exhaust velocity on calculated and measured normalized spectra for the 1/11.5 scale model are compared in figure 16. Data are shown for 60° and 120° polar angles at about 150 and 220 m/sec exhaust velocities. Measured normalized spectra for the flyover plane and large Strouhal numbers are highest for the aft polar angle at both velocities. They are about 8 dB lower for the forward angle and lower velocity. This change in spectrum shape and level is predicted by the UTRC method. Although the GELAC method gave a poor prediction of OASPL at 120° polar angle, it correctly predicted that noise at this direction would be dominated by quadrupole noise. The resulting calculated normalized spectra also match the high-frequency portion of the data. The ANOP normalized spectrum is independent of polar angle and exhaust velocity; it would generally match the data (not shown) for 90° polar angle and both velocities. Measured normalized spectra at large Strouhal numbers were greatly affected by exhaust velocity at 60° polar angle but not at 120° angle. For 60° angle, increasing the exhaust velocity greatly increases the calculated amount of quadrupole noise and therefore the spectrum amplitudes at high Strouhal numbers. It causes only moderate increases of surface-radiated noise which dominates the peak amplitudes and OASPL. The ANOP method overpredicts measured normalized levels by about 3 to 11 dB at high Strouhal numbers. Normalized spectra given by the GELAC method were a few dB closer to data than those from the UTRC method for Strouhal numbers larger than 5.

Three difference flap lengths had been tested with the 1/11.5 scale model at 218 m/sec exhaust velocity. The effect of flap length on directivity and spectrum in the flyover plane is shown in figure 17. As can be seen from the sketch at the top of this figure, the short flap was only slightly shorter than the nominal length but the long flap was considerably longer. The short flap was found to cause 3 to 4 dB increase, and the long flap about 2 dB decrease, of OASPL relative to that for the nominal flap. In contrast, the UTRC method predicted no significant change with the short flap and about 2 dB increase with the long flap. The UTRC method tends to predict an increase of surface-radiated noise due to increased flap length, and a decrease of both quadrupole and surface-radiated noise caused by viscous decay of exhaust velocity at the flap trailing edge. Data given in figure 4 of reference 22 showed 10 percent lower peak velocity at the trailing edge of the long flap. This velocity difference would be expected to cause 3 dB noise decrease below UTRC calculated levels, resulting in a 2 dB overestimate as with the nominal flap. Negligible viscous decay was predicted for the short and nominal flap lengths, and very little for the long flap. The UTRC method therefore could predict the measured effect of increased flap length on OASPL for this configuration if measured velocity at the trailing edge could be supplied as input, rather than calculated as one portion of that method.

Measured normalized 1/3 octave spectra for the three flap lengths at 105° polar angle are plotted in the lower part of figure 17. Also shown is the normalized spectrum calculated by the UTRC method, which was the same for these flaps. This calculation was within 2 dB of data for the nominal and long flap. The normalized spectrum measured with the short flap was 2 to 3 dB higher than the other data near peak amplitude and the same increment lower at high frequencies. That is, for frequencies above 435 Hz full scale (5000 Hz model scale) which strongly affect annoyance-weighted noise, actual measured spectra for the short and nominal flaps agreed within 2 dB with each other and within about 3 dB with the UTRC prediction. Large differences between 1/3 octave spectra for these two flap lengths were concentrated below about 110 Hz full scale (1250 Hz model scale), near peak amplitude of the spectra. Calculated full-scale annoyance levels therefore would underpredict data by about 3 dB for the small and nominal flaps. For the long flap, they would be about 5 dB too high.

All three flap lengths had been tested at 63° sideline angle in addition to the flyover plane. As shown in figure 15, there was no significant effect of flap length on sideline noise reduction. This result is in agreement with predictions by all methods. The measured 5 dB reduction at 90° polar angle was predicted within 1 dB by the UTRC method and underpredicted by the other methods.

QCSEE USB, Approach

Calculated and measured OASPL directivities in the flyover plane for the nominal flap length and approach flap deflection are compared in figure 18. As with the takeoff configuration, the measured directivity pattern changed shape as exhaust velocity was increased. It varied from relatively constant amplitude in the forward quadrant at small exhaust velocities to a shape which resembled jet noise rotated through the flow deflection angle at large exhaust velocities. The ANOP method correctly predicted the measured levels ahead of 60° polar angle but increasingly underestimated peak levels at 90° as exhaust velocity was increased. The UTRC method correctly predicted the change of shape but tended to overestimate by several dB the peak noise for directions below the deflected jet. For the typical critical approach case of 90° polar angle and 189 m/sec exhaust velocity, measured OASPL was about 2 dB above the ANOP prediction and an equal amount below the UTRC prediction. The GELAC prediction for the sum of trailing edge noise and low-amplitude quadrupole noise terms differed greatly from the data. Underestimates of 10 to 13 dB generally occurred near 90° polar angle.

Effects of polar angle on calculated and measured sideline directivity are shown in figure 19 for the approach configuration and 190 m/sec exhaust velocity. The measured 5 dB maximum reduction at 90° polar angle and 63° sideline angle was predicted within 1 dB by the UTRC method and underestimated 2 dB by the ANOP method. Reductions calculated by the GELAC method decrease to zero for directions near the deflected trailing edge, where calculated quadrupole noise components are much larger than the calculated trailing edge noise. Measured maximum noise reduction was only about 1 dB larger at 85° than at 63° sideline angle, contrary to the 4 dB increase calculated by the UTRC method. However, the ANOP method incorrectly predicts an increase of OASPL for that change of sideline angle. This relatively poor prediction by the UTRC method of sideline noise reduction at approach flap deflection and 85° sideline angle may be associated with the underprediction of quadrupole noise at polar angles above the deflected flap in the flyover plane (figure 18). The slot jet should be loudest at directions normal to the narrow side of the jet. For this large sideline angle and large flap deflection, the microphone at 90° polar angle is not shielded from line-of-sight view of the exhaust nozzle. Any underestimate of exhaust jet noise above the wing would cause an overestimate of sideline noise reduction.

Calculated and measured normalized 1/3 octave spectra are compared in figure 20 for noise radiated by the QCSEE USB approach configuration. Results are shown for 60° and 105° polar angles and nominal 150 and 220 m/sec exhaust velocities in the flyover plane, and 60° and 120° polar angles in the 63° sideline plane. In the flyover plane, the UTRC method predicted a small range of variation for normalized spectra. These calculated spectra were

close to that given by the ANOP method. In contrast, the GELAC method predicted a larger range of spectrum shapes that was in closer agreement with data. The same differences occurred between predictions for the 63° sideline plane. Spectra measured in this plane were more closely predicted by the UTRC method at large and small Strouhal numbers.

TF-34 Scale Model

This model, shown in figure 4b, was $1/18.5$ the size of a large-scale USB model having a 4:1 canted slot nozzle and 40° deflection short flap, tested with the mixed exhaust of a TF-34 turbofan engine. Free-field data for this geometrically similar scale model had been compared in reference 22 with data for that large-scale model, taken from reference 34. OASPL directivity at high subsonic exhaust velocities was characterized by a relatively strong peak of noise at directions just below the deflected jet. Data from previous tests of large- and small-scale USB models had not contained this feature. It was not apparent whether this localized apparent quadrupole noise was peculiar to the nozzle and flap geometry or was somehow associated with use of a real turbofan engine as an air supply. Both this scale model and the TF-34 engine installation had uniform exhaust velocities. However, the exhaust of an engine would be hotter and more turbulent than that obtained with unheated compressed air, and could have an incompletely mixed high-velocity core. This small model of the large configuration was tested by NASA to resolve this question. It was shown in reference 22 that the model data, scaled to the large configuration, did reproduce the measured directivity and spectra. Data were obtained only for the flyover plane.

Measured and calculated OASPL directivities are compared in figure 28 for five exhaust velocities. At the lowest velocity (115 m/sec) the measured directivity had no abrupt peak and was closely matched by the ANOP and UTRC methods. Increasing the exhaust velocity caused a large increase of noise radiation at 100° to 130° polar angles, as with the data of reference 34. The ANOP method did not predict this change. The UTRC method predicted the qualitative increase of OASPL but underestimated its magnitude. However, OASPL at 90° polar angle was predicted within 2 dB by that method for all exhaust velocities. The GELAC method of reference 30 again greatly underestimated the data for all but the lowest exhaust velocity and less than 90° polar angle, as if the quadrupole terms were too low.

Calculated and measured normalized spectra are compared in figure 22 for 60° , 90° , and 120° polar angles at 116 and 239 m/sec exhaust velocities. At both velocities the UTRC method predicts a narrower range of spectrum shapes than the GELAC method and lower normalized amplitudes at high frequencies

than the ANOP method. The UTRC method clearly gave the closest prediction of data above 10 kHz model frequency (500 Hz large-scale frequency). This would be the dominant region for predicting annoyance-weighted noise levels of the large-scale configuration tested with the TF-34 engine. The measured rapid decay of normalized amplitudes below 1 kHz model frequency (50 Hz large-scale frequency) was not predicted by any of the three methods. The ANOP method does predict this type of rapid decay but was 5 to 10 dB above the measured levels.

USB Vane Deflector

This configuration, shown in figure 4c and described in reference 28, has a circular nozzle at moderate height above the wing. A vane deflector, mounted on a pivot located above and downstream of the nozzle, forced the exhaust jet down against the wing upper surface for powered-lift flight. External airflow would pass between the wing upper surface and the exhaust jet. During cruise the deflector would be retracted and stowed away, reducing aerodynamic friction drag relative to conventional USB (figure 4a). Additional acoustic data, not given in reference 28, were provided by NASA for use in this evaluation of EBF noise prediction methods.

Calculated and measured OASPL directivities in the flyover plane for this configuration at takeoff flap deflection are compared in figure 23 for three exhaust velocities. The ANOP method predicts the general level but not the shape of these data. The GELAC method matches the measured levels of OASPL near 90° polar angle but gives a very poor prediction of directivity shape. The UTRC method matches the general shape but is about 7 dB too large in amplitude. This large error was caused by the calculated lift fluctuation noise component associated with the large chord. However, measured noise did not exceed that for the TF-34 scale model which had the same nozzle equivalent diameter but 0.425 times this chord. Unpublished velocity distributions measured for this vane deflector show that the exhaust jet was spread over a very large spanwise extent relative to that for USB slot nozzles. Thus the flow field achieved with a vane deflector was not typical of that for which the prediction method is based.

Calculated and measured sideline directivities for this takeoff configuration are compared in figure 24. At 60° sideline angle (figure 24a), the measured reductions relative to those for the same polar angle and the flyover plane were closely predicted by the UTRC method. Maximum measured reductions of about 5 dB at two exhaust velocities were about twice the reduction predicted by the ANOP method. This close agreement with the noise increments predicted by the UTRC method illustrates that the dominant noise radiation process below the exhaust jet at both 0° and 60° sideline angles must be surface-radiated noise.

In contrast, noise radiation measured at 85° sideline angle was stronger than that for 60° sideline angle. This result is predicted by the UTRC method only when the nozzle exit plane and exhaust-deflecting surfaces can be viewed above the wing surface. It is likely that the high-mounted vane deflector was not shielded by the limited-span wing model for any polar angle directions in the 85° sideline plane. Calculated and measured absolute values of OASPL at that sideline angle are compared in figure 24b. All three methods matched the general level of the data, with the UTRC method being about 3 dB low. It is possible that deflection of the exhaust jet by an external circular vane causes more noise than deflection by a nozzle roof inclined at the same angle, as was assumed in the calculation.

Calculated and measured OASPL directivities in the flyover plane for the approach configuration are compared in figure 25 for two velocities. The ANOP and GELAC methods generally match these measured levels. The UTRC method is about 8 dB too high near 90° polar angle and about 3 dB too high at forward positions. That is, the underestimate of surface-radiated noise associated with the highly deflected flap was not as severe as the underestimate of noise associated with the undeflected part of the wing.

Calculated and measured normalized $1/3$ octave spectra in the flyover plane for the USB vane deflector model are compared in figure 26. Data for takeoff flap and vane position, shown in figure 26a, had one broad peak at the relatively low Strouhal number of 0.1 and another broad peak at Strouhal numbers near 2. The ANOP method matched the peak at the low Strouhal number. However, it and the other two methods predicted a second peak at Strouhal numbers from 0.2 to 0.5 where the data had a local minimum. Both the ANOP and UTRC methods generally matched the data for Strouhal numbers larger than 1. The GELAC method predicted a wide envelope of normalized spectra for this range of polar angles. For 120° polar angle the OASPL calculated by the GELAC method was dominated by noise attributed to direct radiation from the wake downstream of the trailing edge. This noise component decays slowly with increasing Strouhal number at this measurement direction. Thus the upper dotted line at large Strouhal numbers, which lies furthest above the average data, corresponds to the open triangle data symbols which lie below the average data.

Measured normalized spectra for the approach configuration, shown in figure 26b, had sharper peaks than those measured for takeoff. The high-frequency peak, centered at a Strouhal number of 2, extended over about an octave of frequency. It protruded more than 6 dB above the remainder of the spectrum at the lower exhaust velocity. All of the noise prediction methods gave smooth curves which did not reproduce this spectrum peak. The UTRC and ANOP methods predicted the general level of data. The GELAC method again

predicted a much larger range of normalized spectrum shape than was measured. These 80° and 100° polar angles are relatively close to the deflected exhaust jet downstream direction. For Strouhal numbers from 1 to 10, noise calculated by the GELAC method for 80° polar angle was predicted to be dominated by quadrupole noise from the wake downstream of the trailing edge. At this moderate angle from the deflected jet downstream direction, the resulting calculated spectrum had a large decay rate. For 100° polar angle the calculated quadrupole noise radiated from the flap upper surface wall jet, and refracted around the trailing edge, was calculated to dominate at large Strouhal numbers. This normalized spectrum has a small decay rate and produced the upper dash curve. For Strouhal numbers near 4, this upper curve is about 8 dB higher than the 100° polar angle (triangle) data symbols. This strong sensitivity of high-frequency spectrum shape to polar angle, at directions within about 60° from the deflected jet downstream direction, is a property of predictions by the GELAC USB method of reference 30. The predicted strong variation is independent of errors in absolute level of quadrupole noise, and is contrary to the data.

Normalized spectra for the takeoff configuration at 90° polar angle and both 60° and 85° sideline angle are shown in figure 27. At 60° sideline angle, shown in figure 27a, the data for high Strouhal numbers were bracketed by the ANOP and UTRC methods. Each method was about 3 dB from the data. For 85° sideline angle, shown in figure 27b, the ANOP and GELAC methods generally were within 3 dB of the data. The UTRC method gave worst agreement with data for this configuration and sideline angle.

Discussion of Error

When EBF noise data are applied to prediction of full-scale flyover noise, calculated levels of perceived noise level (PNL) are dominated by the noise radiated at 90° polar angle. A rough estimate of error incurred by use of each prediction method was obtained from the difference between predicted and measured OASPL for this overhead position. These comparisons were examined only at the second highest exhaust velocity for which directivity data are presented. Error in predicting annoyance-weighted noise was obtained by comparing PNL for scaled predicted and measured spectra at this direction and velocity. Model linear dimensions and far-field distance were each multiplied by 10 in order to weigh the high-frequency portions of the measured spectra in a manner similar to that for PNL at full scale. Atmospheric attenuation over the increased path length was included in these PNL predictions. The resulting prediction errors for each configuration, mean error, and range about that mean for 50% confidence (0.67 times the

standard deviation) are shown in TABLE III for the UTRC, ANOP, and GELAC prediction methods. These calculations of PNL, and the statistical analysis, were conducted by NASA Lewis Research Center using spectra predicted as part of this contract effort.

TABLE III - OASPL AND PNL PREDICTION ERROR FOR 90° FLYOVER POSITION

Notes: Errors = Prediction-Data, PNL calculated for 10 times model scale, Comparisons for the test exhaust velocity closest to 225 m/sec.

Configuration	OASPL Error, dB			PNL Error, PNdB		
	UTRC	ANOP	GELAC	UTRC	ANOP	GELAC
3-Flap UTW, T/O	-3.5	-2.7	-6.7	-6.6	-4.1	-8.4
APP	-1.5	-2.5	+0.6	-0.7	-1.8	+0.5
Slotless 3-Flap	+1.5	NA	+3.0	+2.0	NA	+2.7
QCSEE USB, T/O	+1.5	-3.2	-4.9	+1.1	-5.2	-5.7
APP	+1.9	-2.5	-10.4	+4.6	-1.2	-9.4
TF-34 USB	-1.6	-4.2	-5.8	-3.2	-6.9	-6.7
Vane USB, T/O	+9.0	+0.1	-2.3	+8.0	+2.0	+0.2
APP	+7.1	-0.8	-0.1	+11.2	+2.3	-3.2
Mean Error	+1.8	-2.3	-3.3	+2.0	-2.1	-3.7
50% Confidence	±2.9	±1.0	±3.0	±3.9	±2.3	±3.0

Both the ANOP and UTRC methods have mean errors of about 2 dB in both OASPL and PNL. Mean error of the GELAC method was about 50% larger. The range of scatter about these mean errors (assuming a Gaussian distribution) was about half as large for the ANOP method as for the other two methods. The UTRC method best predicted the shapes of the polar and azimuthal directivity, but it failed to predict OASPL and PNL at the flyover position significantly better than the earlier empirical ANOP method. There are three key reasons for this latter result: (1) calculated noise levels are sensitive to local mean velocity and turbulence level, which are crudely represented in the UTRC method, (2) by summing several components whose levels are maximum at directions determined by the flap geometry, it is easy to miss the level at any one direction, and (3) the ANOP method was based on data correlations for the specific 90° direction angle at which this comparison was made. The resulting ANOP predictions, at this 90° direction angle and exhaust pressure ratios near 1.4, apparently are at least as accurate as those from the UTRC and GELAC methods which are based on summations of separately calculated noise components. If the vane USB configuration had not been included in this comparison, the UTRC method would have achieved mean errors smaller in magnitude than 0.5 dB, with 50% confidence levels of ± 1.5 dB OASPL and ± 2.7 PNdB. These predictions clearly were better than those of the other methods.

One possible alternate method for UTW and USB noise prediction would regard measured noise amplitudes and spectra as a sum of two independent components: surface-radiated noise and quadrupole noise. Quadrupole noise as inferred from the data would be subtracted from those data to find an amplitude at 90° direction, directivity shape, and spectrum shape associated with surface-radiated noise. These quantities would vary with configuration type (UTW or USB) and flap deflection angle but would be independent of the detailed configuration geometry, as with the current ANOP method. Use of these two components, each optimized to give best results at the 90° flyover direction, should give better prediction of amplitudes, spectra, and general directivity shapes for this and other directions. This possible new method would require less computation effort than the noise component methods. It could be used with UTW mixer nozzle configurations and slotless wing configurations. Use of this empirical approach would give up all pretense of describing EBF noise as a sum of simple basic noise processes for which the prediction accuracy is limited only by the accuracy of estimated mean and fluctuating local flow properties.

Comparisons for Additional EBF Configurations

Additional Slotless Wings

The method presented herein for calculating noise radiated by slotless wings had been strongly influenced by data for the UTW slotless version of a triple-slotted wing (reference 19). That paper had included comparisons with the calculated sum of a deflected-jet quadrupole noise component and a trailing edge noise component with amplitude matched with data for the upper forward quadrant. That sum greatly underpredicted the noise measured below the wing at low exhaust velocities. The NASA Lewis method of references 24 and 25 used essentially these same two components. Attention was confined to the limited range of polar angles below the wing and flap. The deflected-jet noise data of reference 3, used in reference 25 for representing quadrupole noise, is similarly limited because half the range of polar angles was shielded behind the large flat surface. Also, data are given therein only for 15° , 30° , 60° , and 90° deflection without a simple method for interpolating to intermediate angles. The UTRC method uses an empirical modification to the accepted prediction (reference 16) of noise radiated by an isolated jet. Therefore it can be readily applied for all deflection angles and exhaust velocities, and includes noise radiated above the deflected exhaust jet downstream of the slotless flap trailing edge.

Calculated and measured OASPL directivities in the flyover plane are plotted in figure 28 for the large double-slotted wing of reference 25 with the slots closed by plug fairings. The calculated curves designated NASA were taken from reference 25; they closely match the data. The UTRC calculated

curves did not match the fine detail of measured directivity near the deflected jet but generally were within 2 dB of the data. Therefore the UTRC method for slotless wings gives acceptable prediction of these directivity data.

Calculated and measured directivities in the flyover plane are compared in figure 29 for the UTW slotless wing of reference 26. This configuration matched the length and contour of a double-slotted wing at approach deflection; it was shorter than the slotless version of the triple-slotted wing. Data were presented for two subsonic and (not shown) one supersonic exhaust velocity. These data have not been corrected to free field, so all of the predicted levels have been increased 2 dB to account approximately for ground reflection.

For the higher exhaust velocity, the NASA Lewis method closely matched the measured trends and levels at directions below the wing, where this method applies. Note that if that method had been assumed to apply at all directions, a broad peak of trailing-edge noise centered at 300° polar angle would be predicted to occur. Maximum amplitude of that peak would exceed the levels calculated by this NASA Lewis method for 20° polar angle. This result is inherent in the analytical description and is contrary to the measured directivity shapes. The UTRC method predicted the general level but not the precise shape of data below the wing. It matched the shape measured above the wing, although levels were underpredicted 3 to 4 dB at most directions. For the lower exhaust velocity the UTRC method closely matched the measured shape and level below the wing and the NASA method was low. The GELAC method was about 5 dB high for both velocities.

Measurements of OASPL directivity and sound power spectra had been presented in reference 35 for a UTW slotless wing at several flap lengths. The test model had a straight section corresponding to an undeflected wing, followed by a circular arc with 45° turning angle. This curved portion extended below the nozzle centerline. Straight flap sections with lengths of 0.75, 3.75, and 12.75 diameters were added to the model. Measured directivity in the flyover plane at a jet exhaust Mach number of 0.84 (exhaust velocity 270 m/sec) was given in figure 13 of reference 35 for these three flap lengths. These data are plotted in figure 30, with the flaps denoted as short, medium, and long.

Calculations by the NASA method of reference 24 required scaling or interpolation of the jet impingement noise data of reference 3 to this deflection angle. Those data have a more sharply peaked directivity shape for 30° than for 60° deflection. The slotless wing data of figure 30 for 45° deflection also have a sharply peaked directivity. Calculations by the NASA

method used an interpolation between the noise data of reference 3 for 30° and 60° deflection to obtain a prediction for the required 45° deflection. Neither the slotless wing data of reference 35 nor the jet impingement noise data of reference 3 were corrected to free field. Values for jet exhaust width, boundary layer thickness, and maximum velocity at the trailing edge were taken from data of reference 24 scaled for variations with flap length. Increased flap length causes increased exhaust cross section area, increased boundary layer thickness, and decreased maximum velocity, producing different calculated noise for the short and medium flaps. The UTRC method predicted a small decrease of noise as flap length was increased from short to medium. Noise levels calculated by the UTRC method were increased 2 dB to account for the measurements being conducted above a reflecting surface. Calculated directivity curves are not plotted for the GELAC method of reference 29. The normalized directivity curves given in figure 5-19 of that report change shape drastically between 20° and 60° flap deflection. If the maximum relative amplitude shown in that figure for 60° was assumed to apply for 45° deflection, the resulting broad peaks of the calculated curves would match the levels of data plotted in figure 30 for the medium flap length at 80° and 200° polar angles. It would not give the sharp peaks of noise measured near the deflected exhaust jet. Because all flap lengths have the same impingement-point location, they would all have the same calculated noise levels.

As shown in the upper part of figure 30, the NASA method matched the measured OASPL shape below the wing for the short and medium flap. It was about 3 dB below data for the short flap and 1 dB above data for the medium flap. The UTRC method did not reproduce the measured sharp peak at 110° and 120° polar angle, 15° to 25° below the deflected jet, and was 4 to 8 dB below data. The UTRC method underestimated angular extent of the noise peak measured above the deflected jet but correctly predicted the measured levels near 270° polar angle. Levels measured with the short flap generally were about 5 dB louder than with the medium flap. Neither method predicted this difference.

Calculated and measured directivities for the long flap are shown in the lower part of figure 30. The NASA method predicted the measured sharply peaked shape and measured levels. The UTRC method poorly predicted the measured directivity shape for polar angles below the wing. A calculated curve is not shown for the GELAC method because its geometry is beyond the range of variables used in that method.

UTW Mixer Nozzle

Noise radiation data for the nominal half-scale UTW mixer nozzle configuration of reference 37 were compared with those calculated by the method given herein. Although the only UTW EBF airplane now flying (McDonnell-Douglas YC-15) uses mixer nozzles, no other method has been published for predicting the noise of such installations. This method calculates UTW surface-radiated noise for an exhaust velocity equal to the average of the two highest peak velocities in the isolated mixer nozzle's measured velocity profile. Measured noise for the isolated mixer nozzle is increased corresponding to the calculated effect of flow deflection by the flaps at the local flow velocity (reference 18). For this configuration, maximum local velocity at the impingement point was 0.64 times the jet exhaust velocity. The resulting increases were 0.1 dB for takeoff and 0.6 dB for approach deflection. This measured, slightly increased noise associated with the mixer nozzle flow field was rotated through the flow deflection angle. For polar angles above the wing and deflected flaps, it was added directly to the calculated surface-radiated noise. For polar angles below the wing and deflected flap, it was increased 3 dB and added to the calculated surface-radiated noise.

These tests were not conducted in a free-field environment and are affected by ground reflections. Acoustic calibration of the test area have shown that wave cancellation tended to occur in the range from 400 to 630 Hz center frequency. This frequency region, and frequencies from 800 to 2000 Hz where ground reflection caused about 1.5 dB increase, generally dominated the measured OASPL. Tabulated values of OASPL, plotted herein, are believed to be about 1.5 dB too large.

Measured OASPL directivities in the flyover plane, and those calculated by the method given herein, are compared in figure 31 for both takeoff and approach flap deflections. Results are shown for nominal exhaust pressure ratios of 1.2, 1.4, and 1.7 at both deflections. Calculated levels and directivity shapes closely match the data. At directions near 30° above and below the deflected jet, the calculated levels are dominated by measured noise from the mixer nozzle as modified in the manner described above. Because data for the UTW configuration and the isolated mixer nozzle contain the same ground reflection effect, the relative difference between calculated curves and measured data symbols is unaffected by ground reflection at these angles. Further away from the deflected jet, calculated levels are primarily surface-radiated noise. Maximum OASPL was approximately independent of flap deflection because it was dominated by noise associated with the mixer nozzle rather than the flaps. Increasing the pressure ratio caused the measured, nearly flat directivity shape below the wing to develop a peak near the deflected jet. This change was correctly predicted.

For direction angles of practical interest, the portion of the frequency spectrum which would dominate annoyance-weighted noise would be predicted to be associated with the mixer nozzle. Surface-radiated noise would be significant only at lower frequencies. Measured spectra therefore are not compared with predictions. Such comparisons were given in reference 18. The best evaluation of this noise prediction method for UTW mixer nozzles would be comparisons with flyover noise data for the USAF YC-15 Advanced Medium STOL Transport. This comparison would have to include measured, rather than calculated, forward flight effects on noise from the mixer nozzles.

Engine in Front of Wing

Calculated and measured OASPL directivities for this configuration at two exhaust velocities for takeoff and approach flap deflection are shown in figure 32. Data for this small model (reference 37) were not measured under free-field conditions and are plotted 3 dB below the tabulated levels for this comparison. Measured levels were unaffected by axial position of the wing leading edge relative to the nozzle exit plane, and this parameter does not affect the noise prediction. As compared with UTW and USB configurations, the measured directivities are relatively unaffected by flap deflection. Calculated noise levels beneath the wing were underestimated 2 to 4 dB at the higher velocity but were closely predicted at all directions at the lower velocity.

Calculated and measured spectra at the directions for maximum OASPL are compared in figure 33. These spectra are characterized by a 12 dB per octave decay at high frequencies. This decay is more rapid than that associated with either UTW or USB. Measured spectra generally were closely predicted but were underestimated at low frequencies which dominated the contributions to OASPL.

Noise Predictions for Full-Scale QCSEE Configurations

Zero Forward Speed

Noise radiation caused by the presence of the wing and trailing edge flaps was calculated for the full-scale QCSEE engine, wing, and flap installations. Both the UTW and USB configurations were represented at the engine exhaust velocities specified as the design takeoff and landing conditions. NASA tests of these configurations at zero forward speed are scheduled to be run within the next two years. Calculations discussed in this subsection were conducted for a 100 m (305 ft) far-field distance and zero forward speed. Configuration geometries supplied by NASA are shown in figure 34.

The UTW configuration had a double-slotted flap with relatively large forward flap chord. The aft flap panel extends relatively far into the exhaust jet at takeoff flap deflection. Therefore it is likely that the predictions given herein will underestimate the flap-radiated noise for this condition, as occurred with the UTW triple-slotted flap model previously discussed. Model tests of this QCSEE configuration are recommended, to determine whether the increased noise does occur. The high bypass ratio engine had coaxial fan and core exhaust jets. Equivalent exhaust velocity V_E was defined in terms of the fan exhaust velocity V_F and exhaust area A_F , and core exhaust velocity V_C and exhaust area A_C , in the same manner as with the NASA ANOP method of reference 27. That is, $(A_F + A_C)V_E^6 = A_F V_F^6 + A_C V_C^6$. Other velocity weighting functions for defining an equivalent exhaust velocity, such as a mass flow weighted velocity (references 22 and 34), could also have been used. Determination of the correct weighting function for two-stream UTW installations also requires additional model-scale tests. The sum of fan and core exhaust area was 1.96 m^2 (21.1 ft^2) corresponding to 1.581 m (5.188 ft) diameter. Velocities specified by NASA for UTW takeoff and approach are:

	Fan Velocity, m/sec (ft/sec)	Core Velocity, m/sec (ft/sec)	Equivalent Velocity, m/sec (ft/sec)
Takeoff	204 (670)	245 (803)	215 (704)
Approach	146 (480)	194 (636)	161 (528)

The USB configuration had an internal mixer nozzle. Fully mixed exhaust velocities were specified as 220 m/sec (722 ft/sec) for takeoff and 190 m/sec (623 ft/sec) for approach. Nozzle equivalent diameter was 1.491 m (4.893 ft). Atmospheric properties were taken as those for standard sea level.

Because actual exhaust velocities for these planned full scale tests may differ from those specified here, and other definitions of equivalent velocity may be examined, it is necessary to predict the effect of small changes in exhaust velocity. This was done by regarding OASPL at each polar angle, sideline angle, and flap deflection as varying with equivalent exhaust velocity raised to some exponent n . OASPL was calculated to two decimal places for the nominal and 1.0233 times nominal velocity. Ten times the difference between the two values of OASPL was then equal to the velocity exponent.

The calculated OASPL directivities in the flyover plane and at 63° and 85° sideline angles are plotted in figure 35 for UTW takeoff. Also shown are the calculated variations of velocity exponent with polar angle for these three sideline angles. The velocity exponent at 90° polar angle is largest

for 85° sideline angle because calculated noise at this direction is dominated by quadrupole noise. Calculated OASPL directivities at these sideline angles for UTW approach, and the associated velocity exponents, are plotted in figure 36. For both takeoff and approach, the calculated OASPL in the flyover plane increases by 1 to 3 dB as polar angle is increased from upstream toward the deflected jet. Predicted velocity exponents have maximum values of about 9 near the edge of the jet exhaust refraction region. These values are somewhat larger than tend to be actually measured. Calculated 1/3 octave spectra at 90° polar angle and the three sideline angles are plotted in figure 37 for both takeoff and approach. Maximum 1/3 octave SPL is predicted to occur below 50 Hz center frequency, the lowest frequency used in many methods for prediction of annoyance-weighted noise, for five of these six spectra. If OASPL is measured as the sum of 1/3 octave SPL's for center frequencies from 50 to 10,000 Hz, this quantity would be about 3 dB less than the actual OASPL plotted in figures 35 and 36.

Calculated OASPL directivities and velocity exponents for the QCSEE USB configuration at take off and approach conditions are plotted in figures 38 and 39. OASPL in the flyover plane is predicted to have very little variation with polar angle at directions beneath the deflected exhaust jet. Again, the calculated velocity exponents near the edge of the exhaust jet refraction region seem unrealistically high. Calculated levels of OASPL at 90° polar angle in the flyover plane are between 102 and 103 dB for both UTW and USB at takeoff. They are about 97 and 98 dB for the two configurations at approach. The specified geometries and exhaust velocities therefore are well balanced to provide calculated conditions of about equal noise for both UTW and USB. Calculated 1/3 octave spectra at 90° polar angle for USB takeoff and approach are plotted in figure 40. As with the UTW spectra, only about half the OASPL was predicted to be radiated above 50 Hz center frequency.

Effects of Forward Flight

Calculations were conducted of the effects of forward flight on spectra at a position 100 m (328 ft) directly beneath the QCSEE configurations. The flight speed was taken as 41 m/sec (80 knots), the QCSEE nominal design condition for both takeoff and approach. As was previously mentioned, this calculation method predicts spectra that would be measured in a coordinate system which is fixed relative to the airframe. Such predictions are appropriate for comparison with data for models tested in open jets or acoustic wind tunnels. They include the effects of a reduction in noise source strength caused by changes in turbulence level of the exhaust jet. They do not include the changes in directivity pattern caused by motion of the noise sources relative to the atmosphere. This change would divide the mean square acoustic pressure by the quantity $1 - M_F \cos \theta$ raised to some positive exponent, where M_F is the flight Mach number. However, EBF noise

annoyance is predicted to be largest for polar angles θ near 90° , and EBF flight Mach numbers for takeoff and landing are near 0.2. Thus the omitted correction is unimportant for conditions of practical importance. Predictions for a coordinate system fixed relative to the aircraft can be converted to those for ground-fixed microphones by dividing mean square acoustic pressure by $1 - M \cos \theta$ and Doppler-shifting the frequency. This correction also is small for cases of practical interest. Calculated spectra are shown for the flyover position, at which the omitted factors do not change the predicted noise.

The calculated effect of 41 m/sec flight velocity on flyover spectra for the QCSEE UTW takeoff and approach configurations is shown in figure 41. Each predicted spectrum is decreased by nearly a constant increment at all frequencies. The decrease is slightly larger for approach, with its larger ratio of flight velocity to exhaust velocity, than for takeoff. In contrast, the same comparison for the QCSEE USB configuration (figure 42) shows only about 1 dB predicted noise reduction at frequencies of interest for noise annoyance. This small effect occurs because forward flight is predicted not only to reduce the spectrum amplitudes but to shift each amplitude to a higher frequency. It was shown in references 18 and 20 that these qualitative trends have been reported for tests of EBF configurations in acoustic wind tunnels.

CONCLUSIONS

1. The UTRC method best predicted the variations of EBF noise amplitude with polar and azimuthal angle. The UTRC, ANOP, and GELAC methods adequately predicted normalized spectrum shapes.
2. All three methods poorly predicted OASPL at the flyover position for some configurations. The UTRC method failed badly for a USB circular nozzle with vane deflector at both takeoff and approach flap deflections, but generally was closest to data for the more conventional UTW and USB installations. This discrepancy probably was caused by differences between the actual and calculated or assumed local flow-field properties. The consequence of this poor agreement for two of the eight example cases was that the ANOP method gave more accurate predictions of average PNL at 90° direction than did the UTRC or GELAC methods.

RECOMMENDATIONS FOR FUTURE RESEARCH

Flow-field turbulence properties such as turbulence streamwise and transverse integral scale length and turbulence convective velocity, along with mean and rms fluctuating velocity, should be measured for simple slotted UTW and unslotted USB configurations. These data should be utilized along with available theories for calculating the spectrum of lift force fluctuation and noise radiation. For USB, it may be necessary to develop a numerical simulation for the pressure field induced by a random distribution of discrete vortices representing the wall-jet boundary layer and upper shear layer.

Noise measurements should be obtained for USB configurations having conventional nozzles and at least a factor of 2 variation in the ratio of upper surface flow length to nozzle diameter. These data would be utilized to determine whether discrepancies between measured noise radiation for USB models and levels predicted by the method given herein were caused by incorrect prediction of the effect of this parameter. If so, the prediction method should be modified.

Noise measurements should be obtained with a scale model of the QCSEE UTW configuration at takeoff flap deflection. Current EBF noise prediction techniques poorly predict data for this type of flap position relative to the exhaust nozzle.

Flyover noise data should be obtained and compared with predictions by this and other methods. Ideally, these tests should be obtained with a powered sailplane or some other type of aircraft having highly suppressed engine noise. Tests could be conducted with the two USAF Advanced Medium STOL Transport configurations (a USB and a mixer nozzle UTW) if it is predicted that flight conditions exist for which EBF noise exceeds noise radiated directly from the propulsive systems.

REFERENCES

1. Fink, M. R.: Mechanisms of Externally Blown Flap Noise. *Progress in Aeronautics and Astronautics*, Vol. 38, Aeroacoustics, ed. by H. T. Nagamatsu, M.I.T. Press, Cambridge, Ma., 1975, pp 113-128. Also, Paper 73-1029, AIAA, Oct. 1973.

REFERENCES (Continued)

2. Sharland, I. J.: Sources of Noise in Axial Flow Fans. J. Sound and Vib., Vol. 1, No. 3, July 1964, pp 302-322.
3. Olsen, W. A., Miles, J. H., and Dorsch, R. G.: Noise Generated by Impingement of a Jet Upon a Large Flat Board. NASA TN D-7075, Dec. 1972.
4. Fink, M. R.: Investigation of Scrubbing and Impingement Noise. NASA CR-134762, Feb. 1975.
5. Fink, M. R.: Experimental Evaluation of Theories for Trailing Edge and Incidence Fluctuation Noise. AIAA J., Vol. 13, No. 11, Nov. 1975, pp 1472-1477. Also, Paper 75-206, AIAA, Jan. 1975.
6. Fink, M. R.: Scrubbing Noise of Externally Blown Flaps. Progress in Aeronautics and Astronautics, Vol. 45, Aeroacoustics: STOL Noise; Airframe and Airfoil Noise, ed. by I. R. Schwartz, M.I.T. Press, Cambridge, Ma., 1976, pp 3-25. Also, Paper 75-469, AIAA, Mar. 1975.
7. Fink, M. R.: A Method for Calculating Strut and Splitter Plate Noise in Exit Ducts - Theory and Verification. NASA CR-2955, 1978.
8. Hayden, R. E.: Sound Generation by Turbulent Wall Jet Flow Over a Trailing Edge. MS Thesis, Purdue Univ., 1969.
9. Ffowcs Williams, J. and Hall, L. H.: Aerodynamic Sound Generation by Turbulent Flow in the Vicinity of a Scattering Half Plane. J. Fluid Mech., Vol. 40, Part 4, Mar. 1970, pp 657-670.
10. Chase, D. M.: Sound Radiated by Turbulent Flow Off a Rigid Half Plane as Obtained From a Wavevector Spectrum of Hydrodynamic Pressure. J. Acoust. Soc. Am., Vol. 52, No. 3, Part 2, Sept. 1972, pp 1011-1023.
11. Hayden, R. E.: Noise from Interaction of Flow with Rigid Surfaces: A Review of Current Status of Prediction Techniques. NASA CR 2126, Oct. 1972.
12. Hayden, R. E., Fox, H. L., and Chanaud, R. C.: Some Factors Influencing Radiation of Sound From Flow Interaction with Edges of Finite Surfaces. NASA CR-145073, 1976.

REFERENCES (Continued)

13. Siddon, T. E.: Surface Dipole Strength by Cross-Correlation Method. J. Acoust. Soc. Am., Vol. 53, No. 2, Feb. 1973, pp 619-633.
14. Neuwerth, G.: Acoustic Feedback of a Subsonic and Supersonic Free Jet Impinging on a Foreign Body. NASA TT F-15719, 1974.
15. Dorsch, R. G., Goodykoontz, J. H., and Sargent, N. B.: Effect of Configuration Variation on Externally Blown Flap Noise. Paper 74-190, AIAA, Jan. 1974.
16. Stone, J. R.: Interim Prediction Method for Jet Noise. NASA TM X-71618, Dec. 1974.
17. Fink, M. R.: Prediction of Externally Blown Flap Noise and Turbo-machinery Noise. NASA CR-134883, Aug. 1975.
18. Fink, M. R.: Additional Studies of Externally Blown Flap Noise. NASA CR-135096, Aug. 1976.
19. Fink, M. R. and Olsen, W. A.: Comparison of Predictions and Under-the-Wing EBF Noise Data. Paper 76-501, AIAA, July 1976.
20. Fink, M. R.: Forward Flight Effects on EBF Noise. Paper 77-134, AIAA, Oct. 1977.
21. Tam, C. K. W. and Reddy, N. N.: Sound Generated in the Vicinity of Trailing Edge of Upper Surface Blown Flaps. Paper 76-503, AIAA, July 1976.
22. Olsen, W. A., Burns, R., and Groesbeck, D.: Flap Noise and Aerodynamic Results for Model QCSEE Over-the-Wing Configurations. Paper 77-23, AIAA, NASA TM X-73588, Jan. 1977.
23. Olsen, W. A.: Noise Generated by Impingement of Turbulent Flow on Airfoils of Varied Chord, Cylinders, and Other Flow Obstructions. NASA TM X-73464, July 1976.

REFERENCES (Continued)

24. McKinzie, D. J., Jr., and Burns, R. J.: Analysis of Noise Produced by Jet Impingement Near the Trailing Edge of a Flat and Curved Plate. NASA TM X-3171, Jan. 1975.
25. McKinzie, D. J., Jr., Burns, R. J., and Wagner, J. M.: Noise Reduction Tests of Large-Scale-Model Externally Blown Flap Using Trailing-Edge Blowing and Partial Flap Slot Covering. NASA TM X-3379, Apr. 1976.
26. Olsen, W. A., Dorsch, R. G., and Miles, J. H.: Noise Produced by a Small-Scale, Externally Blown Flap. NASA TN D-6636, Mar. 1972.
27. Dorsch, R. G., Clark, B. J., and Reshotko, M.: Interim Prediction Method for Externally Blown Flap Noise. NASA TM X-71768, Aug. 1975.
28. Von Glahn, U. H. and Groesbeck, D. E.: Effect of External Jet-Flow Deflector Geometry on OTW Aero-Acoustic Characteristics. Paper 76-499, AIAA, July 1976.
29. Guinn, W. A., Blakney, D. F., and Gibson, J. S.: V/STOL Noise Prediction and Reduction. FAA-RD-73-145, Aug. 1973.
30. Reddy, N. N., Blakney, D. F., Tibbetts, J. G., and Gibson, J. S.: V/STOL Aircraft Noise Prediction. Lockheed-Georgia Co. LG75ER0054, June 1975. Also, FAA Report No. FA-RD-75-125.
31. Filler, L.: Prediction of Far-Field Jet/Trailing Edge Interaction Noise for Engine-Over-the-Wing Installation. Paper 76-518, AIAA, July 1976.
32. Clark, L. R. and Yu, J. C.: Effects of Geometry and Jet Velocity on Noise Associated with an Upper-Surface-Blowing Model. NASA TN D-8386, Mar. 1977.
33. Evertz, E., Kloppel, V., Neuwerth, G., and Quick, A.: Noise Generated by Interaction Between Subsonic Jets and Blown Flaps. Deutsche Luft-und Raumfahrt DLR-FB 76-20, Jan. 1976.
34. Heidelberg, L. J., Homyak, L., and Jones, W. L.: Full-Scale Upper-Surface-Blown Flap Noise. SAE Paper 750609, May 1975.
35. Reddy, N. N. and Yu, J. C.: Radiated Noise from an Externally Blown Flap. NASA TN D-7908, July 1975.

REFERENCES (Concluded)

36. Goodykoontz, J. H., Dorsch, R. G., and Groesbeck, D. E.: Noise Tests of Mixer Nozzle-Externally Blown Flap System. NASA TN D-7236, May 1973.
37. Karchmer, A. M. and Friedman, R.: Noise Tests on an Externally Blown Flap with the Engine in Front of the Wing. NASA TM X-2842, Dec. 1973.
38. Hayden, R. E.: Exploratory Investigation of Aerodynamic Optimization of the Variable Impedance Edge Concept Applied to Upper Surface Blown Configurations. NASA CR-145072, BBN Report 3245, Nov. 1976.
39. Brown, W. H. and Reddy, N. N.: USB Flow Characteristics Related to Noise Generation. Powered-Lift Aerodynamics and Acoustics, NASA SP-406, May 1976, pp 213-226.
40. Lee, H. K. and Ribner, H. S.: Direct Correlation of Noise and Flow of a Jet. J. Acoust. Soc. Am., Vol. 52, No. 5, Pt. 1, Nov. 1972, pp 1280-1290.
41. Becker, R. S. and Maus, J. R.: Acoustic Source Location in a Jet-Blown Flap Using a Cross-Correlation Technique. Final Report for NASA Grant NGR 43-001-135, Univ. of Tenn. Space Inst., Feb. 1977. Also Paper 77-1364, AIAA, Oct. 1977.
42. Yu, J. C. and Tam, C. K. W.: An Experimental Investigation of Trailing Edge Noise Mechanism. Paper 77-1291, AIAA, Oct. 1977.

APPENDIX A: LIST OF SYMBOLS

a	Speed of sound, m/sec
c	Total wing and flap chord, m
c_n	Chord of nth flap panel, m
D	Nozzle exit diameter or hydraulic diameter, m
f	One-third octave center frequency, Hz
h	Average distance from flap panel to assumed vortex trajectory, m
K_n	Amplitude function for fluctuating lift noise of nth flap panel
M_c	Convective Mach number for jet, $0.62 M_j$
M_j	Jet exhaust Mach number relative to ambient speed of sound
M_{jj}	Jet exhaust Mach number relative to jet speed of sound
P_{ref}	Reference acoustic pressure, $2 \times 10^{-5} \text{ N/m}^2$
r	Far-field distance, m
St	Strouhal number, fD/V
U_i	Maximum exhaust velocity at impingement distance, m/sec
V	Nozzle exhaust velocity, m/sec
X	Axial distance from nozzle exit to impingement point, m
δ_F	Deflection angle of last flap segment, deg
θ	Polar angle relative to nozzle upstream direction, deg
θ_n	Polar angle relative to upstream direction along chord of nth flap segment, deg
ρ	Density, kg/m^3
ϕ	Azimuth angle relative to flyover plane, deg
Subscripts	
a	Ambient atmosphere
ISA	International standard atmosphere
J	Jet exhaust
L	Lift fluctuation noise
n	Nth flap segment

Q Directly radiated quadrupole noise

T Trailing edge noise

APPENDIX B: LIST OF PUBLICATIONS PRODUCED

The following three annual reports and two final reports were prepared under this Contract and published as NASA Contractor Reports.

Fink, M. R.: Investigation of Scrubbing and Impingement Noise. NASA CR-134762, Feb. 1975.

Fink, M. R.: Prediction of Externally Blown Flap Noise and Turbomachinery Strut Noise. NASA CR-134883, Aug. 1975.

Fink, M. R.: Additional Studies of Externally Blown Flap Noise. NASA CR-135096, Aug. 1976.

Fink, M. R.: A Method for Calculating Strut and Splitter Plate Noise in Exit Ducts - Theory and Verification. NASA CR-2955, 1978.

Fink, M. R.: A Method for Calculating Externally Blown Flap Noise. NASA CR-2954, 1978.

The following AIAA papers, and subsequent publications of some of these papers, provided wider distribution of major results obtained under this Contract.

Fink, M. R.: Experimental Evaluation of Theories for Trailing Edge and Incidence Fluctuation Noise. AIAA J., Vol. 13, No. 11, Nov. 1975, pp 1472-1477. Also, Paper 75-206, AIAA, Jan. 1975.

Fink, M. R.: Scrubbing Noise of Externally Blown Flaps. Progress in Astronautics and Aeronautics, Vol. 45, Aeroacoustics: STOL Noise, Airframe and Airfoil Noise, M.I.T. Press, Cambridge, Ma., pp 3-25, 1976. Also, Paper 75-469, AIAA, Mar. 1975.

Fink, M. R. and Olsen, W. A.: Comparison of Predictions and Under-the-Wing EBF Noise Data. Paper 76-501, AIAA, July 1976.

Fink, M. R.: Forward Flight Effects on EBF Noise. Paper 77-1314, AIAA, Oct. 1977.

The following AIAA Paper, prepared by NASA Lewis Research Center, compared NASA data with predictions calculated under this Contract.

Olsen, W. A., Burns, R., and Groesbeck, D.: Flap Noise and Aerodynamic Results for Model QCSEE Over-the-Wing Configurations. Paper 77-23, AIAA, Jan. 1977.

The following AIAA paper and publication, while not conducted under this Contract, described a direct extension of contract results to an additional practical application.

Fink, M. R.: Approximate Prediction of Airframe Noise. J. Aircraft, Vol. 13, No. 11, Nov. 1976, pp 833-834. Paper 76-526, AIAA, July 1976.

APPENDIX C: COMPUTER PROGRAM FOR CALCULATING EBF NOISE

General Description

This digital computer program, written in FORTRAN IV, predicts externally blown flap noise that would be measured in the free field at points on a sphere centered at the nozzle exit. These points are equally spaced in polar angle, in planes of designated sideline angle. The reference angle direction (zero polar angle for all azimuth angles) is forward along the nozzle centerline. If atmospheric properties are not specified as input but allowed to remain at their sea-level standard default values, all linear dimensions should have the dimensions of meters and velocities should be input as meters per second. Comment statements are placed throughout the program listing to describe the purpose of each portion of the program and to define the program variables. The program is relatively small, requiring less than 12K of computer memory.

Input quantities include geometric properties of the EBF configuration as sketched in figure 43. For under-the-wing (UTW, CONFIG=1) and engine-in-front-of-the-wing (IFW, CONFIG=3) installations, these properties include the coordinates of the wing and flap leading edges in a coordinate system centered at the nozzle exit. Here, positive X is downstream and positive Y is upward, normal to the wing plane. Other geometric properties are the wing incidence relative to the nozzle centerline, deflection of each flap segment relative to the wing, number of flap segments, chord of the last flap segment, nozzle exit diameter, and far-field radius. Geometric lengths required for upper surface blowing (USB, CONFIG=2) installations are the coordinates of the wing leading edge and flap trailing edge, nozzle exit hydraulic diameter, and far-field radius. Geometric angles for these installations are the nozzle roof angle (also called cant angle or kickdown angle) relative to the nozzle upstream centerline, wing incidence relative to the nozzle upstream centerline, and flap deflection relative to the wing. An USB configuration without a flap is described as having zero flap deflection.

Two special cases are under-the-wing configurations having slotless wings or mixer nozzles. Slotless wings are represented by CONFIG=1 and NFLAP=0 input. Wing geometry is input as the leading edge coordinates XW, YW, the deflected trailing edge coordinates X(2), Y(2), incidence DELW of the forward undeflected portion of the slotless wing relative to the nozzle centerline, and deflection DEL(1) of the aft portion relative to the forward portion. Slotted under-the-wing configurations having mixer nozzles are designated separately (CONFIG=4). They require the same input as CONFIG=1 plus the isolated-nozzle centerline velocity ratio at the impingement distance, input as ROOF.

A flow chart for the calculation process is shown as figure 44. The first portion of the computer program calculates various geometric quantities such as chord lengths. For UTW and USB, it also calculates distances from the nozzle exit plane to the impingement point and the trailing edge, average distance from each wing and flap segment to the assumed far edge of the jet shear layer, and resulting spanwise-coherent lift force fluctuation. Axial distances downstream of the nozzle exit plane are utilized to calculate the ratio of local maximum velocity to nozzle axial velocity. The program variables XW and $XL(N)$ are the ratios of wing and N th flap segment maximum fluctuating-lift mean square acoustic pressure to reference pressure squared. (This noise component has also been called scrubbing noise or inflow noise.) The program variable XTE is the ratio of maximum trailing edge noise mean square acoustic pressure to reference pressure squared, calculated only for the most rearward trailing edge. Calculated quadrupole noise from an isolated exhaust jet, in the direction perpendicular to the jet centerline, is adjusted for local velocity ratio and jet deflection angle to yield the acoustic pressure ratios for quadrupole noise of a jet deflected by UTW flaps or an USB nozzle and wing assembly, and of such a jet downstream of the trailing edge. These pressure ratios apply for the direction perpendicular to the deflected jet.

Next, the noise components are calculated at equally spaced increments $DELTH$ of polar angle at up to ten designated sideline angles PHI . For each polar angle, the components of fluctuating lift noise from the wing and flaps are computed and summed. Similarly, the viewing angle relative to the centerline of the deflected jet must be computed so that quadrupole noise can be determined. Calculations of quadrupole noise pressure ratio $GJET$ must take into account whether the combination of polar angle and sideline angle yields a direction within the jet refraction region and, for USB, whether the direction is shielded from noise generated near the nozzle exit. Individual $1/3$ octave spectra for the different noise components are computed and added to obtain the spectrum and OASPL of the UTW or USB configuration.

In contrast, quadrupole noise from engine-in-front-of-the-wing installations is taken as that from an undeflected isolated exhaust jet. Lift fluctuation noise is calculated for loading distributions which become acoustically noncompact along the scrubbed span. The $1/3$ octave spectra of noise from the wing and flap is calculated taking this into account, and this spectrum is summed to obtain overall noise.

Input Variables

The following is a list and definition of the input variables and their default values.

<u>Program Symbol</u>	<u>Definition</u>	<u>Default Value</u>
CONFIG	Integer equal to 1 for UTW, 2 for USB, 3 for IFW, or 4 for UTW with mixer nozzle	1
NFLAP	Integer, number of flaps	1
NPHI	Integer, number of sideline angles (maximum allowable number is 10)	1
V	Exhaust velocity	100.
VINF	Flight velocity	0.
D	Nozzle hydraulic diameter	1.
R	Far-field radius	1.
THL	Lower value for polar angle, deg	0.
THU	Upper value for polar angle, deg	180.
DELTH	Increment between successive polar angles, deg	10.
PHI(1)	First polar angle, deg	0.
PHI(2)	Second polar angle, deg	0.
.		
.		
.		
PHI(10)	Tenth polar angle, deg	0.
FL	Lower limit for 1/3 octave center frequency, Hz	50.
FU	Upper limit for 1/3 octave center frequency, Hz	.1E5
CA	Ambient speed of sound	340.3
RHOA	Ambient air density	1.225

<u>Program Symbol</u>	<u>Definition</u>	<u>Default Value</u>
PREF	Reference acoustic pressure	.2E-6
DELW	Wing deflection relative to nozzle, deg	0.
DEL(1)	Deflection of first flap relative to wing, deg	0.
DEL(2)	Deflection of second flap relative to wing, deg	45.
.		
.		
DEL(NFLAP)	Deflection of last flap relative to nozzle, deg	45.
ROOF	USB nozzle roof angle, deg, and mixer nozzle velocity ratio at impingement distance	0.
XW	Axial position of wing leading edge	0.
X(1)	Axial position of first flap leading edge	1.
.		
.		
X(NFLAP)	Axial position of last flap leading edge	1.
YW	Vertical position of wing leading edge	0.
Y(1)	Vertical position of first flap leading edge	0.
.		
.		
Y(NFLAP)	Vertical position of last flap leading edge	0.
CLAST	Chord of last flap	1.

The input variables CONFIG, NFLAP, and NPHI must be integers. This program can be utilized with English-system units (ft,ft/sec) for lengths and velocities if CA, RHOA, and PREF are supplied in English units. For standard atmosphere, these are set equal to 1116., .2377E-2, and .41773E-6, respectively. Data input uses the standard NAMELIST format. A title card, prepared for each run, provides a printed title to identify each specific configuration.

Test Case

The following cards provide a test case for this computer program. All of these cards are punched starting in column 2. The first card provides a title to identify the print-out. Input dimensions are in meters and exhaust velocities are in meters per second, so the default values for standard sea-level air density and reference acoustic pressure are used. This test had been performed during cold weather, and speed of sound is input for the actual air temperature. The inputs for direction angle will cause calculations to be performed for polar angles from 60° to 120° in 20° increments, at 0° and 63° sideline angles, for both exhaust velocities.

```
QCSEE USB 1/11.5 SCALE MODEL, TAKEOFF FLAP SETTING
$INPUT
CONFIG=2, NPHI=2, PHI(1)=0., PHI(2)=63.
THL=60., THU=120., DELTH=20., FL=50., FU=20000.
DELW=5., XW=-.20, YN=-.024, D=.123, R=6.1
DEL(1)=30., X(2)=.42, Y(2)=-.122, CA=330.
V=191.
$END
$INPUT
V=219.
$END
$INPUT
IEND=2
$END
```

```

1*  C*** THIS PROGRAM CALCULATES FAR-FIELD EXTERNALLY BLOWN FLAP NOISE FOR
2*  C*** UNDER-THE-WING (CONFIG=1), UPPER SURFACE BLOWING (CONFIG = 2) AND
3*  C*** IN-FRONT-OF-THE-WING (CONFIG = 3) ENGINE INSTALLATIONS. OASPL AND SPECTRA
4*  C*** ARE CALCULATED FOR THE FREE FIELD AT POINTS ON A SPHERE CENTERED AT THE
5*  C*** EXHAUST NOZZLE AND MOVING WITH THE AIRCRAFT AT A LOW SUBSONIC FLIGHT
6*  C*** SPEED. DEFAULT ATMOSPHERIC PROPERTIES AND REFERENCE ACOUSTIC PRESSURE ARE
7*  C*** IN METRIC SYSTEM UNITS CORRESPONDING TO INPUT DISTANCES IN METERS AND
8*  C*** EXHAUST VELOCITY AND FLIGHT VELOCITY IN METERS PER SECOND.
9*  C*** CONFIG=4 FOR UNDER-THE-WING EBF WITH MIXER NOZZLE
10*  INTEGER CONFIG
11*  REAL KW,K,M,L,LTE,MJ
12*  DIMENSION DTHETA(37),DEL(4)
13*  DIMENSION FB(40),X(4),Y(4),PHI(10),CC(4),HL(4),HT(4),K(4),XL(3),
14*  1 SPL(40,37), OASPL(37)
15*  DATA V,VINF,D,R,THL,THU,DELTH,PHI(1),PHI(2),PHI(3),PHI(4),PHI(5),
16*  1 PHI(6),PHI(7),PHI(8),PHI(9), PHI(10), CA,RHOA,PREF,DELW,
17*  2 DEL(1),DEL(2),DEL(3),DEL(4),ROOF,FL,FU,XW,X(1),X(2),X(3),
18*  3 Y(1),Y(2),Y(3), CLAST,YW/
19*  4 100.,0.,1.,1.,0.,180.,10.,10*0., 340.3,1.225, .00002, 0.,
20*  5 0.,3*45.,0.,50.,10000.,0.,3*1.,3*0.,1.,0./
21*  NAMELIST/INPUT/ IEND,CONFIG,NFLAP,NPHI,
22*  1 V,VINF,D,R,THL,THU,DELTH,PHI(1),PHI(2),PHI(3),PHI(4),PHI(5),
23*  1 PHI(6),PHI(7),PHI(8),PHI(9), PHI(10), CA,RHOA,PREF,DELW,
24*  2 DEL(1),DEL(2),DEL(3),DEL(4),ROOF,FL,FU,XW,X(1),X(2),X(3),
25*  3 YW,Y(1),Y(2),Y(3), CLAST
26*  DIMENSION TITLE(13)
27*  READ(5,850) (TITLE(I),I=1,13)
28*  FB(1) = 10.
29*  FB(2) = 12.5
30*  FB(3) = 16.
31*  FB(4) = 20.
32*  FB(5) = 25.
33*  FB(6) = 31.5
34*  FB(7) = 40.
35*  FB(8) = 50.
36*  FB(9) = 63.
37*  FB(10) = 80.
38*  DO 4 I=1,10
39*  FB(I+10) = 10.* FB(I)
40*  FB(I+20) = 100.* FB(I)
41*  4 FB(I+30) = 1000.* FB(I)
42*  6 READ(5,INPUT)
43*  NTHETA= (THU-THL)/DELTH +1.00001
44*  IF(NTHETA.GT.37.1)NTHETA=37.00001
45*  WRITE(6,7)
46*  7 FORMAT(1H1)
47*  IF(IEND.NE.0) GO TO 2000
48*  WRITE(6,INPUT)
49*  IF=1

```



```

50*      DO 10 I=1,38
51*      IF(FL.LT.FB(1)) GO TO 20
52*      IF=1
53*      10 CONTINUE
54*      20 LF=38
55*      DO 30 I=1,39
56*      J = 39-I
57*      IF(FU.GT.FB(J)) GO TO 40
58*      LF=J
59*      30 CONTINUE
60*      40 IF(IF.LT.LF) GO TO 50
61*      LF=IF
62*      50 CONTINUE
63*      DEGRAD = .01745329
64*      IF(XW.LT.0.)XW=0.
65*      IF(CONFIG.EQ.4) GO TO 60
66*      IF(CONFIG.NE.1) GO TO 200
67*      60 CONTINUE
68*      C*** GEOMETRY CALCULATIONS FOR UNDER-THE-WING BLOWN FLAPS
69*      IF(NFLAP.NE.0) GO TO 100
70*      C*** SLOTTLESS UNDER-THE-WING CONFIGURATION
71*      GO TO 205
72*      65 LTE=X(1)+CC(1)
73*      L=LTE
74*      C= 3.*CW
75*      IF(Y(2).GE.0.) C=CW
76*      ARG=(DELW+DEL(1))*DEGRAD
77*      IF(Y(2).LE.0.)L=X(1)+Y(1)*COS(ARG)/SIN(ARG)
78*      IF(Y(1).LE.0.)L=XW+YW/TAN(DEL)
79*      GO TO 120
80*      C*** SLOTTED FLAPS
81*      100 CW = SQRT((X(1)-XW)**2. +(Y(1)-YW)**2.)
82*      ARG = DELW*DEGRAD + DEL(NFLAP)*DEGRAD
83*      X(NFLAP+1)= X(NFLAP) + CLAST * COS(ARG)
84*      Y(NFLAP+1)= Y(NFLAP) - CLAST * SIN(ARG)
85*      SUM=CW
86*      DO 110 N=1,NFLAP
87*      CC(N) = SQRT((X(N+1)-X(N))**2.+(Y(N+1)-Y(N))**2.)
88*      110 SUM = SUM+CC(N)
89*      C = SUM
90*      C*** SHEAR LAYER TRAJECTORY AND FLAP LIFT FLUCTUATIONS
91*      120 HLW = .5*D +YW
92*      HTW = HLW -CW*SIN(DELW*DEGRAD)
93*      IF(HTW.LT..5*D) HTW =.5*D
94*      KW = 1.E-7 *C *CW *(HLW**(-2.) + HTW**(-2.))
95*      IF(NFLAP.EQ.0) GO TO 500
96*      LTE = X(NFLAP) + CLAST * COS(ARG)
97*      L = X(NFLAP) +Y(NFLAP)/TAN(ARG)
98*      IF((Y(NFLAP)-CLAST*SIN(ARG)).GE.0.) L=LTE
99*      DO 130 N =1,NFLAP
100*      HL(N) = .5*D +Y(N)

```

```

101*      HT(N) = HL(N) - CC(N) * SIN(DELW*DEGRAD + DEL(N)*DEGRAD)
102*      IF(HL(N).LT..5*D) HL(N) = .5*D
103*      IF(HT(N).LT..5*D) HT(N) = .5*D
104*      130 K(N) = 1.E-7*C*CC(N) * (HL(N)**(-2.)*HT(N)**(-2.))
105*      GO TO 500
106*      200 IF(CONFIG.NE.2) GO TO 300
107*      C*** GEOMETRY CALCULATIONS FOR UPPER SURFACE BLOWN FLAPS
108*      NFLAP=1
109*      ARG=(DELW+DEL(1))*DEGRAD
110*      205 CONTINUE
111*      DELL=DELW*DEGRAD
112*      IF(DEL(1).LT..01) X(1)=X(2)
113*      IF(DEL(1).LT..01) GO TO 210
114*      X(1)=X(2)-(YW-Y(2)-(X(2)-XW)*TAN(DELL))/(TAN(DELL+DEL(1)*DEGRAD)-T
115*      AN(DELL))
116*      210 Y(1)=YW-(X(1)-XW)*TAN(DELL)
117*      CW = SQRT((X(1)-XW)**2. + (Y(1)-YW)**2.)
118*      CC(1)=SQRT((X(2)-X(1))**2.+(Y(2)-Y(1))**2.)
119*      IF(CONFIG.EQ.1)GO TO 65
120*      C = CW * CC(1)
121*      L=X(1)*CC(1)
122*      LTE=L
123*      KW=2.E-7*C*X(1)/(D*D)
124*      K(1)=1.5E-7*C*CC(1)/(D*D)
125*      GO TO 500
126*      300 CONTINUE
127*      C*** ENGINE IN FRONT OF THE WING
128*      CRD=CLAST
129*      IF(NFLAP.EQ.0) GO TO 320
130*      CW = SQRT((X(1)-XW)**2. + (Y(1)-YW)**2.)
131*      X(NFLAP+1) = XINFLAP + CLAST * COS(DELW*DEGRAD+DEL(NFLAP)*DEGRAD)
132*      Y(NFLAP+1) = YINFLAP - CLAST * SIN(DELW*DEGRAD+DEL(NFLAP)*DEGRAD)
133*      DO 310 N=1,NFLAP
134*      CC(N) = SQRT((X(N+1)-X(N))**2. + (Y(N+1)-Y(N))**2. )
135*      310 IF(NFLAP.EQ.0) IUPPER=1
136*      IF(NFLAP.EQ.1) IUPPER=2
137*      IF(NFLAP.GT.1) IUPPER=NFLAP
138*      M = V/CA
139*      XJET= (1.-VINFL/V)**6.*1.E14 * D*D*M**7.5/(R*R*(1.+.01*M**4.5))
140*      B= .62*M /((1.+(.62*M)**5.)*.0.2)
141*      MJ =(0.62*M)**0.1
142*      PI =3.14159
143*      PLK= 1.45E-4 *D *(PI *RHOA*V**3.* D/(2.*CA*R*REF))**2.
144*      GO TO 530
145*      500 M=V/CA
146*      C*** VELOCITY RATIOS AT IMPINGEMENT POINT AND AT TRAILING EDGE
147*      IF(CONFIG.EQ.4) GO TO 501
148*      VR=(1.+((.14*L/?) /SQRT(1.*M))**4.)*.25)
149*      VRTE=(1.+((.14*LTE/D)/SQRT(1.*M))**4.)*.25)
150*      GO TO 502

```

```

151*      501 V=V*ROOF
152*      VR=1.
153*      VRTE=1.
154*      502 CONTINUE
155*      P=(1.-VIN/V)**2.*C*D*(VR*RH0A*(V*VR)**3./((CA*PREF*R))**2.
156*      IF(CONF16.EQ.4)P=2.*P
157*      PP4I = PHI(I*PHI) *DEGRAD
158*      C*** MAXIMUM TRAILING EDGE NOISE
159*      XTE=1.E-5*CA*P*D*(VRTE/VR)**3./((C*V)
160*      IF(CONF16.EQ.1.AND.NFLAP.NE.0)P=.5*P
161*      XLW=P*KW
162*      IF(NFLAP.EQ.0) GO TO 506
163*      C*** MAXIMUM LIFT FLUCTUATION NOISE FOR EACH FLAP
164*      DO 505 N=1,NFLAP
165*      505 XLIN)=P*(IN)
166*      506 CONTINUE
167*      C*** NOISE PERPENDICULAR TO JET WITH VELOCITY EVALUATED AT NOZZLE EXIT, IMPACT
168*      C*** POINT, OR TRAILING EDGE
169*      IF(CONF16.NE.4) GO TO 507
170*      M=.1*M
171*      507 CONTINUE
172*      XJET=(1.-VIN/V)**2.*1.E14*D*D*M**7.5/(R*R*(1.+.01*M**4.5))
173*      XMVR=M*VR
174*      XIMJET=(1.-VIN/V)**2.*1.E14*D*D*XMVR**7.5/(R*R*(1.+.01*XMVR**4.5))
175*      1)
176*      XMVRTE = M*VRTE
177*      XTEJET=(1.-VIN/V)**2.*1.E14*D*D*XMVRTE**7.5/(R*R*(1.+.01*XMVRTE**
178*      1 4.5))
179*      IF(CONF16.NE.2)GO TO 510
180*      C*** INCREASED QUADRUPOLE NOISE FROM DEFLECTION OF JET BY USB NOZZLE ROOF AND
181*      C*** WING SURFACE
182*      AMPDEL=1.*6.*SIN(ROOF*DEGRAD)**2.
183*      XIMJET=XJET*AMPDEL
184*      XTEJET=XTEJET*AMPDEL
185*      GO TO 520
186*      510 CONTINUE
187*      C*** INCREASED QUADRUPOLE NOISE FROM DEFLECTION OF JET BY UTM FLAPS
188*      AA=(1.-VIN/V)**4.
189*      XTEJET=XTEJET*(1.*COS(PPHI)**2.)*(AA*6.*VR**8.*SIN(ARG)**2.)/2.
190*      XIMJET=XIMJET*(1.*COS(PPHI)**2.)*(AA*6.*SIN(ARG)**2.)/2.
191*      IF(NFLAP.EQ.0) XIMJET=.25*XIMJET
192*      IF(NFLAP.EQ.0) XTEJET=.10*XTEJET
193*      520 B=.62*M/(1.+(.62*M)**5.))**0.2
194*      MJ=(.62*M)**0.1
195*      530 CONTINUE
196*      DO 999 IPHI=1,NPHI
197*      WRITE(6,860) (TITLE(III),III=1,13)
198*      WRITE(6,810) PHI(IPHI)
199*      DO 998 ITHETA=1,NTHETA
200*      THETA = (THL + (ITHETA-1)*DELTH) *DEGRAD

```

```

201*      DTHETA(I,THETA)=THETA/DEGRAD
202*      TRIG = SIN(THETA)*SIN(PPHI)
203*      ANGF = (COS(ATAN(TRIG/SQRT(1.-TRIG * TRIG))))**2.
204*      IF(CONFIG.EQ.3) GO TO 740
205*      C*** CALCULATING SUM OF LIFT FLUCTUATION NOISE COMPONENTS
206*      IF(NFLAP.EQ.0) GO TO 605
207*      GW=XLW*(COS(DELW*DEGRAD)*SIN(THETA)*COS(PPHI)+SIN(DELW*DEGRAD)*COS
208*      I(THETA))**2.
209*      SUM =0.
210*      DO 600 N=1,NFLAP
211*      600 SUM=SUM+XL(N)*(COS((DELW+DEL(N))*DEGRAD)*SIN(THETA)*COS(PPHI)+SIN(
212*      I(DELW+DEL(N))*DEGRAD)*COS(THETA))**2.
213*      GL=GW+SUM
214*      GO TO 607
215*      605 GL=1.
216*      IF((THETA+ARG).LE.3.1416) GO TO 606
217*      IF(THETA.GE.6.283) GO TO 606
218*      GO TO 607
219*      606 GL=XLW*(COS(ARG)*SIN(THETA)*COS(PPHI)+SIN(ARG)*COS(THETA))**2.
220*      607 CONTINUE
221*      GF = ANGF *XTE *COS((THETA+ARG)*.5)**2.
222*      C*** VIEWING ANGLE RELATIVE TO DEFLECTED JET
223*      ANGJ=SIN(PPHI)*SIN(THETA)
224*      ANGJ =ATAN(ANGJ/SQRT(1.-ANGJ*ANGJ) )
225*      ANGJ=ATAN(COS(ANGJ)**2.*SIN(ARG)/COS(ARG))
226*      IF((THETA+ANGJ)*MJ).LE.2.618) GO TO 680
227*      IF((THETA+ANGJ).LE.3.1416) GO TO 610
228*      IF((6.2832-THETA-ANGJ)*MJ).GE.2.618) GO TO 660
229*      GO TO 690
230*      610 IF(CONFIG.EQ.2) GO TO 640
231*      620 GJET=(XIMJET+XTEJET)*(1.+B*COS(THETA+ANGJ))**(-3.)
232*      IF(CONFIG.EQ.2) GO TO 650
233*      C*** REFRACTION IN QUADRUPOLE NOISE
234*      630 GJET=GJET*10.**(-1.8*(1.-ABS(6.-(THETA+ANGJ)*1.91*MJ)))
235*      GO TO 700
236*      640 GJET=XTEJET*(1.+B*COS(THETA+ANGJ))**(-3.)
237*      IF(CONFIG.EQ.2) GO TO 630
238*      C*** REFRACTION IN QUADRUPOLE NOISE
239*      650 GJET=GJET*10.**(-1.8*(1.-ABS(6.-(6.2832-THETA-ANGJ)*1.9)*MJ)))
240*      GO TO 700
241*      660 IF(CONFIG.EQ.2) GO TO 620
242*      GO TO 690
243*      670 GJET=XTEJET*(1.+B*COS(THETA+ANGJ))**(-3.)
244*      GO TO 700
245*      680 IF(CONFIG.EQ.2) GO TO 670
246*      690 GJET=(XIMJET+XTEJET)*(1.+B*COS(THETA+ANGJ))**(-3.)
247*      IF(CONFIG.EQ.2) GO TO 730
248*      IF((THETA+ANGJ)*MJ).LT.2.618)GO TO 700
249*      IF((6.2832-THETA-ANGJ)*MJ).LT.2.618)GO TO 700
250*      GO TO 650

```

```

251*      700 GJET=GJET*(1.+(SIN(ANGJ)/SIN(ARG))**2.)
252* C*** SUM OF NOISE COMPONENTS
253*      G= GL + GE + GJET
254*      OASPL(ITHETA) = 10.* ALOG10(G)
255*      IF(CONFIG.EQ.2) GE=GE+GL
256*      PLL=0.
257*      DO 730 I=IF,LF
258* C*** CALCULATION OF 1/3 OCTAVE SPECTRA
259*      S =FB(I)*D/V
260*      PLJET = GJET *S**4./ (8. * (.125 + S**1.333)**4.)
261*      IF(CONFIG.EQ.1) GO TO 710
262*      S=S/(1.+VINF/V)
263*      GO TO 720
264*      710 PLL = GL *.037 * S**4./ (0.038 +S**2.667)**2.
265*      720 PLE = GE *.029 * S**4./ (0.05 +S**1.5 )**4.
266*      PL = PLL + PLE + PLJET
267*      730 SPL(I,ITHETA) = 10.*ALOG10(PL)
268*      GO TO 998
269* C*** ENGINE IN FRONT OF WING
270*      740 CONTINUE
271* C*** QUADRUPOLE NOISE OF UNDEFLECTED JET
272*      GJET= XJET *(1.+B*COS(THETA))**(-3.)
273*      IF((THETA*MJ).LE.2.618) GO TO 744
274*      IF(THETA.LE.3.1416) GO TO 742
275*      IF((16.2832-THETA)*MJ).LE.2.618) GO TO 744
276*      GJET = GJET *10.**(-.9 *(1.-ABS(6.-(6.2832-THETA)*1.91* MJ)))
277*      GO TO 744
278*      742 GJET = GJET *10.**(-.9 *(1.-ABS(6.- THETA*1.91* MJ)))
279*      744 CONTINUE
280* C*** LIFT FLUCTUATION NOISE FROM WING AND ALL BUT LAST FLAP, BY METHOD OF
281* C*** FILOTAS
282*      SUM1=0.
283*      DO 800 I=IF,LF
284*      SUM=0.
285*      CRD= CW
286*      DELL= DELW*DEGRAD
287*      DO 790 J=1,UPPER
288*      IF(J.EQ.1) GO TO 750
289*      CRD = CC(J-1)
290*      DELL=(DELW *DEL(J-1))*DEGRAD
291*      750 SC = FB(I) * CRD/V
292*      SIGMA = PI*SC
293*      BETA = 2.*CRD/D
294*      IF(SIGMA.GE.BETA) GO TO 770
295*      AAA = BETA
296*      760 XLS = (LOG(1.7 +(PI*AAA)**2.))/(LOG(1.2) +3.*(PI*AAA)**2.)
297*      GO TO 780
298*      770 AAA= SIGMA
299*      GO TO 760
300*      780 PLF = SC**3.*(4./ (1.+(1.5)*SIGMA*D/CPD)**2.))*XLS/(1.+(SIGMA*M)**2.)

```


[illegible]

Test Case Output

```

$INPUT
IEND = +0
CONFIG = +2
NFLAP = +1
NPHI = +2
V = .21900000E+J3
VINP = .00000000E+00
D = .12300000E+00
R = .61000000E+01
THL = .60000000E+J2
THU = .12000000E+03
DELTH = .20000000E+J2
PHI (1) = .00000000E+00
PHI (2) = .63000000E+J2
PHI (3) = .00000000E+00
PHI (4) = .00000000E+00
PHI (5) = .00000000E+00
PHI (6) = .00000000E+00
PHI (7) = .00000000E+00
PHI (8) = .00000000E+00
PHI (9) = .00000000E+00
PHI (10) = .00000000E+00
CA = .33000000E+J3
RHOA = .12250000E+01
PREF = .20000000E+04
DEL* = .50000000E+J1
DEL (1) = .30000000E+02
DEL (2) = .45000000E+02
DEL (3) = .45000000E+02
DEL (4) = .45000000E+02
ROOF = .00000000E+00
FL = .50000000E+02
FU = .20000000E+05
X* = .20000000E+00
X (1) = .32002793E+00
X (2) = .42000000E+00
X (3) = .10000000E+01
Y* = -.24000000E-J1
Y (1) = -.51996811E-01
Y (2) = -.12200000E+00
Y (3) = .00000000E+00
CLAST = .10000000E+01

$END

```

COSEL USE 1/41.5 SCALE MODEL, TAKEOFF FLAP SETTING

SIDELINE ANGLE, PHI = .00 DEGREES

1/3 OF
CTR FREQ: AZIMUTH ANGLE, DEG
(HERTZ) 60. 80. 100. 120.

50.00	76.41	75.93	74.86	73.04
60.00	74.81	74.34	73.29	71.49
80.00	83.11	82.65	81.60	79.84
100.00	93.92	93.47	92.45	90.76
120.00	98.42	97.96	96.98	95.32
140.00	99.74	99.38	98.37	96.81
160.00	98.34	97.99	96.97	95.60

250.00	93.58	93.22	92.41	91.13
315.00	94.32	94.02	93.31	92.25
400.00	94.60	94.36	93.61	93.01
500.00	94.45	94.31	93.93	93.40
630.00	93.96	93.93	93.75	93.51
800.00	93.15	93.26	93.31	93.36
1000.00	92.20	92.44	92.70	92.96
1250.00	91.09	91.46	91.94	92.43
1600.00	89.74	90.29	90.95	91.63
2000.00	88.44	89.12	89.95	90.77
2500.00	87.09	87.90	88.87	89.81
3150.00	85.65	86.58	87.69	88.73
4000.00	84.13	85.19	86.41	87.54
5000.00	82.71	83.86	85.18	86.37
6300.00	81.22	82.47	83.88	85.13
8000.00	79.69	81.03	82.51	83.82
10000.00	78.26	79.66	81.23	82.57
12500.00	76.84	78.33	79.93	81.31
16000.00	75.28	76.83	78.49	79.90
20000.00	73.88	75.48	77.18	78.62

OVERALL 104.01 103.98 103.81 103.57

QCSEE USB 1/11.5 SCALE MODEL, TAKEOFF FLAP SETTING

SIDELINE ANGLE, PHI = 63.00 DEGREES

1/3 OB
CTR FREQ:
(HERTZ) 60. 80. 100. 120. AZIMUTH ANGLE, DEG

50.00	71.65	69.52	68.04	66.83
63.00	75.06	72.93	71.47	70.31
80.00	78.36	76.24	74.80	73.70
100.00	81.18	79.07	77.66	76.65
125.00	83.68	81.59	80.22	79.34
160.00	86.01	83.95	82.64	81.95
200.00	87.66	85.64	84.42	83.96
250.00	88.86	86.89	85.79	85.61
315.00	89.62	87.72	86.78	86.96
400.00	89.92	88.12	87.39	87.97
500.00	89.80	88.12	87.62	88.59
630.00	89.34	87.81	87.57	88.92
800.00	88.58	87.22	87.25	88.95
1000.00	87.67	86.48	86.76	88.73
1250.00	86.62	85.59	86.09	88.29
1600.00	85.32	84.47	85.20	87.59
2000.00	84.07	83.37	84.27	86.80
2500.00	82.76	82.21	83.25	85.89
3150.00	81.37	80.95	82.12	84.85
4000.00	79.90	79.60	80.89	83.70
5000.00	78.51	78.31	79.69	82.57
6300.00	77.06	76.96	78.42	81.35
8000.00	75.57	75.55	77.08	80.06
10000.00	74.17	74.23	75.82	78.83
12500.00	72.77	72.90	74.54	77.58
16000.00	71.24	71.43	73.12	76.18
20000.00	69.86	70.10	71.83	74.91
OVERALL	99.40	97.86	97.62	98.98

```

$INPUT
IEND == +0
CONFIG == +2
NFLAP == +0
NPHI == +2
V == .19100000E+03
VINP == .00000000E+00
D == .12300000E+00
R == .61000000E+01
THL == .60000000E+02
THU == .12000000E+03
DELTH == .20000000E+02
PHI (1) == .00000000E+00
PHI (2) == .63000000E+02
PHI (3) == .00000000E+00
PHI (4) == .00000000E+00
PHI (5) == .00000000E+00
PHI (6) == .00000000E+00
PHI (7) == .00000000E+00
PHI (8) == .00000000E+00
PHI (9) == .00000000E+00
PHI (10) == .00000000E+00
CA == .33000000E+03
RHOA == .12250000E+01
PREF == .20000000E-04
DELW == .50000000E+01
DEL (1) == .30000000E+02
DEL (2) == .45000000E+02
DEL (3) == .45000000E+02
DEL (4) == .45000000E+02
ROOF == .00000000E+00
FL == .50000000E+02
FU == .20000000E+05
XW == -.20000000E+00
X (1) == .10000000E+01
X (2) == .42000000E+00
X (3) == .10000000E+01
YW == -.24000000E-01
Y (1) == .00000000E+00
Y (2) == -.12200000E+00
Y (3) == .00000000E+00
CLAST == .10000000E+01

$END

```

QCSEE USB 1/11.5 SCALE MODEL, TAKEOFF FLAP SETTING

SIDELINE ANGLE, PHI = .00 DEGREES

1/3 OB
CTR FREQ: AZIMUTH ANGLE, DEG
(HERTZ) 60. 80. 100. 120.

50.00	75.12	74.55	73.35	71.31
63.00	78.41	77.84	76.65	74.63
80.00	81.55	80.98	79.81	77.81
100.00	84.17	83.61	82.45	80.49
125.00	86.44	85.89	84.76	82.85
160.00	88.47	87.94	86.84	85.02
200.00	89.83	89.32	88.27	86.55

250.00	90.72	90.24	89.26	87.68
315.00	91.15	90.72	89.83	88.45
400.00	91.14	90.77	90.01	88.86
500.00	90.75	90.45	89.84	88.94
630.00	90.03	89.83	89.39	88.75
800.00	89.04	88.95	88.70	88.32
1000.00	87.93	87.96	87.88	87.74
1250.00	86.69	86.84	86.94	87.00
1600.00	85.22	85.50	85.78	86.03
2000.00	83.82	84.22	84.66	85.06
2500.00	82.38	82.90	83.47	84.00
3150.00	80.87	81.49	82.20	82.83
4000.00	79.29	80.02	80.84	81.58
5000.00	77.80	78.63	79.56	80.37
6300.00	76.27	77.19	78.21	79.09
8000.00	74.69	75.70	76.80	77.74
10000.00	73.22	74.31	75.48	76.47
12500.00	71.77	72.93	74.15	75.19
16000.00	70.17	71.40	72.69	73.76
20000.00	68.75	70.03	71.37	72.47
OVERALL	100.54	100.29	99.74	98.95

QCSEE USB 1/11.5 SCALE MODEL, TAKEOFF FLAP SETTING

SIDELINE ANGLE, PHI = 63.00 DEGREES

1/3 OB CTR FREQ: (HERTZ)	60.	80.	100.	120.
--------------------------------	-----	-----	------	------

50.00	70.43	68.14	66.54	65.00
63.00	73.72	71.44	69.85	68.35
80.00	76.86	74.58	73.01	71.58
100.00	79.49	77.22	75.68	74.33
125.00	81.76	79.51	78.01	76.77
160.00	83.80	81.57	80.13	79.08
200.00	85.16	82.98	81.62	80.78
250.00	86.06	83.93	82.68	82.11
315.00	86.52	84.45	83.35	83.12
400.00	86.53	84.56	83.65	83.80
500.00	86.17	84.31	83.61	84.13
630.00	85.49	83.78	83.31	84.19
800.00	84.54	82.99	82.77	83.98
1000.00	83.48	82.08	82.09	83.56
1250.00	82.30	81.06	81.27	82.96
1600.00	80.88	79.81	80.23	82.12
2000.00	79.54	78.62	79.20	81.23
2500.00	78.15	77.37	78.09	80.25
3150.00	76.69	76.04	76.89	79.14
4000.00	75.16	74.63	75.60	77.94
5000.00	73.72	73.30	74.36	76.77
6300.00	72.23	71.91	73.05	75.52
8000.00	70.69	70.47	71.69	74.20
10000.00	69.26	69.12	70.40	72.95
12500.00	67.84	67.77	69.10	71.69
16000.00	66.28	66.28	67.67	70.29
20000.00	64.88	64.93	66.36	69.01
OVERALL	95.98	94.18	93.58	94.25

APPENDIX D: NOISE SOURCE LOCATION FOR UPPER SURFACE BLOWING

Purpose of Experiment

Several analyses have been presented for the acoustic process by which noise is generated by USB externally blown flaps. The physical situation along the jet centerline plane is sketched in figure 45. An engine exhaust nozzle is located on a wing upper surface. The presence of the wing causes observers beneath the wing to be shielded from much of the aft-radiated engine noise. When the trailing edge flaps are deflected, their upper surfaces form a smooth low-curvature surface. The exhaust jet remains attached to this curved upper surface and is deflected downward, generating significant increases of wing lift at low flight speeds. Broadband noise with a velocity exponent less than that for isolated exhaust jet noise is also generated.

At small distances downstream of the exhaust nozzle, the exhaust jet can be regarded as containing a potential core having uniform mean flow properties and low turbulence level. A boundary layer exists between the potential core and the wing upper surface, and a shear layer exists above the potential core. The upper shear layer has a faster growth rate and higher turbulence level than the boundary layer. Depending on the configuration, these two layers of strong viscous effects may merge upstream of the flap trailing edge. The boundary layer can still be denoted as a distinct region because of its larger gradients of streamwise mean velocity and smaller normal turbulence levels, caused by the boundary constraint at a solid surface. Downstream of the trailing edge, the upper surface boundary layer becomes a shear layer. The large gradient of mean velocity within the boundary layer produces a large growth rate and high turbulence levels in the initial part of this shear layer. Thus the largest turbulence levels in any portion of the exhaust jet near the trailing edge are those of the shear layer downstream of the trailing edge and below the exhaust jet.

One analysis of USB noise, developed by Tam and Reddy (reference 21), assumed that one of the dominant components was quadrupole noise generated in the lower shear layer. The calculated levels depend upon measured properties of the turbulence and the mean velocity profile. Some USB noise reduction concepts tested by Hayden (reference 38) have assumed that the noise is caused by turbulent eddies convected past the trailing edge and spatially very near that edge. Thus the noise is implicitly assumed to depend on turbulence properties of the wing upper surface boundary layer immediately upstream of the trailing edge. A noise prediction method developed by Fink (reference 17) represented USB noise at low exhaust velocities as a sum of two simple surface-radiation noise processes: trailing-edge noise and

whole-body lift fluctuation noise caused by large-scale structure of the exhaust jet as it is convected along the airfoil and past the trailing edge. The upper shear layer ahead of the trailing edge, with a combination of large turbulence scale length and large turbulence intensity, was regarded as the dominant region. It seemed likely that crosscorrelation between local flow velocities and far field acoustic pressure should indicate which region, if any, contains the dominant noise source.

Apparatus and Procedure

Test Apparatus

Tests were conducted in the anechoic chamber of the UTRC acoustic wind tunnel. A 15 cm (6 in.) inside diameter duct brought a regulated muffled supply of high-pressure air into the chamber. This air supply duct was connected to a 4.9 cm (1.925 in.) exit diameter axisymmetric nozzle. A 23 cm (9 in.) chord NACA 0018 airfoil was mounted such that for zero deflection relative to the nozzle centerline, the airfoil leading edge was vertical. Its closest position to the nozzle was 2.5 cm (1.0 in.) downstream and 2.0 cm (0.8 in.) to one side of the nozzle lip. The airfoil was rotated about its 30 percent chord line to 9° deflection, trailing edge toward the exhaust jet. This nozzle and airfoil had previously been used in tests reported in references 17, 18, and 20. When positioned in this manner, the aft 70 percent of the airfoil surface adjacent to the jet was nearly in line with the nozzle lip. A conventional 0.635 cm (1/4 in.) microphone was located 2.13 m (7 ft) to the side of the nozzle exit centerline shielded by the wing, to measure far-field acoustic pressure. Thus the test configuration was an USB installation rotated 90° .

When this test program was planned, it was intended to measure the exhaust jet flow properties with a miniature hot film gage used in tests described in reference 20. However, repeated irregular output spectra occurred. A conventional single hot wire gage, which generally is less rugged than hot film gages, was therefore used. This hot wire gage was mounted on a traverse mechanism which could be manually positioned axially in a plane normal to the airfoil chord and containing the nozzle centerline. The hot wire could be remotely actuated in horizontal position within this plane. The amplified output signal could be connected to circuits which measured mean output and rms fluctuation, corresponding to mean and rms axial velocity.

Procedure

Far-field acoustic spectra were measured with and without the hot wire gage and its support strut extended across the exhaust jet at 100 m/sec (328 ft/sec) exhaust velocity. The presence of the support strut caused up to 2 dB noise increase at 2500 Hz frequency and up to 7 dB increase at 6300 Hz. This larger frequency was the expected Strouhal frequency for vortex shedding by the 0.32 cm (1/8 in.) diameter hot-wire support strut. Output of the far-field microphone and the hot wire was therefore sent through matched filters adjusted to pass only the frequency region between 100 and 2000 Hz. The resulting filtered far-field acoustic signal was essentially unaffected by hot-wire position. The dominant broadband peak amplitude occurred at about 400 Hz frequency and was unaffected by the filters.

The hot wire was traversed across the exhaust jet to obtain profiles of mean velocity and rms velocity fluctuation in the direction parallel to the nozzle centerline. These traverses were conducted at axial locations half a nozzle diameter upstream and downstream of the trailing edge. Positions of maximum rms turbulence in the wing boundary layer, lower shear layer, and upper shear layer at both axial stations were located during these traverses. The hot wire was then positioned at each of these four locations. Far-field acoustic spectrum was measured in the frequency range from 100 to 2000 Hz to assure that the spectrum was unaffected by the presence of the hot-wire support strut. The measured difference between noise signals with and without the probe was largest at the support probe Strouhal frequency near 10,000 Hz but was greater than 0.2 dB down to 3150 Hz. Autocorrelations of the resulting filtered broadband hot-wire and acoustic-pressure signals, and a crosscorrelation of those signals, were obtained. Tests were also conducted with the hot wire located at the same vertical distances relative to the airfoil surface at axial positions one diameter upstream and downstream of the trailing edge. All data were obtained at 100 m/sec exhaust velocity.

Hot-wire autocorrelation traces were integrated with respect to time to obtain the Eulerian integral time scale. This time scale was multiplied by the mean velocity at the measurement position to determine the streamwise integral length scale of the local turbulence.

Crosscorrelations generally contained a large positive peak followed by a large negative peak. This portion of the signal was approximately anti-symmetric about the delay time at zero amplitude. Maximum negative slope, corresponding (reference 13) to maximum surface-radiated noise source-strength, occurred approximately at this delay time. Normalized cross-correlation was taken as the average maximum amplitude of the two peaks,

divided by the square root of the product of the maximum values of the autocorrelation. These latter maxima occurred at zero delay time.

Presentation and Interpretation of Data

Velocity and Turbulence Profiles

Mean axial velocity profiles half a diameter upstream and downstream of the airfoil trailing edges are plotted in figure 46. Flow around the slightly curved airfoil surface caused the largest local velocity at these positions to exceed the nozzle exhaust velocity. The upper surface shear layer became thicker with increased downstream distance. Axial turbulence profiles are plotted in figure 47. Minimum turbulence within the exhaust jet, and maximum mean velocity, occurred approximately half a nozzle diameter above the airfoil surface. Peak axial turbulence level in the airfoil boundary layer was less than 11 percent and occurred where the mean velocity was about 85 percent of exhaust velocity. Peak axial turbulence level in the lower shear layer was about 15 percent. It occurred at the vertical position of the trailing edge, where mean velocity was about 70 percent of exhaust velocity. Maximum turbulence levels in the upper shear layer were about 14 and 15 percent for positions upstream and downstream of the trailing edge. These maximum levels occurred at a height roughly one nozzle diameter above the trailing edge, at local mean velocities 65 to 70 percent of nozzle exhaust velocity. Peak turbulence levels of 15 percent in the upper and lower shear layers at these positions are slightly less than the 17 percent levels shown in figure 7 of reference 39 for a position just downstream of the trailing edge, for a model with circular exhaust nozzle.

Crosscorrelation Traces

Crosscorrelations have been measured between static pressures on the upper surface of this USB model with far-field acoustic pressures below the model. Those crosscorrelation curves, shown in figure 7b of reference 18, had negative peaks followed by positive peaks. From the analysis given in reference 13, surface pressures on one side of an airfoil crosscorrelated with dipole acoustic pressures in the far field on the same side of that airfoil should cause a positive peak followed by a negative peak. Maximum negative slope and zero amplitude occur at a delay time which, for a noise source location, is equal to the acoustic travel time r/a . The change to a USB configuration, with acoustic pressures beneath the airfoil occurring 180° out of phase with those above the airfoil, produces one reversal of sign. However, in isentropic flow an increase of static pressure corresponds to a decrease of flow velocity. Use of a hot wire rather than a pressure transducer

therefore reverses the signs. Thus a crosscorrelation between a hot wire above an airfoil and within a flow that causes dipole noise, and a far field microphone below the airfoil, should produce a positive peak followed by a negative peak. In contrast, directly radiated or refracted quadrupole noise should produce a single negative peak centered at delay time r/a (references 40 and 41).

Crosscorrelation signals are plotted in figure 48 for hot-wire locations in the airfoil boundary layer and lower shear layer. Amplitudes of the original data traces were replotted such that all curves have the same scale for normalized crosscorrelation coefficient. All four curves have the same basic shape of a positive peak followed by a negative peak, with maximum negative slope at zero amplitude, corresponding to dipole noise. For the two positions in the airfoil boundary layer, the zero crossing with maximum negative slope occurred at times which exceeded the time required for an acoustic wave to travel from the model to the far-field microphone. The zero-crossing time approached this acoustic travel time as the trailing edge was approached. Similarly, the zero-crossing time measured half a diameter downstream of the trailing edge was smaller than the acoustic travel time. This behavior would occur if the hot wires were detecting turbulence which maintains its identity as it is convected along the airfoil and into the near wake, but causes surface-radiated noise only as it passes close to the trailing edge. A convection velocity can be inferred from the change of zero-crossing times with streamwise distance. This convection velocity is about 60 percent of nozzle exhaust velocity, and is approximately equal to the mean velocity at these locations of maximum turbulence (figure 46). Approximately this same convection velocity ratio was reported in reference 40 for tests of a USB configuration having a 10:1 slot nozzle rather than the circular nozzle used with the tests reported herein.

The crosscorrelation trace which was measured half a diameter downstream of the trailing edge has a negative peak at approximately the far-field acoustic travel time, preceded by a positive peak. The negative peak corresponds to quadrupole noise radiated directly to the far field by the local high-intensity turbulent flow. As previously mentioned, the combination of a positive and negative peak at this position corresponds to surface-radiated noise generated by a portion of this turbulence at an earlier time. The measurement at one diameter downstream has a positive peak followed by a negative peak, followed in turn by a positive peak at the acoustic delay time. Here the first pair of peak levels occurs at a time consistent with generation of surface-radiated noise near the trailing edge, followed by convection of turbulence within the lower shear region to the hot wire. Interpretation of the positive peak at the acoustic travel time is not obvious. The analysis given in reference 40 showed that a positive second derivative of the

crosscorrelation corresponded to direct acoustic radiation from the turbulence-measuring hot wire to the far-field microphone. Maximum positive second derivative corresponds to zero slope and minimum amplitude. However, positive rather than negative peaks of the crosscorrelation were reported in reference 41 as representing directly radiated quadrupole noise. Perhaps the positive peak at the far-field acoustic travel time then represents quadrupole noise from the lower shear layer, and the preceding positive and negative peaks represent surface-radiated noise generated when the measured turbulence had convected past the trailing edge.

The largest peak values for normalized crosscorrelation in the lower shear layer were those for the measurement location half a diameter upstream of the leading edge. However, a comparison of these peak amplitudes alone does not give a direct measure of the relative strength of surface-radiated and volume-radiated noise sources (references 13, 40, and 41).

Crosscorrelations between the far-field acoustic pressure and velocities in the upper shear region are given in figure 49. These traces contain a weak positive peak followed by a strong negative and then a strong positive peak. If the two largest peaks are considered to be the dominant feature, they represent the downstream convection of a flow disturbance of opposite sign to that which produced the far-field noise. The delay times at the zero crossing with positive slope are about a millisecond larger than those for zero crossings shown in figure 48. If these flow disturbances lie in planes skewed about 45° to the jet axis, with their slower-moving portion in the upper shear layer, the observed differences in delay times would occur.

Another viewpoint might be that the first positive peak followed by the large negative peak is the important feature. These portions of the crosscorrelations have zero crossing times approximately equal to those in figure 48 for the airfoil boundary layer and the lower shear region. The large-scale structure would then be approximately perpendicular to the exhaust jet as with an isolated jet. Interpretation of the final positive peak, and in particular its decrease of occurrence time with increasing downstream distance, then becomes difficult. The most likely interpretation of these data for the upper shear layer is that the upper shear layer of an axisymmetric-nozzle USB is related to noise radiation in a complicated manner that cannot be readily approximated as a sum of distinct volume-radiated and surface-radiated components.

Results of Crosscorrelation

Spatial distributions of axial integral length scale within the surveyed region are plotted in figure 50a. This length scale generally was about $1/3$ the nozzle diameter. It increased to about 45 percent of this diameter in the upper shear layer downstream of the trailing edge. Thus the positions of maximum turbulence intensity are associated with large-scale structure of the jet turbulence similar to that of an isolated jet.

Maximum normalized crosscorrelation coefficients between the jet velocity and far-field acoustic pressure are shown in figure 50b. They were evaluated for the largest adjacent positive and negative crosscorrelation peaks in figures 48 and 49. Maximum normalized crosscorrelation coefficient ranged from 0.08 to 0.10 for most locations. The only significantly larger value, 0.13, was measured in the airfoil boundary layer half a diameter upstream of the trailing edge. Normalized crosscorrelations of upper surface pressures and far field acoustic pressures for this USB configuration were shown in figure 10d of reference 18 for a somewhat higher exhaust velocity (125 m/sec). The measured value of nearly 0.4 at a position nearly half a diameter upstream of the trailing edge is much larger than the largest value measured with the hot wire. Evidently, the hot wire measured far more details of the local unsteady flow than the area average provided by a surface pressure transducer.

From the crosscorrelation amplitudes, and the delay times for zero crossings with large-amplitude slopes, it is concluded that USB configurations with axisymmetric nozzles and short flap lengths have two important noise processes. One is convection of airfoil upper-surface boundary layer turbulence past the neighborhood of the trailing edge, generating a surface-radiated edge noise. The other is direct radiation of quadrupole noise from the high-turbulence lower shear layer at moderate distances downstream of the trailing edge.

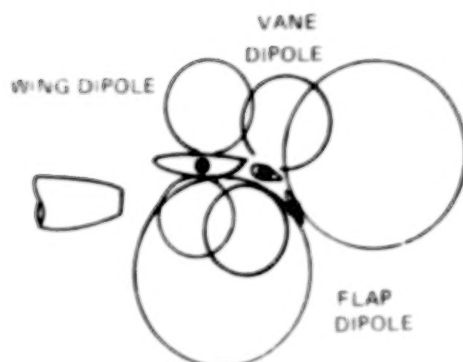
It should be noted that two concurrent studies (references 41 and 42) have investigated noise radiation from USB slot nozzle configurations. Both experimental programs used an aspect ratio 10 slot nozzle and a flat-plate wing having zero flap deflection. Both wing models were longer than the jet potential core, unlike the situation for the configuration described herein. Both programs used crosscorrelations between flow-field hot wires and far-field microphones. In reference 41 it was concluded that the dominant process was quadrupole noise radiated directly from a small region of high turbulence, several slot heights downstream of the trailing edge. However, for the nearly identical configuration and test program described in reference 42,

trailing-edge noise caused by turbulence in the upper shear layer was reported to dominate. If noise radiation from USB configurations can be approximated by a sum of several simplified noise components, associated with discrete source locations, the location of the dominant source cannot be conclusively identified for all cases.

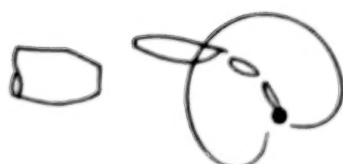
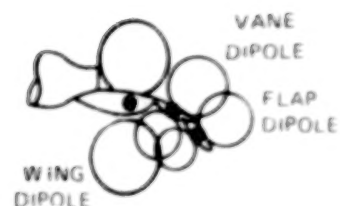
UNDER THE WING
(UTW) CONFIGURATION

NOISE MECHANISM

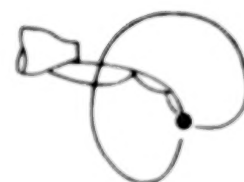
UPPER SURFACE BLOWING
(USB) CONFIGURATION



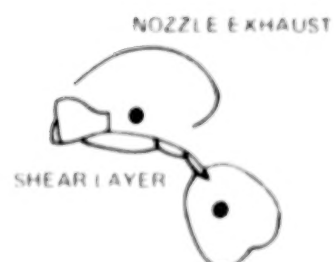
FLUCTUATING
LIFT NOISE,
INFLOW NOISE



TRAILING EDGE NOISE



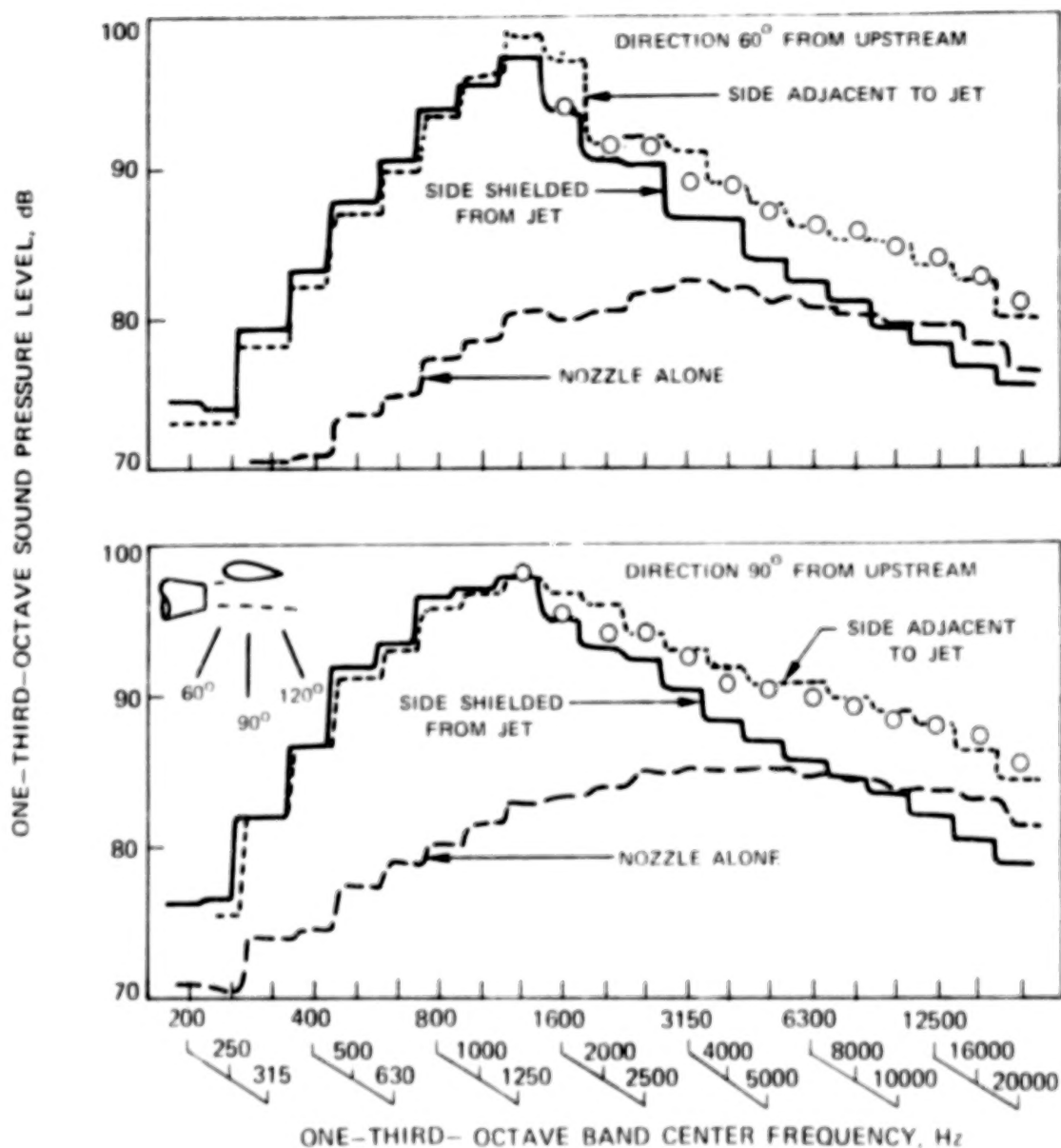
QUADRUPOLE NOISE FROM
DEFLECTED JET
(IMPACT NOISE)



DEFLECTOR DIPOLE NOISE



FIGURE 1. – SKETCH OF DIRECTIVITIES FOR DIFFERENT MECHANISMS
OF EXTERNALLY BLOWN FLAP NOISE



CIRCLE SYMBOLS ARE SUM OF MEASURED SOUND ON SIDE SHEILED FROM JET, PLUS MEASURED NOZZLE-ALONE SOUND INCREASED 3dB BY REFLECTION FROM WING

FIGURE 2. - COMPARISON OF FAR-FIELD SPECTRA IN THE SCRUBBED AND UNSCRUBBED DIRECTIONS FROM AN UNDEFLECTED EXTERNALLY BLOWN WING AT 250 M/SEC VELOCITY

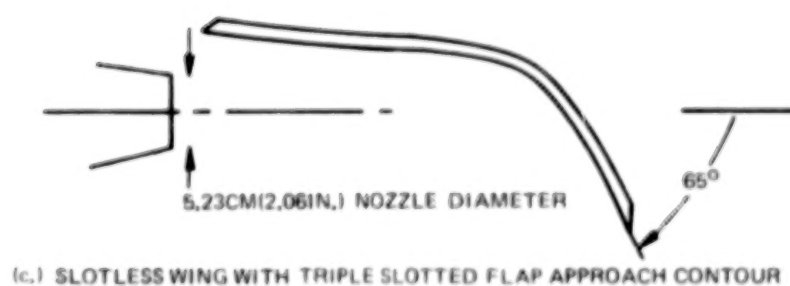
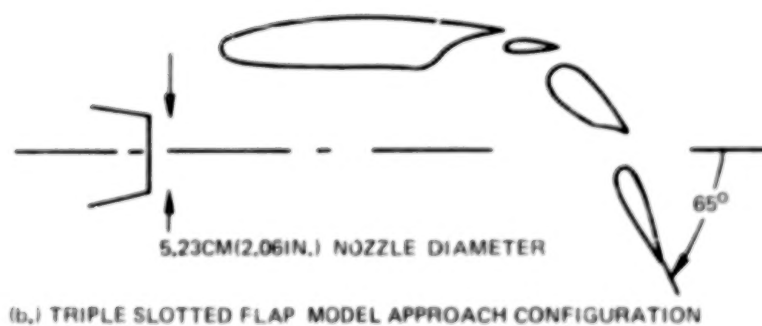
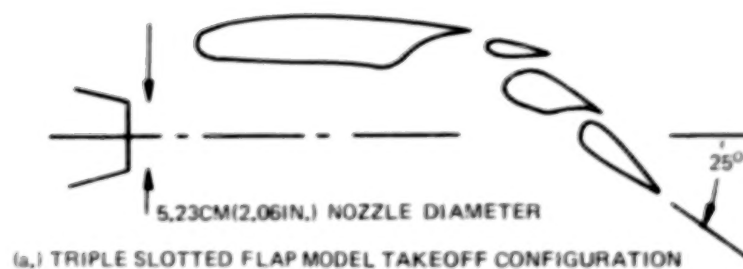


FIGURE 3. -UNDER-THE-WING CONFIGURATIONS FOR EVALUATION OF EBF NOISE PREDICTION METHODS. MODEL CONFIGURATIONS ARE DRAWN TO SCALE.

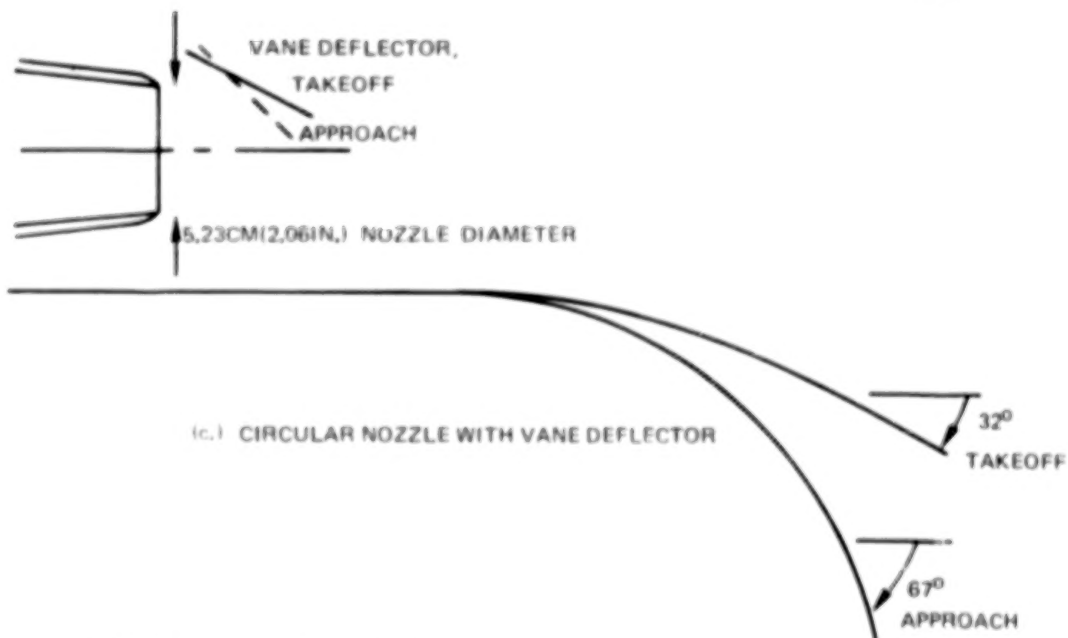
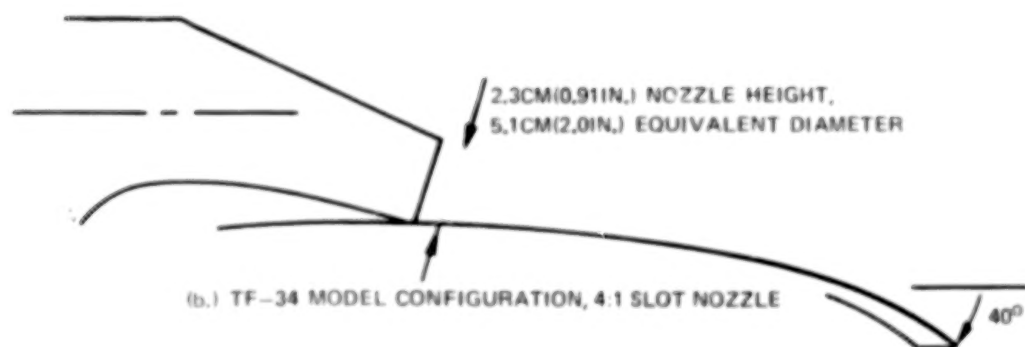
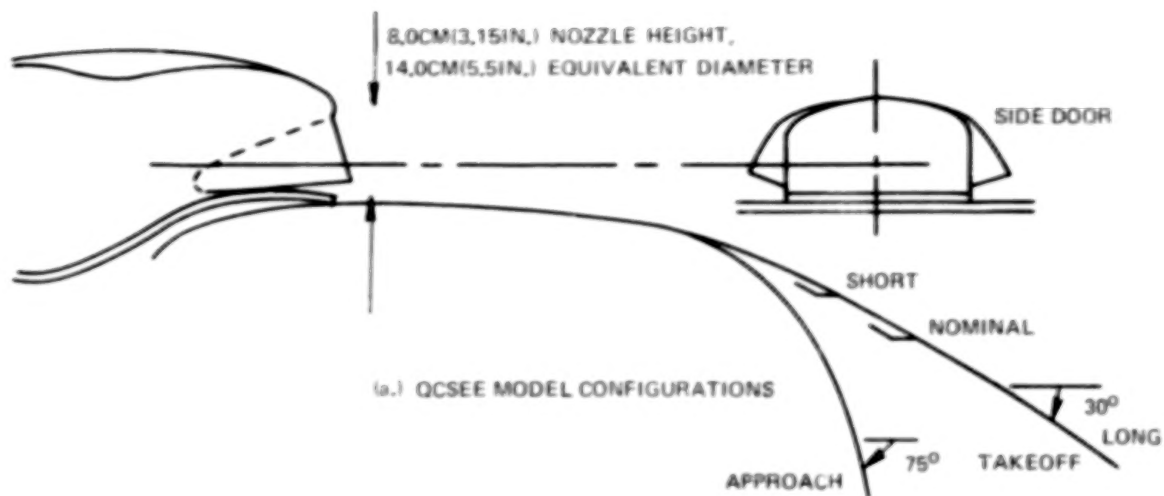


FIGURE 4. —UPPER SURFACE BLOWING CONFIGURATIONS FOR
EVALUATION OF EBF NOISE PREDICTION METHODS.
MODEL CONFIGURATIONS DRAWN TO SCALE.

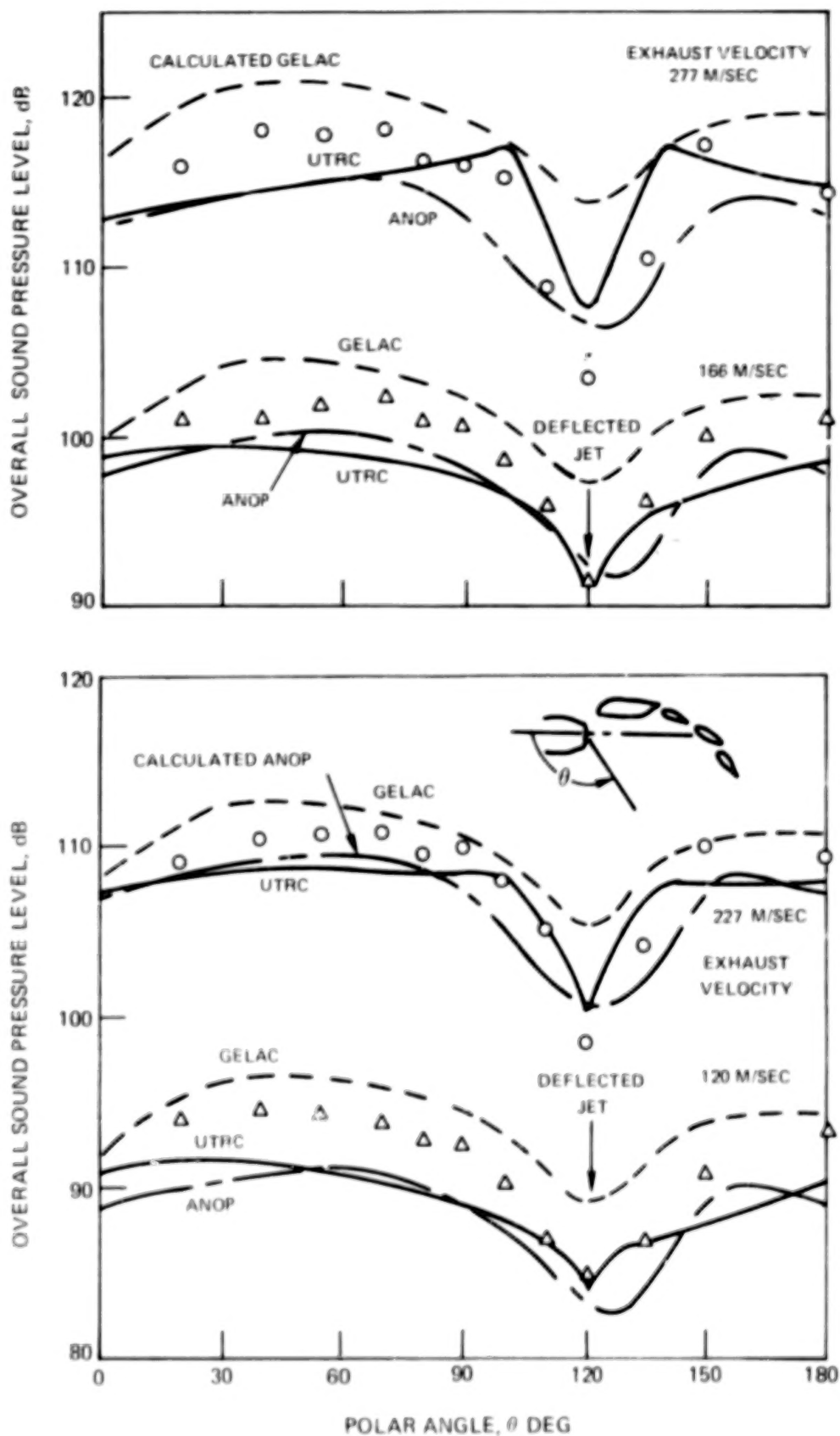


FIGURE 5. – CALCULATED AND MEASURED OASPL DIRECTIVITY IN THE FLYOVER PLANE FOR UTW MODEL APPROACH CONFIGURATION

OVERALL SOUND PRESSURE LEVEL AT SIDELINE ANGLE MINUS OVERALL SOUND PRESSURE LEVEL IN FLYOVER PLANE, (OASPL)_{φ=0}, dB

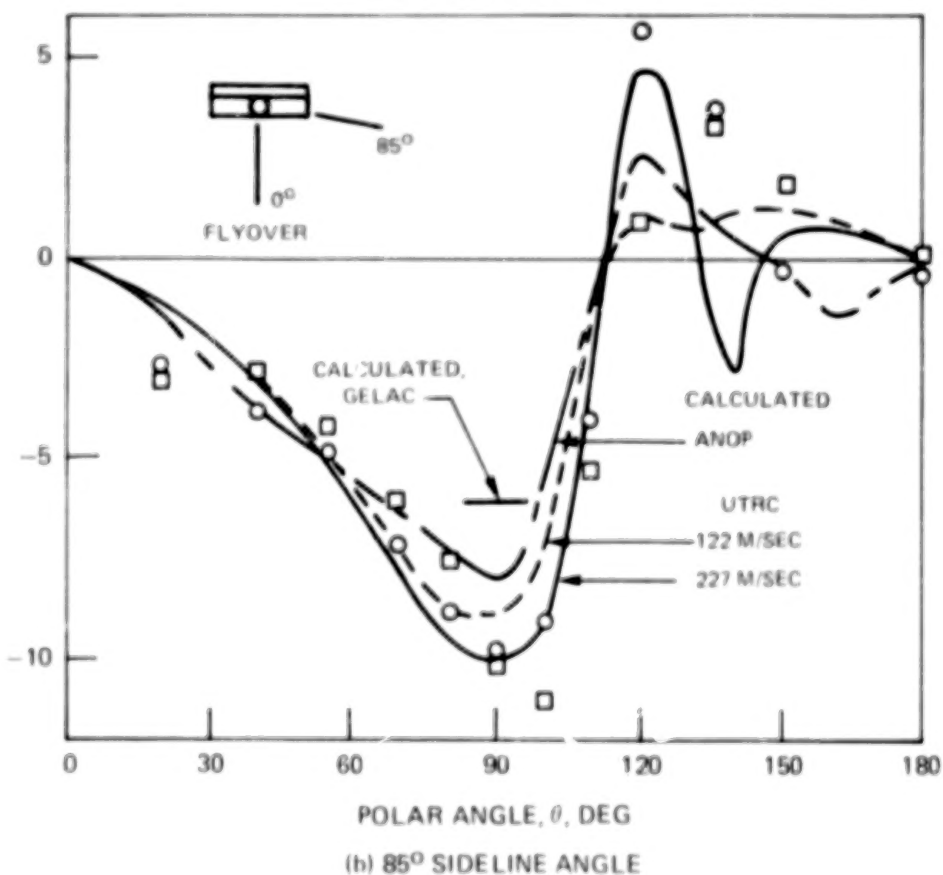
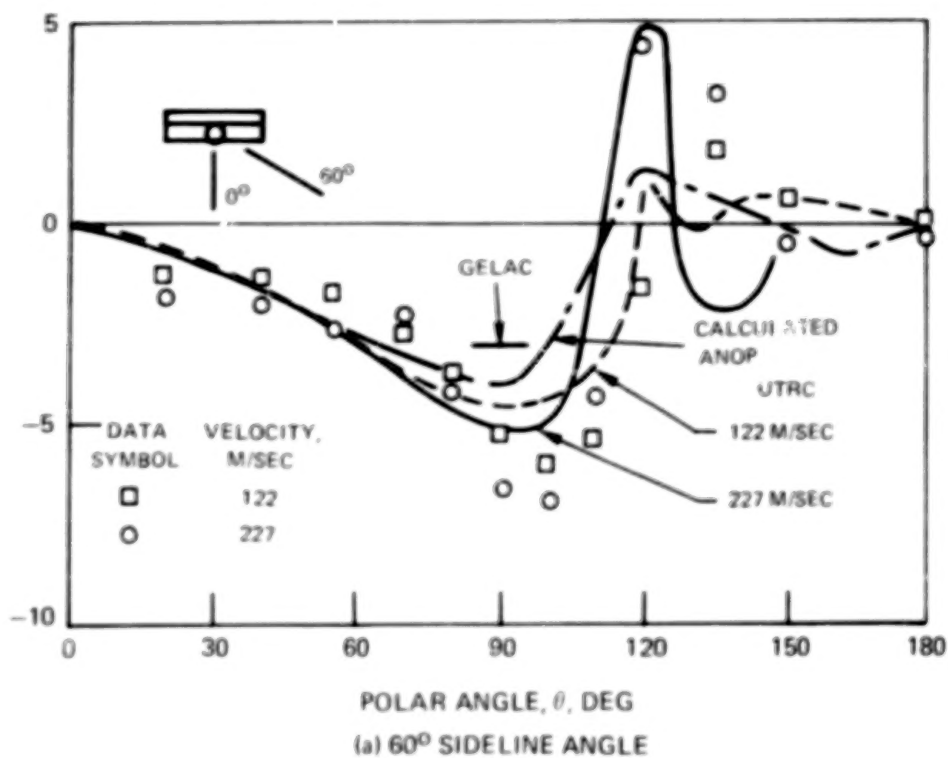


FIGURE 6. - EFFECT OF SIDELINE ANGLE ON CALCULATED AND MEASURED OASPL DIRECTIVITY FOR UTW MODEL APPROACH CONFIGURATION

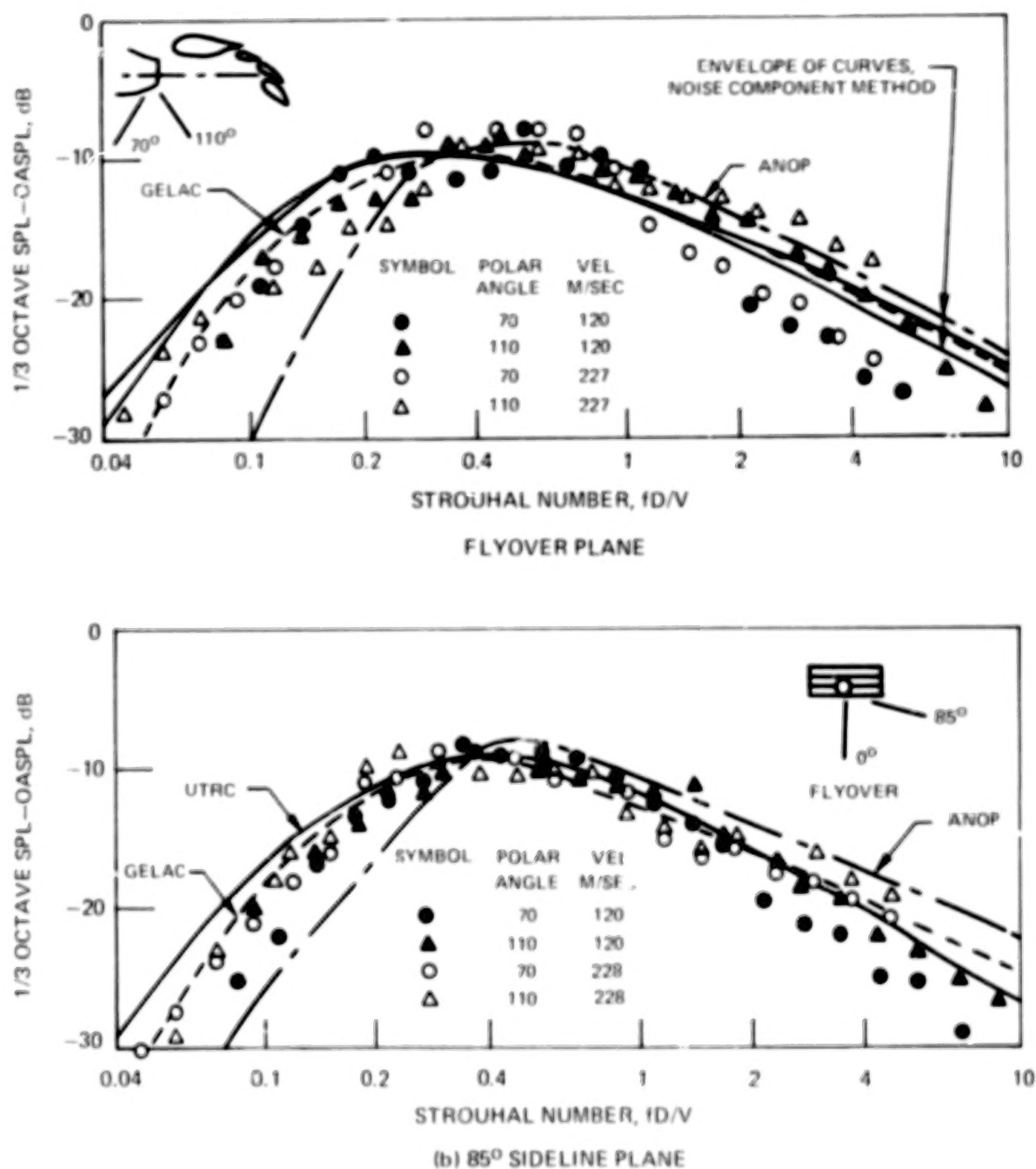


FIGURE 7. - EFFECT OF POLAR ANGLE AND EXHAUST VELOCITY ON CALCULATED AND MEASURED NORMALIZED 1/3 OCTAVE SPECTRA FOR UTW MODEL APPROACH CONFIGURATION

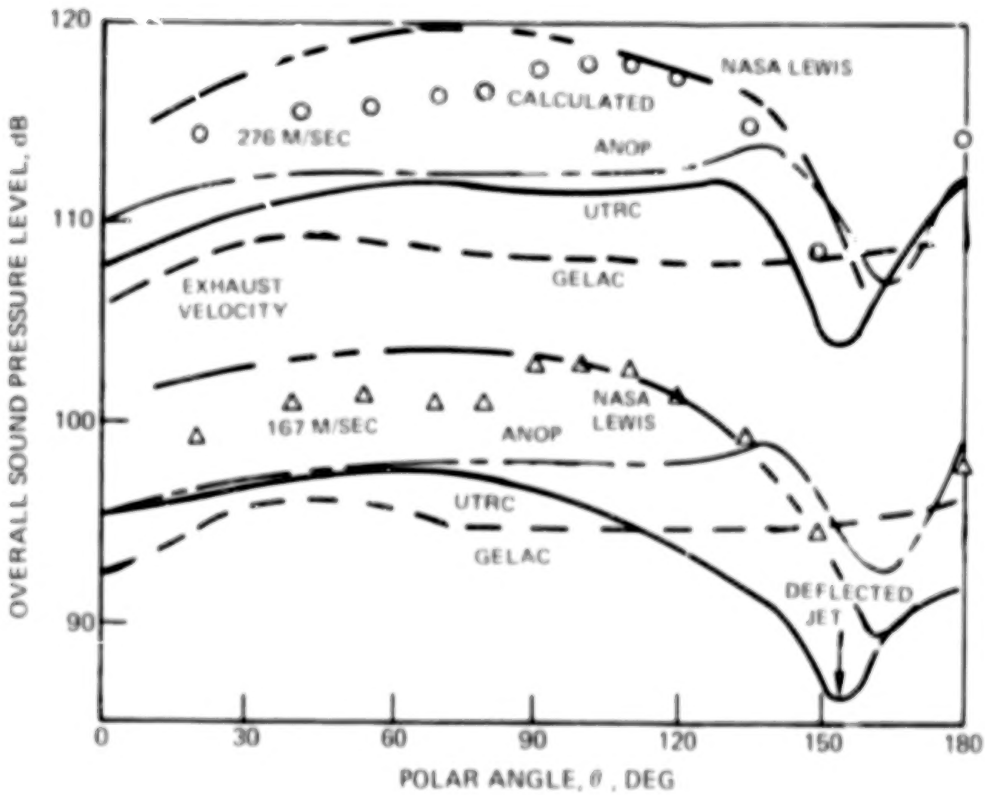
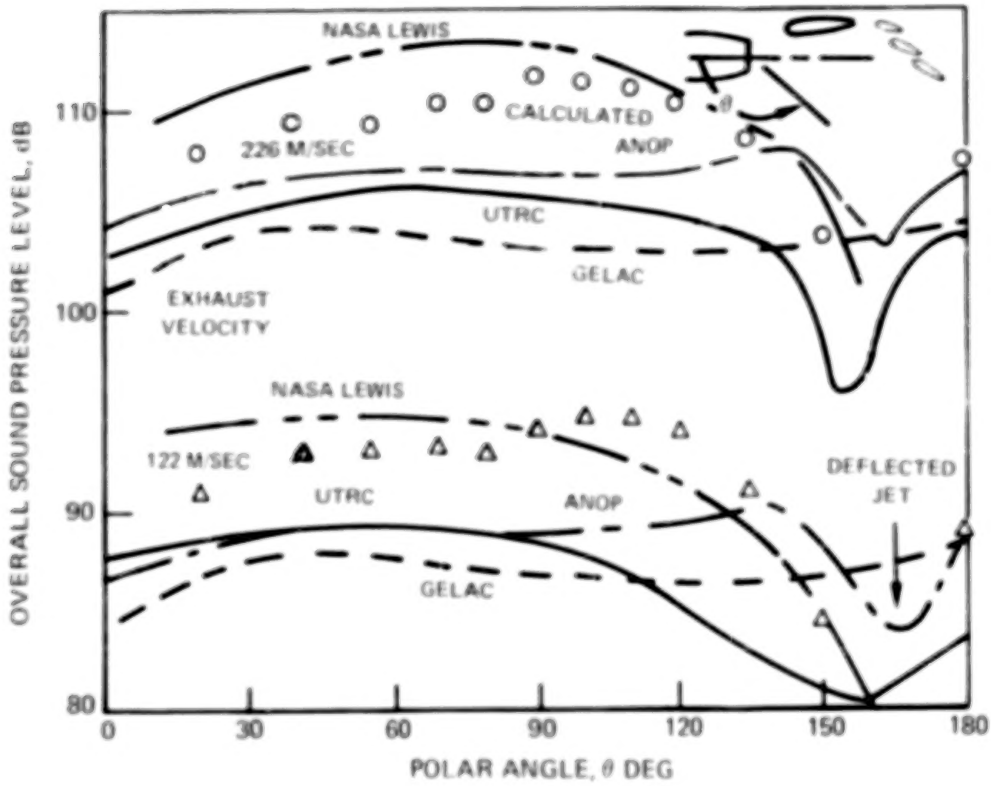


FIGURE 8. — CALCULATED AND MEASURED OASPL DIRECTIVITY IN THE FLYOVER PLANE FOR UTRC MODEL TAKEOFF CONFIGURATION

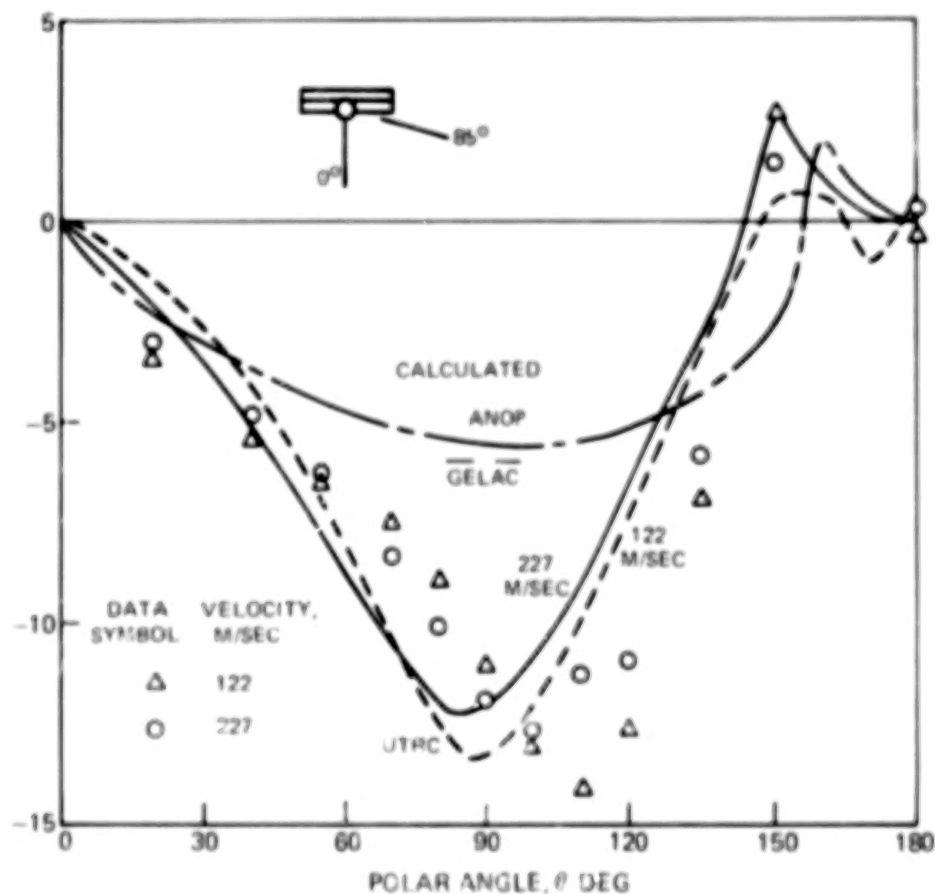
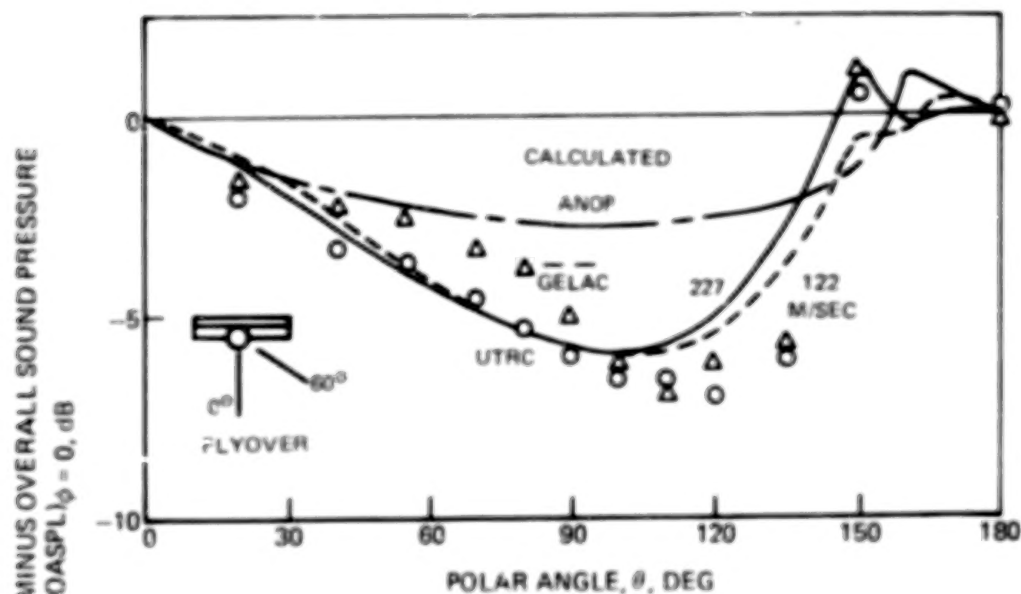
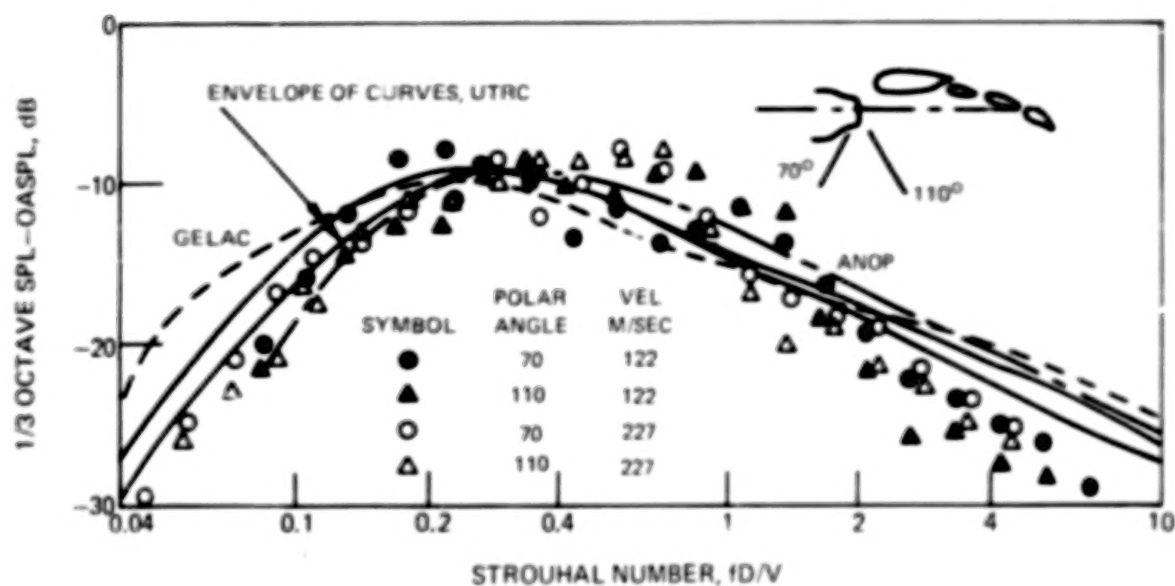
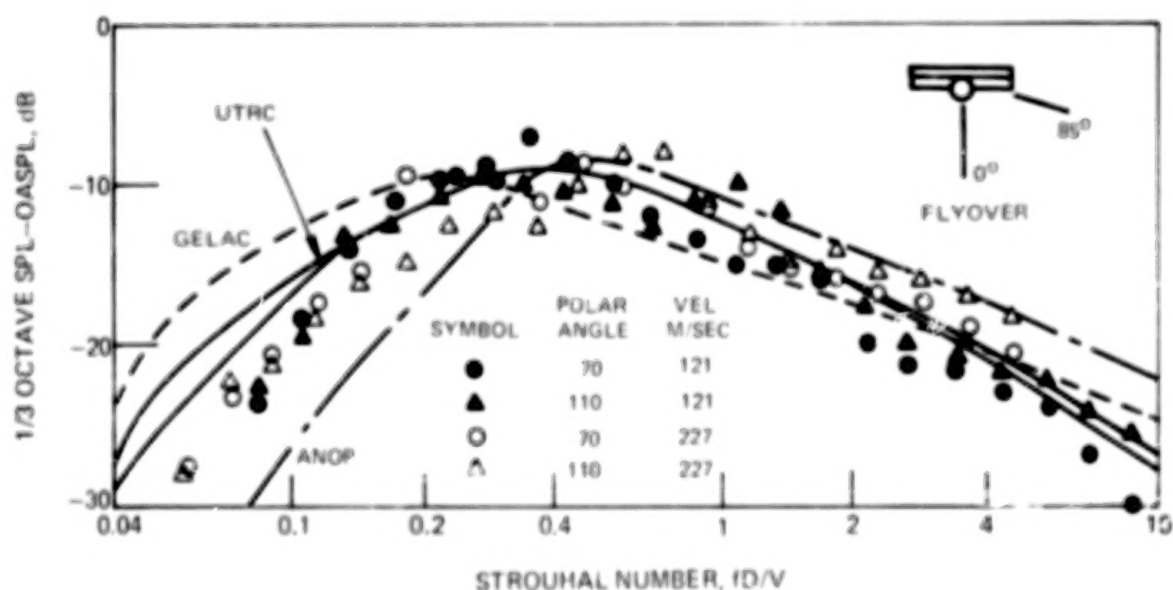


FIGURE 9. - EFFECT OF SIDELINE ANGLE ON CALCULATED AND MEASURED OASPL DIRECTIVITY FOR UTRC MODEL TAKEOFF CONFIGURATION



(a) FLYOVER PLANE



(b) 85° SIDELINE ANGLE

FIGURE 10. - EFFECT OF POLAR ANGLE AND EXHAUST VELOCITY ON CALCULATED AND MEASURED NORMALIZED 1/3 OCTAVE SPECTRA FOR UTW MODEL TAKEOFF CONFIGURATION

CONTENTS

	<u>Page</u>	
SUMMARY.	1	1/A6
INTRODUCTION	2	1/A7
DESCRIPTION OF EBF NOISE PREDICTION METHOD		
Development of Analysis Under This Contract	3	1/A8
Assumptions Within UTRC Method		
Basic Concepts	7	1/A12
UTW Slotted Wing	10	1/B1
UTW Mixer Nozzle	15	1/B6
Upper Surface Blowing.	15	1/B6
UTW Slotless Wing.	17	1/B8
Engine in Front of Wing.	17	1/E8
EVALUATION OF EBF NOISE PREDICTION METHODS		
Other EBF Noise Prediction Methods.	18	1/B9
Designated EBF Model Configurations	21	1/B12
Comparisons With Designated UTW Data		
Triple Slotted Flap, Approach.	22	1/B13
Triple Slotted Flap, Takeoff	24	1/C1
Slotless Version of Three-Flap Wing.	25	1/C2
Comparisons With Designated USB Data		
QCSEE USB, Takeoff	27	1/C4
QCSEE USB, Approach.	30	1/C7
TF-34 Scale Model.	31	1/C8
USB Vane Deflector	32	1/C9
Discussion of Error	34	1/C11
Comparisons for Additional EBF Configurations		
Additional UTW Slotless Wings.	36	1/C13
UTW Mixer Nozzle	39	1/D2
Engine in Front of Wing.	40	1/D3
Noise Predictions for Full-Scale QCSEE Configurations		
Zero Forward Speed	40	1/D3
Effects of Forward Flight.	42	1/D5
CONCLUSIONS.	43	1/D6
RECOMMENDATIONS FOR FUTURE RESEARCH.	44	1/D7
REFERENCES	44	1/D7

	<u>Page</u>
TABLE I: EXTERNALLY BLOWN FLAP MODELS FOR COMPARISON OF MEASURED AND PREDICTED NOISE.	5 1/A10
TABLE II: CAPABILITIES AND LIMITATIONS OF EBF NOISE PREDICTION METHOD	19 1/B10
TABLE III: OASPL AND PNL PREDICTION ERROR FOR 90° FLYOVER POSITION. .	35 1/C1
APPENDIX A: LIST OF SYMBOLS.	49 1/D12
APPENDIX B: LIST OF PUBLICATIONS PRODUCED.	50 1/D13
APPENDIX C: COMPUTER PROGRAM FOR CALCULATING EBF NOISE	
General Description.	52 1/E1
Input Variables.	54 1/E3
Test Case.	56 1/E5
Program Listing.	57 1/E6
Test Case Output	64 1/F7
APPENDIX D: NOISE SOURCE LOCATION FOR UPPER SURFACE BLOWING	
Purpose of Experiment.	68 1/F11
Apparatus and Procedure	
Test Apparatus.	69 1/F12
Procedure	70 1/F13
Presentation and Interpretation of Data	
Velocity and Turbulence Profiles.	71 1/F14
Crosscorrelation Traces	71 1/F14
Results of Crosscorrelation	74 1/G3

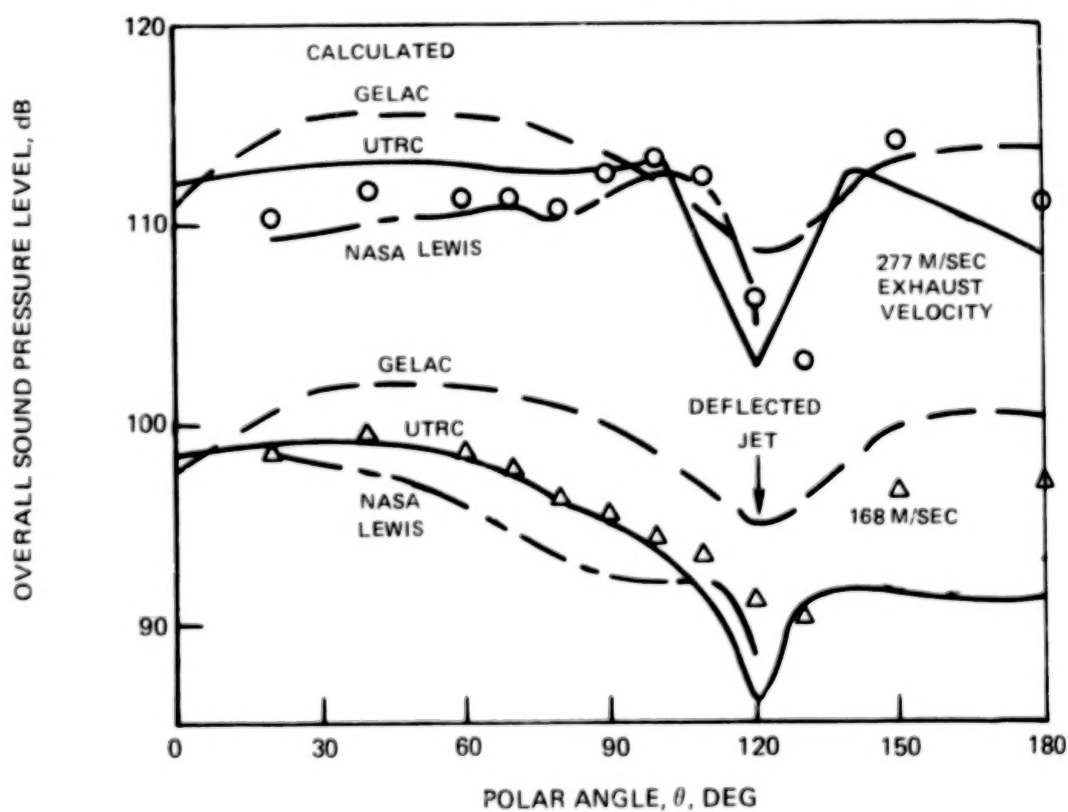
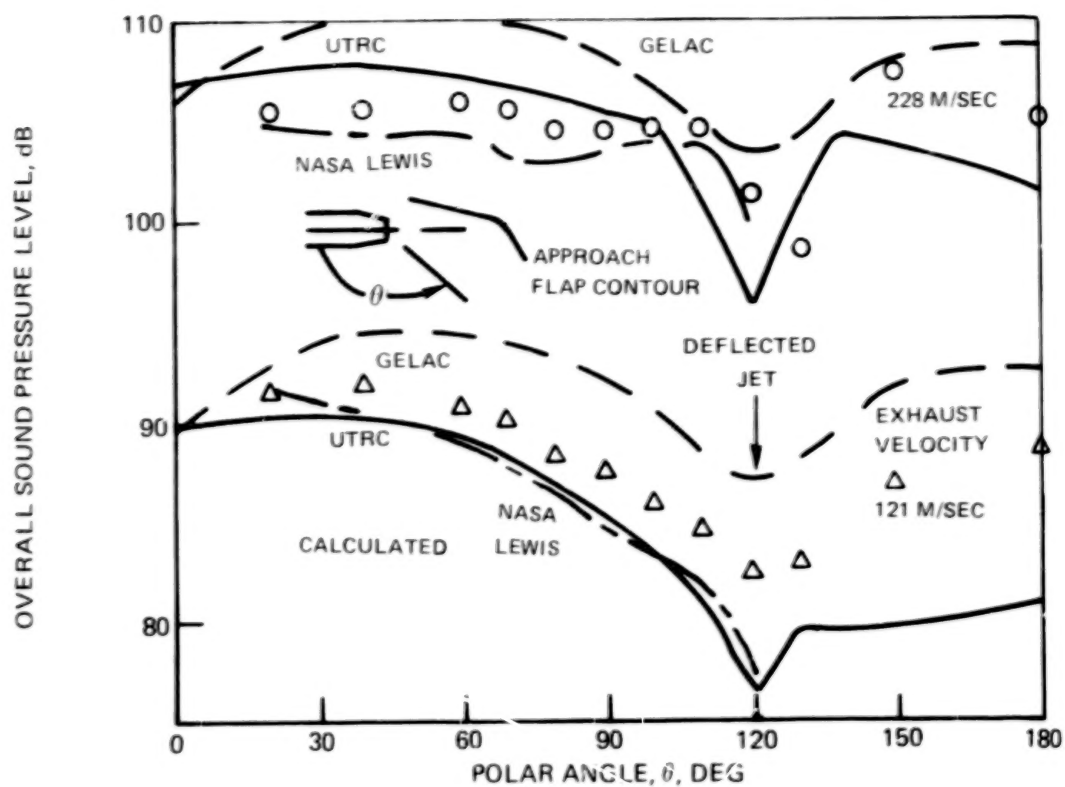


FIGURE 11.— CALCULATED AND MEASURED DIRECTIVITY IN THE FLYOVER PLANE FOR UTW MODEL SLOTLESS WING

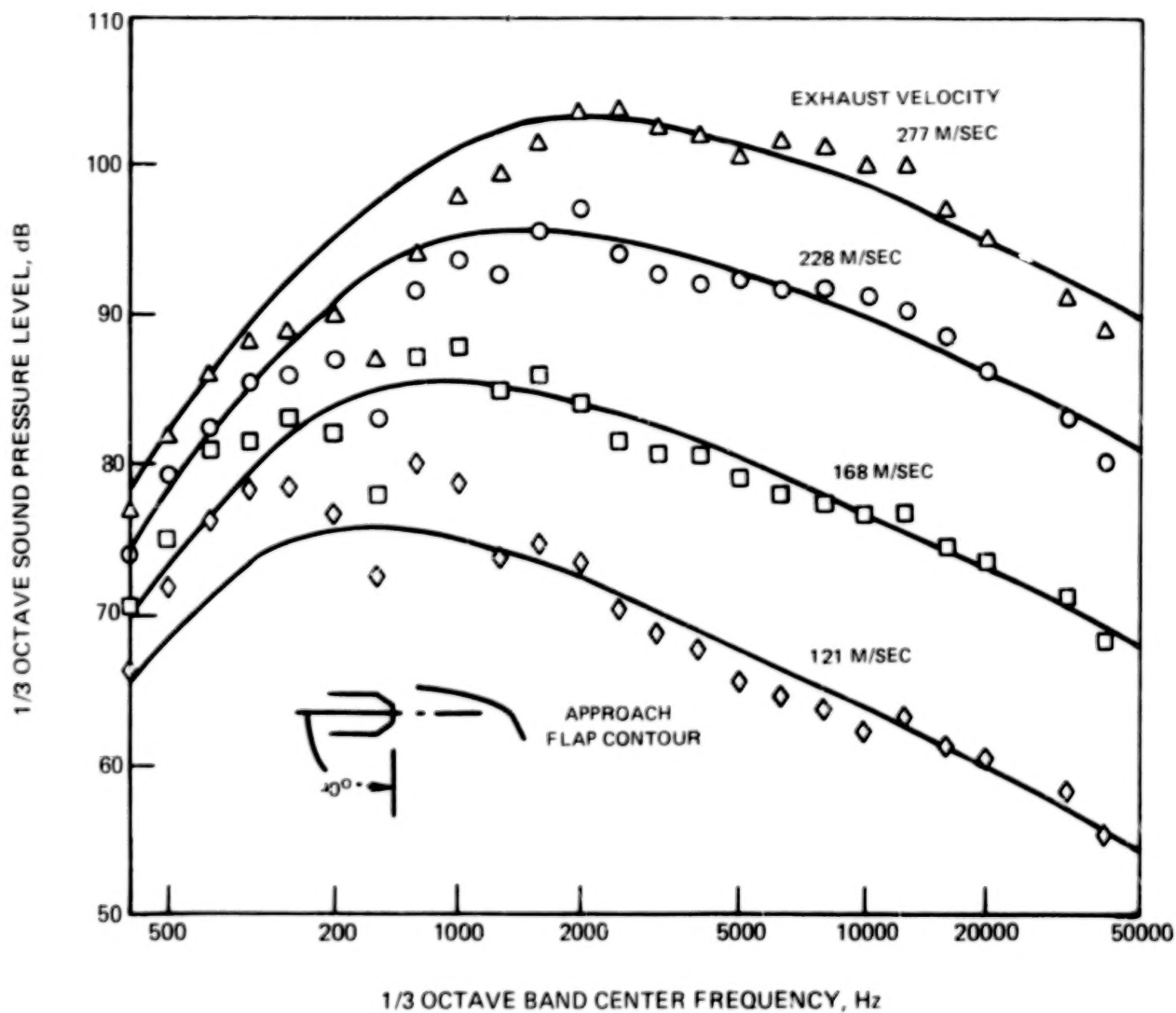


FIGURE 12 COMPARISON OF MEASURED SPECTRA WITH THOSE CALCULATED BY UTRC METHOD FOR POSITION DIRECTLY BENEATH SLOTLESS WING

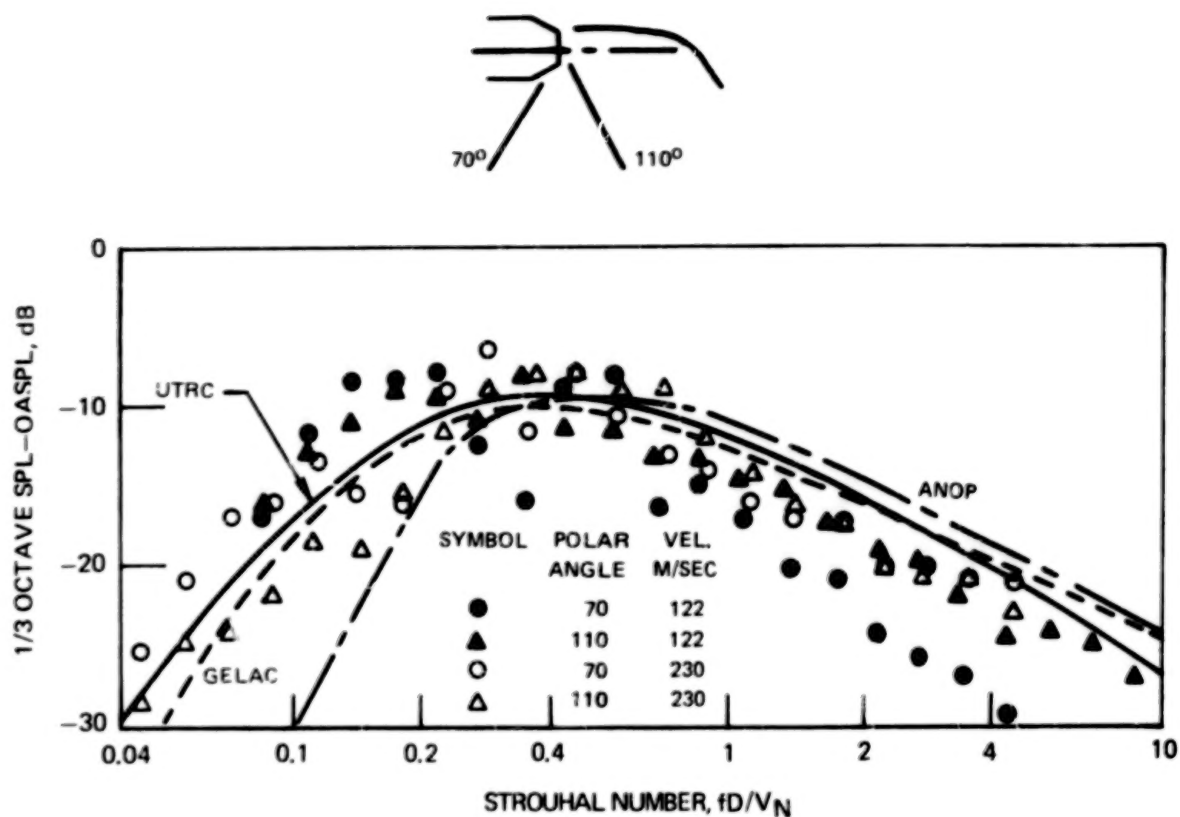


FIGURE 13. - EFFECT OF POLAR ANGLE AND EXHAUST VELOCITY ON CALCULATED AND MEASURED NORMALIZED 1/3 OCTAVE SPECTRA FOR UTW MODEL SLOTLESS WING IN FLYOVER PLANE

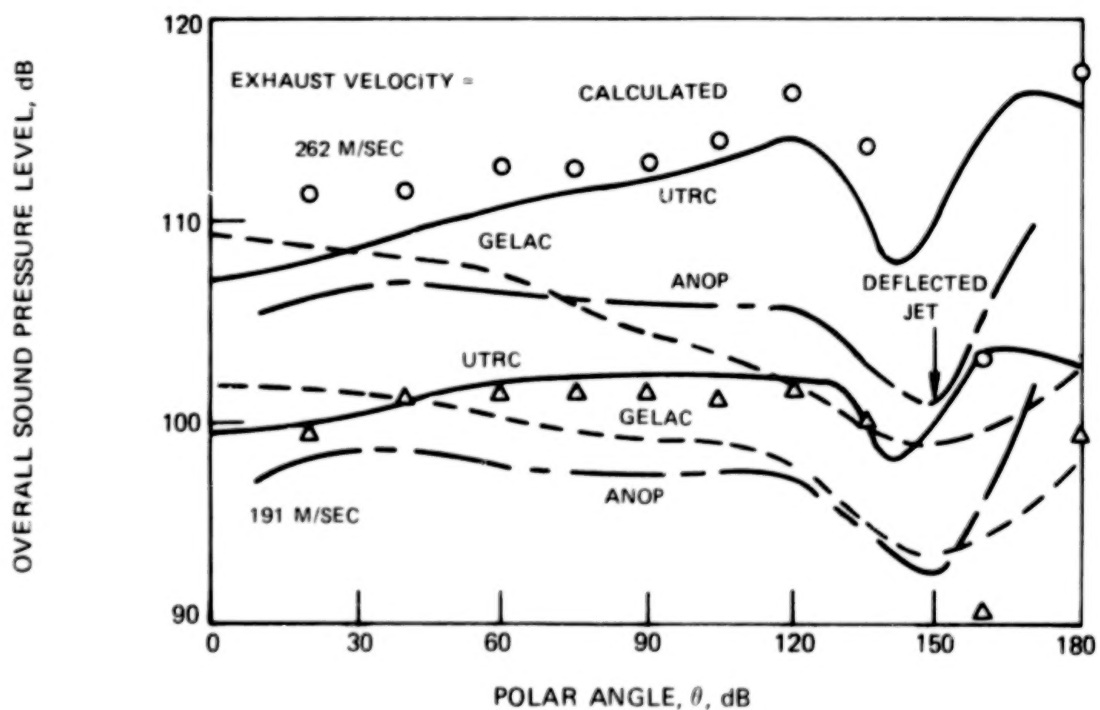
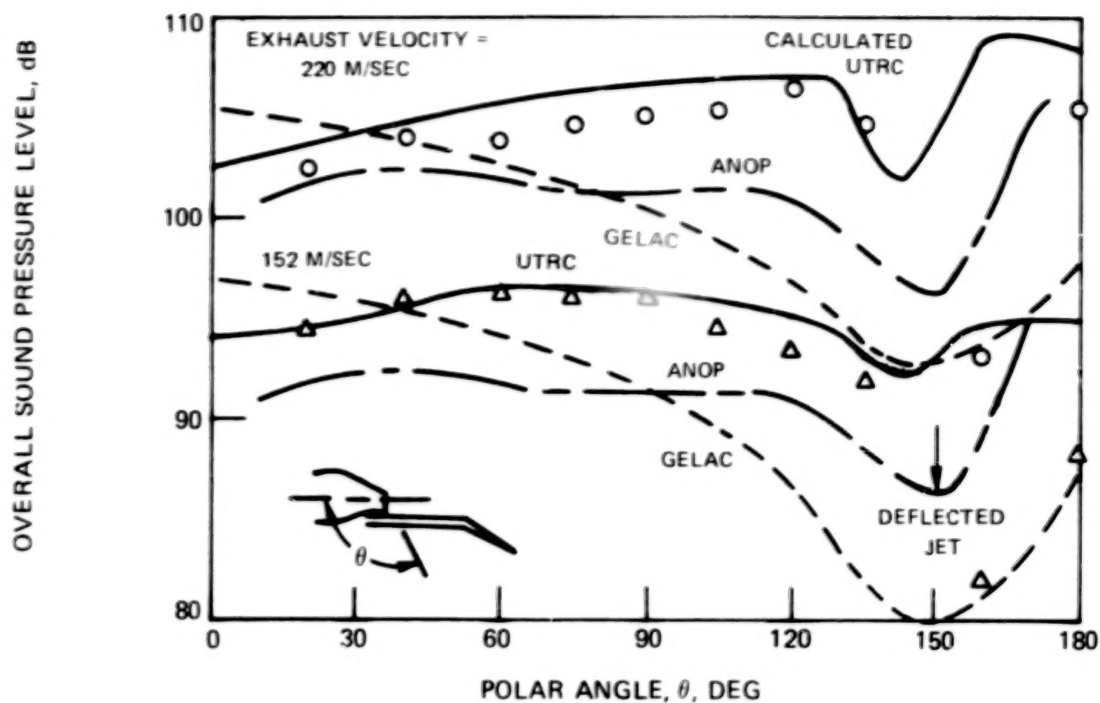


FIGURE 14. — CALCULATED AND MEASURED OASPL DIRECTIVITY IN THE FLYOVER PLANE FOR QCSEE USB 1/11.5 SCALE MODEL, TAKEOFF CONFIGURATION

OVERALL SOUND PRESSURE LEVEL AT SIDELINE ANGLE MINUS
OVERALL SOUND PRESSURE LEVEL AT FLYOVER PLANE, OASPL - OASPL_{φ=0}, dB

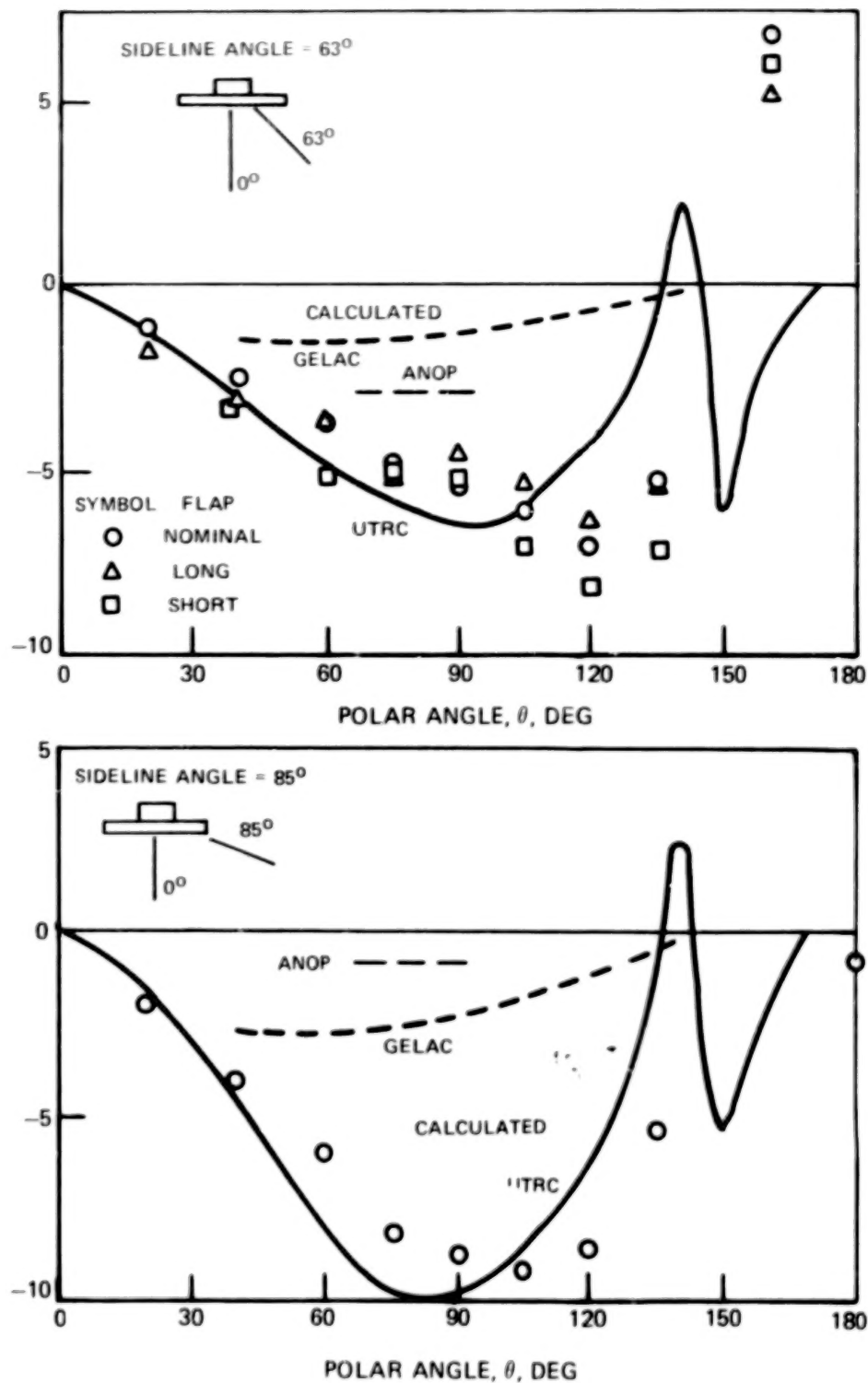
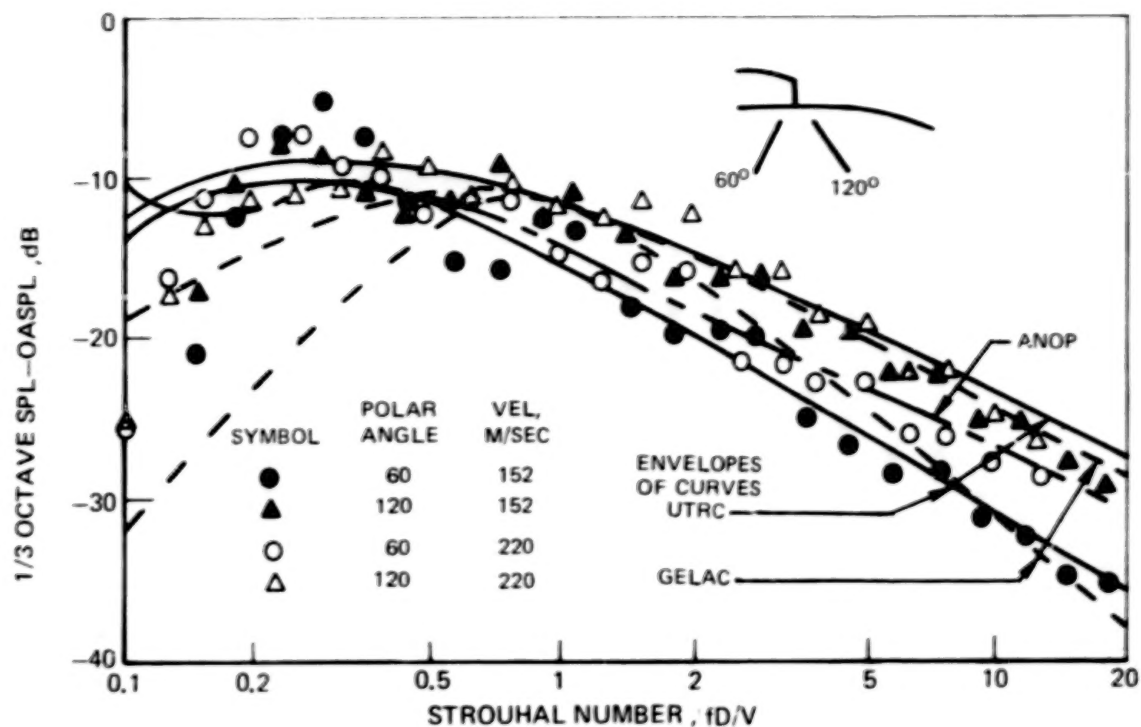
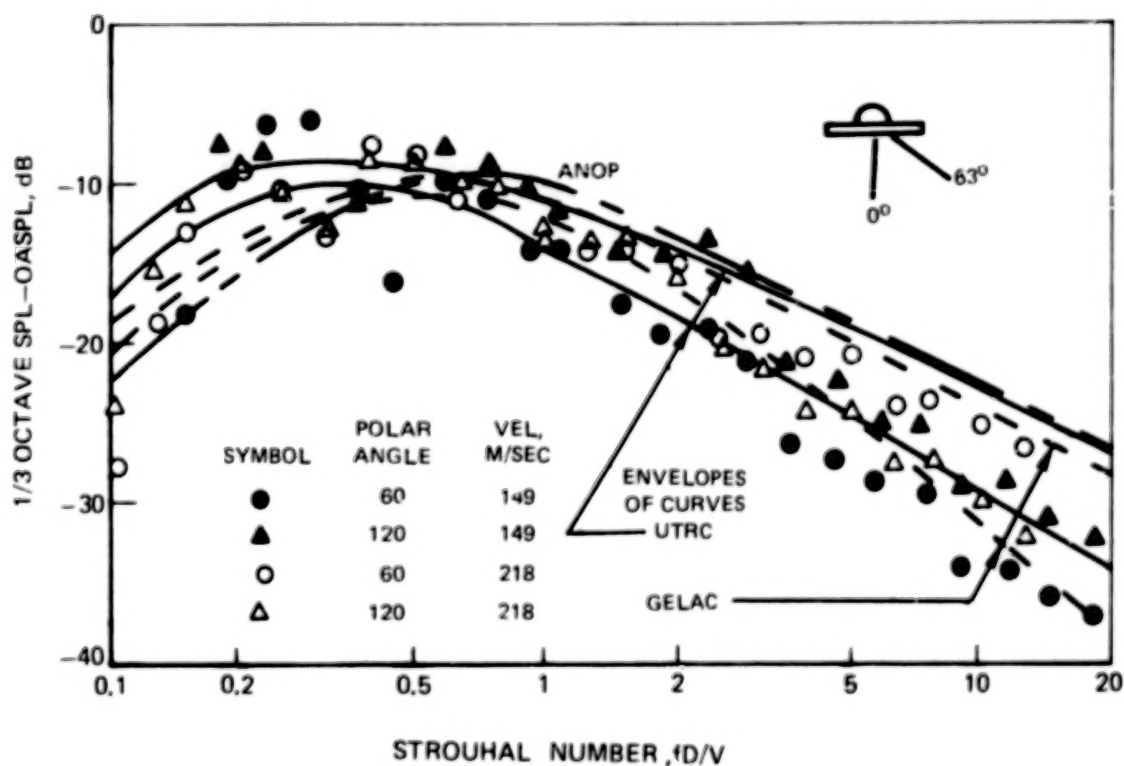


FIGURE 15. — EFFECT OF POLAR ANGLE ON CALCULATED AND MEASURED SIDELINE DIRECTIVITY FOR QCSEE USB 1/1.5 SCALE MODEL, TAKEOFF CONFIGURATION, 218 M/SEC EXHAUST VELOCITY



(a) FLYOVER PLANE



(b) 63° SIDELINE PLANE

FIGURE 16. - EFFECT OF POLAR ANGLE AND EXHAUST VELOCITY ON CALCULATED AND MEASURED NORMALIZED 1/3 OCTAVE SPECTRA FOR QCSEE 1/11.5 SCALE USB MODEL TAKEOFF CONFIGURATION

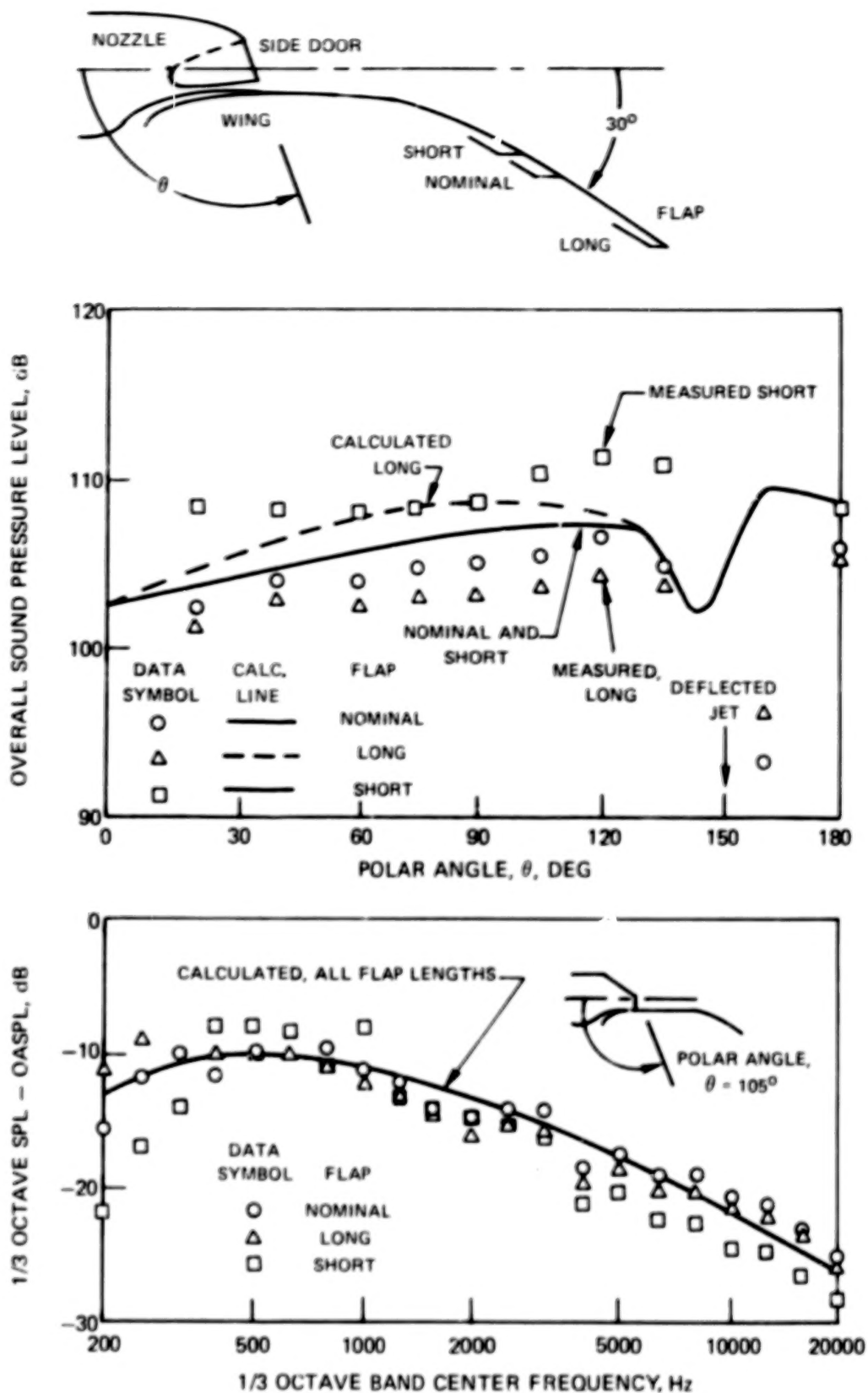


FIGURE 17. — EFFECT OF FLAP LENGTH ON DIRECTIVITY AND NORMALIZED SPECTRUM OF NOISE FROM QCSEE USB 1/11.5 SCALE MODEL, TAKEOFF CONFIGURATION, 218 M/SEC EXHAUST VELOCITY

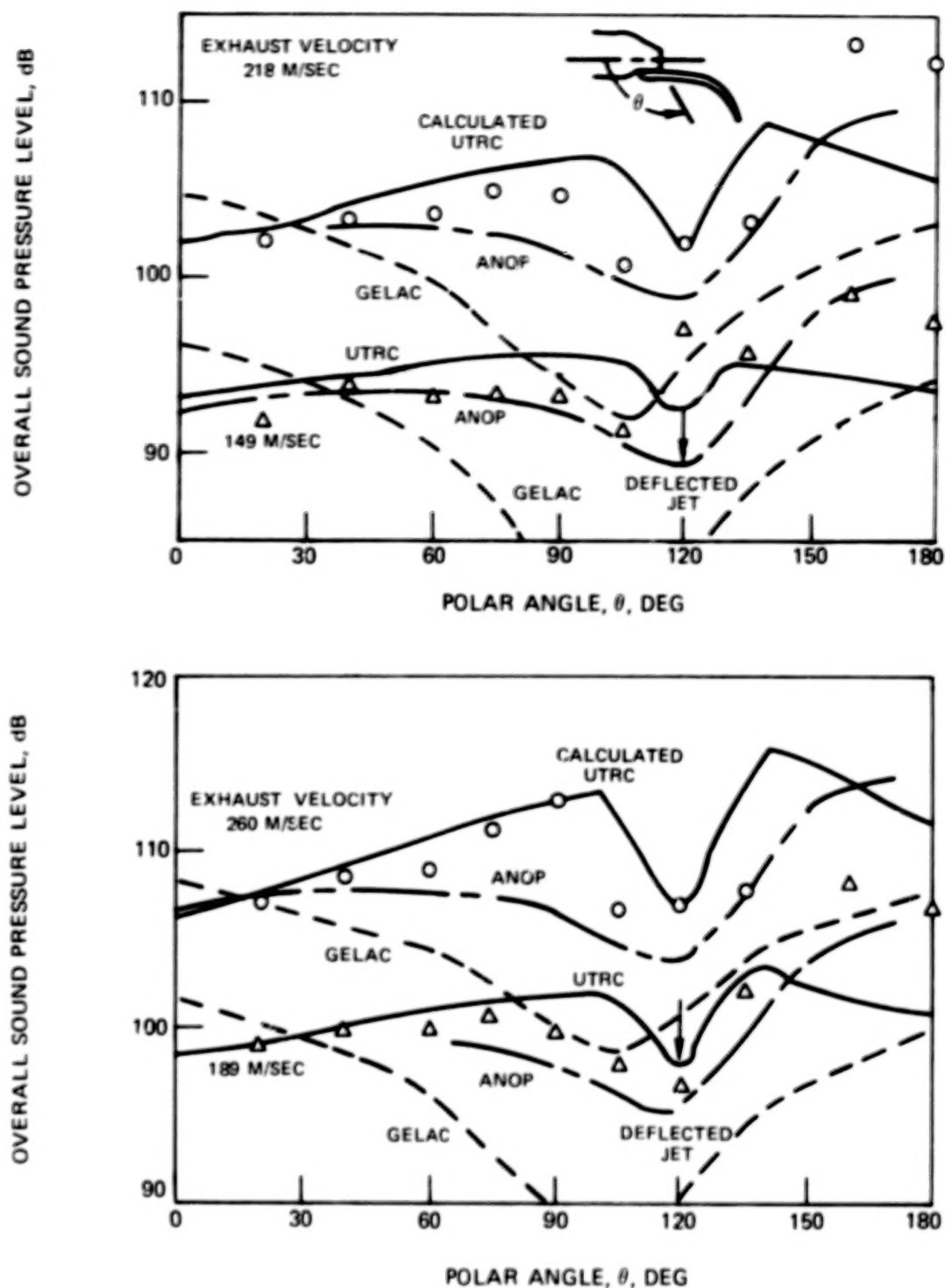


FIGURE 18. – CALCULATED AND MEASURED OASPL DIRECTIVITY IN THE FLYOVER PLANE FOR QCSEE USB 1/11.5 SCALE MODEL APPROACH CONFIGURATION

OVERALL SOUND PRESSURE LEVEL AT SIDELINE ANGLE MINUS
OVERALL SOUND PRESSURE LEVEL AT FLYOVER PLANE, OASPL - OASPL₀ = 0, dB

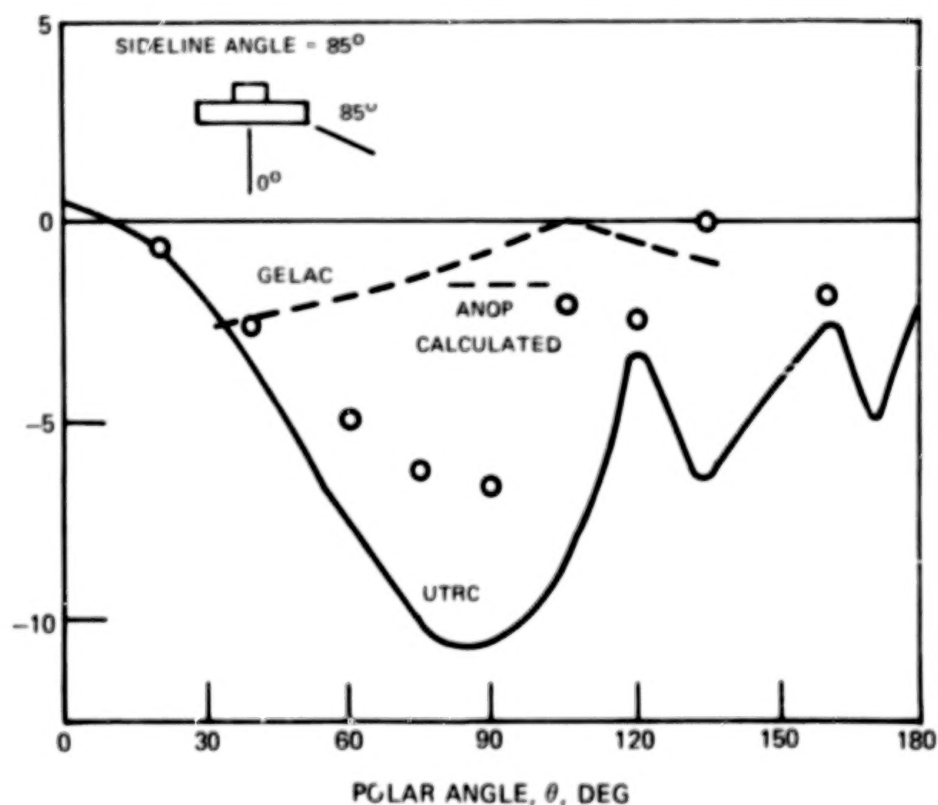
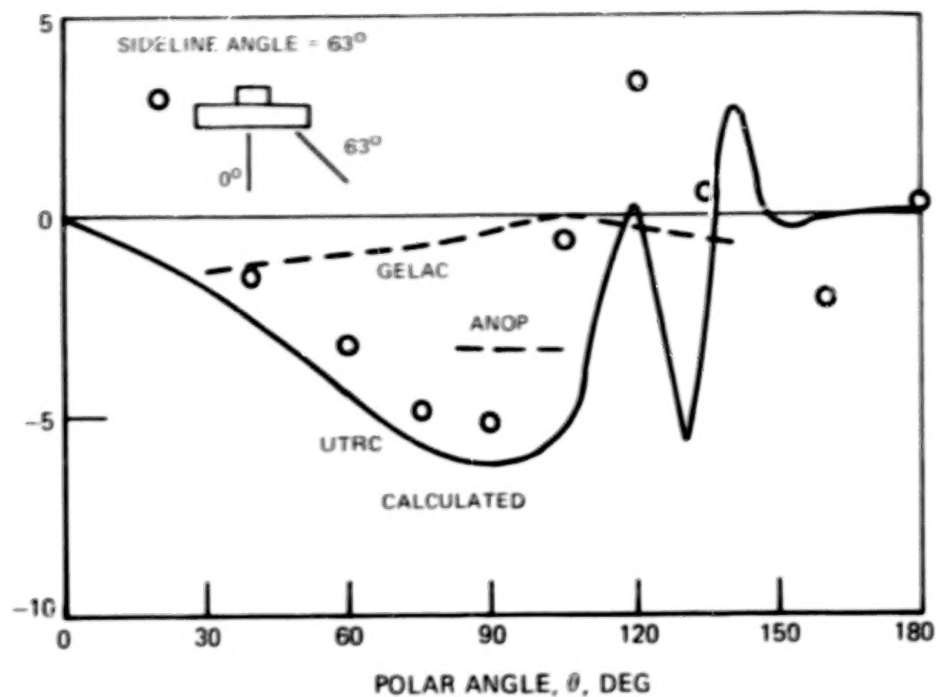
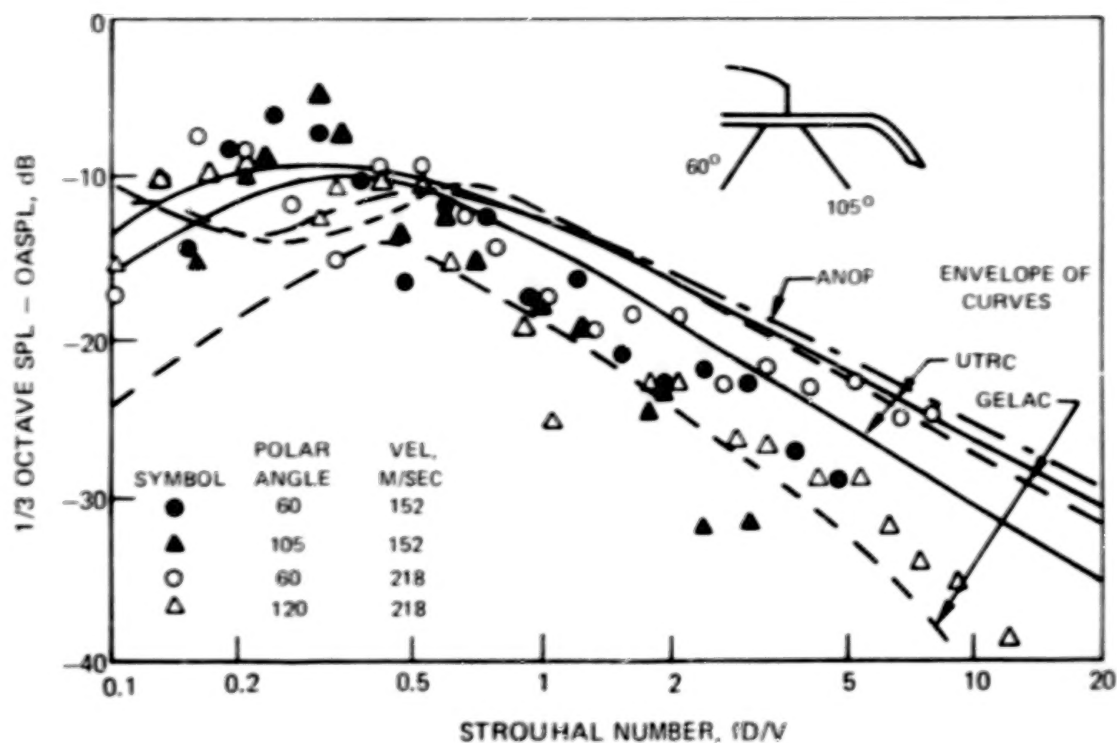
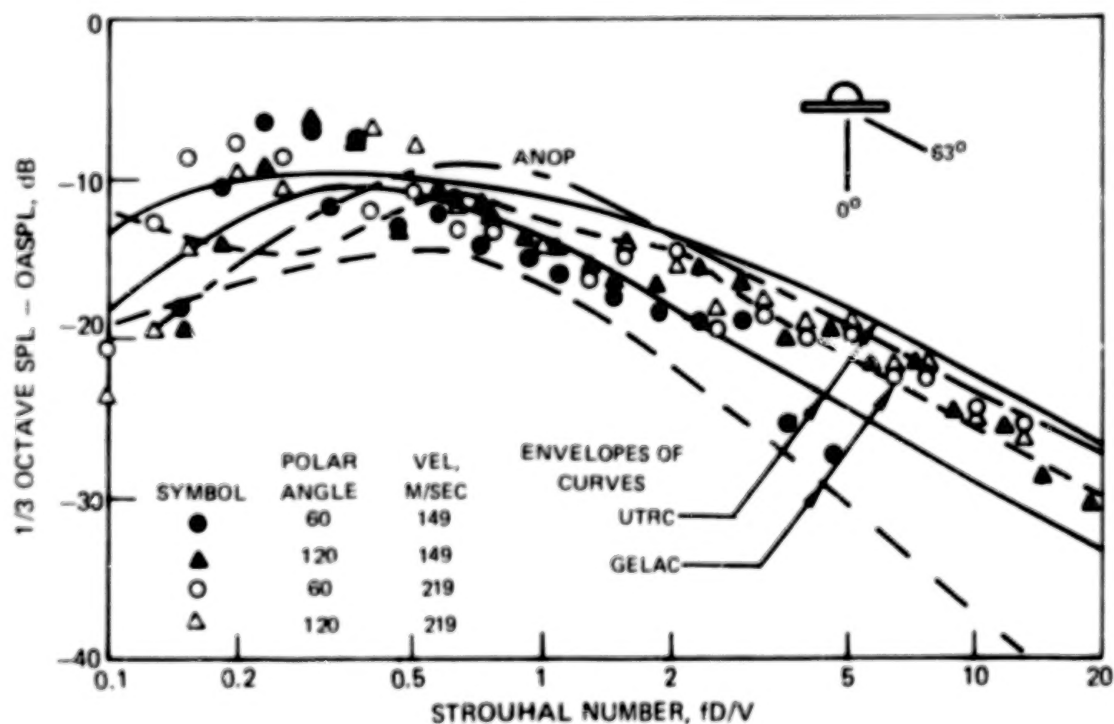


FIGURE 19. - EFFECT OF POLAR ANGLE ON CALCULATED AND MEASURED SIDELINE DIRECTIVITY FOR QCSEE USB 1/11.5 SCALE MODEL, APPROACH CONFIGURATION, 190 M/SEC EXHAUST VELOCITY



(a) FLYOVER PLANE



(b) 63° SIDELINE PLANE

FIGURE 20.- EFFECT OF POLAR ANGLE AND EXHAUST VELOCITY ON CALCULATED AND MEASURED NORMALIZED 1/3 OCTAVE SPECTRA FOR QCSEE 1/11.5 SCALE USB MODEL APPROACH CONFIGURATION

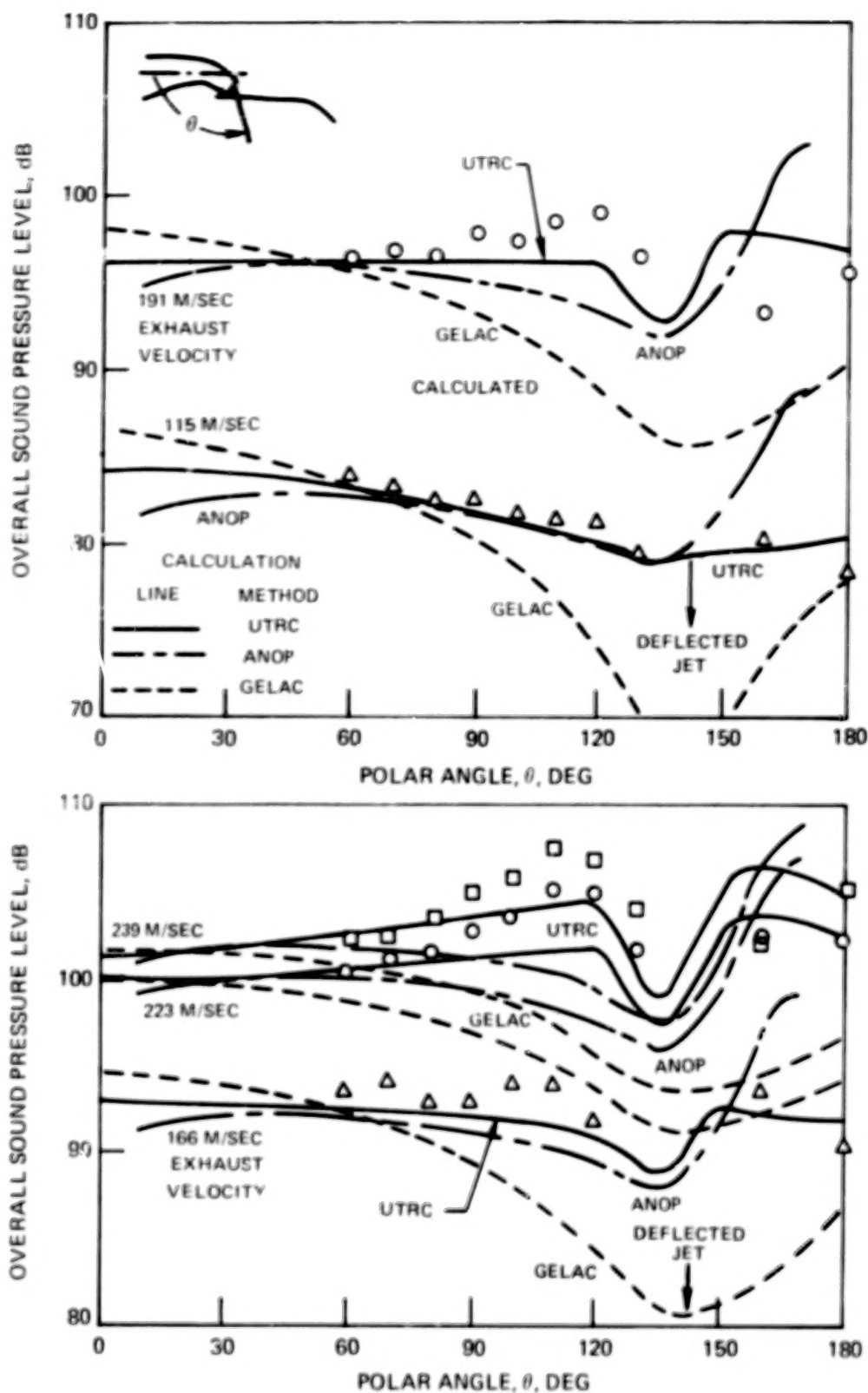


FIGURE 21. — CALCULATED AND MEASURED OASPL DIRECTIVITY IN THE FLYOVER PLANE FOR TF-34 USB 1/18.5 SCALE MODEL WITH SLOT NOZZLE AND 40° DEFLECTION SHORT FLAP

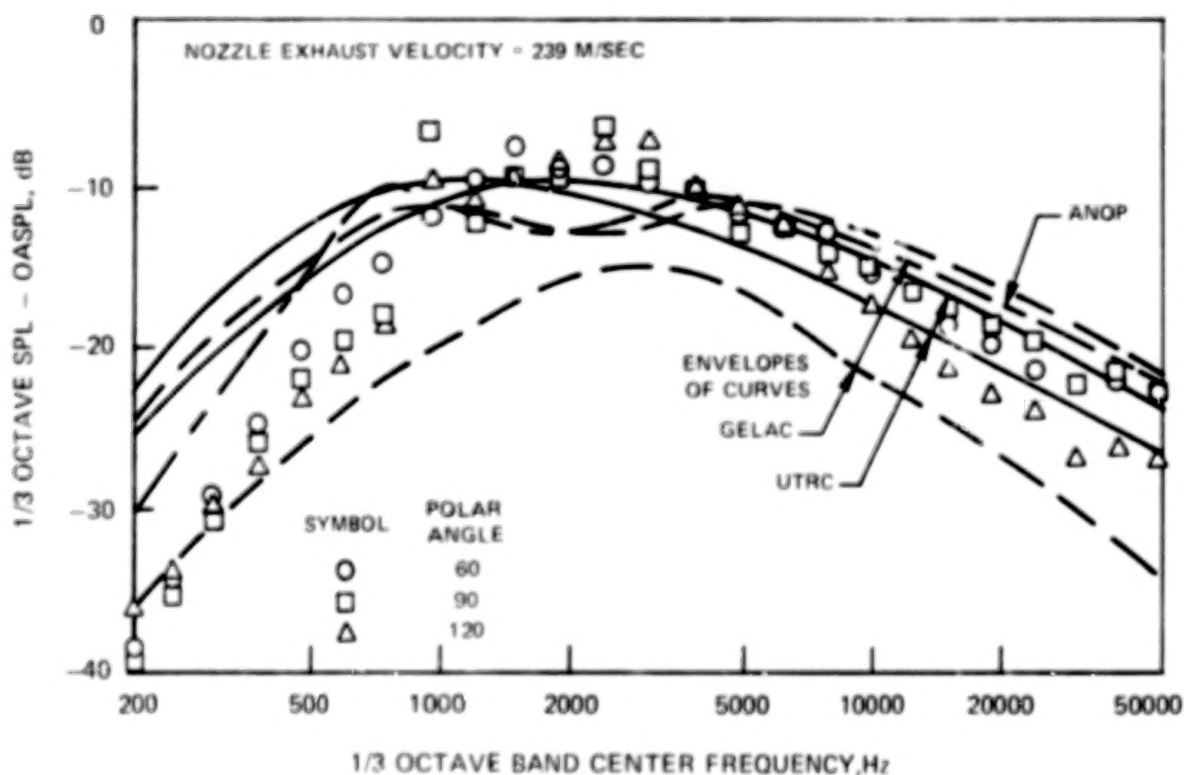
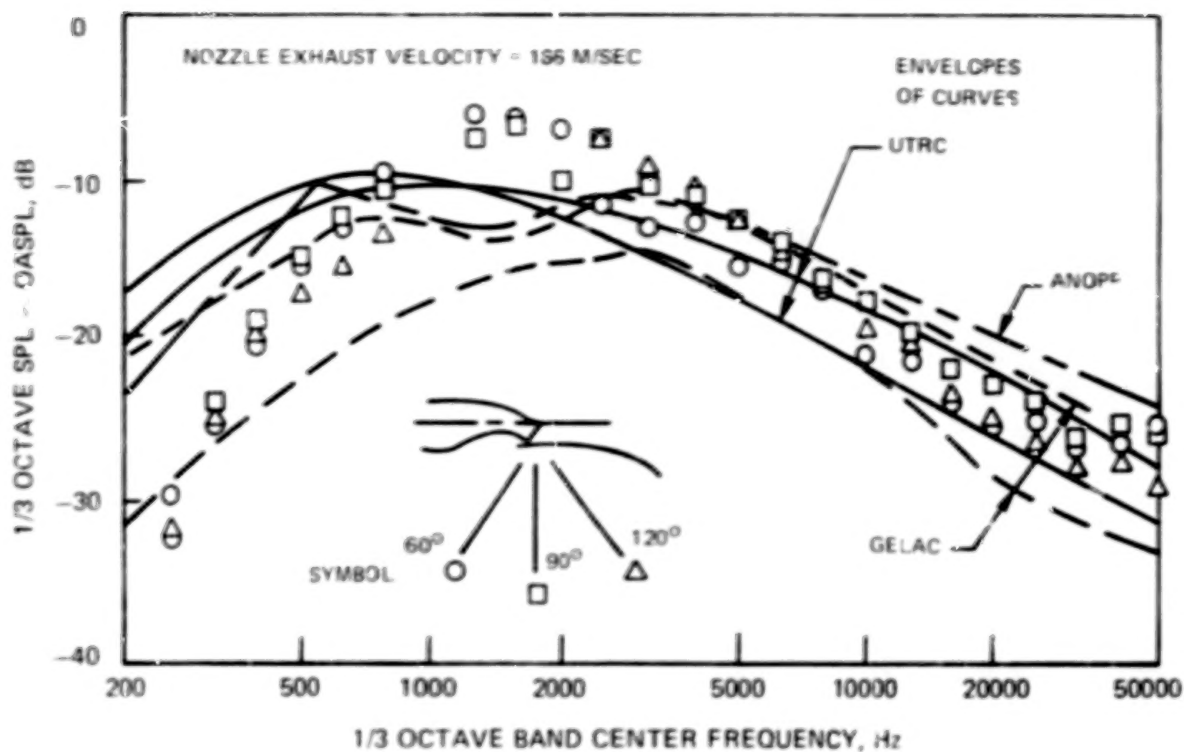


FIGURE 22. - EFFECT OF POLAR ANGLE AT TWO EXHAUST VELOCITIES ON CALCULATED AND MEASURED NORMALIZED 1/3 OCTAVE SPECTRA FOR TF-34 USB 1/18.5 SCALE MODEL WITH SLOT NOZZLE AND 40° DEFLECTION SHORT FLAP

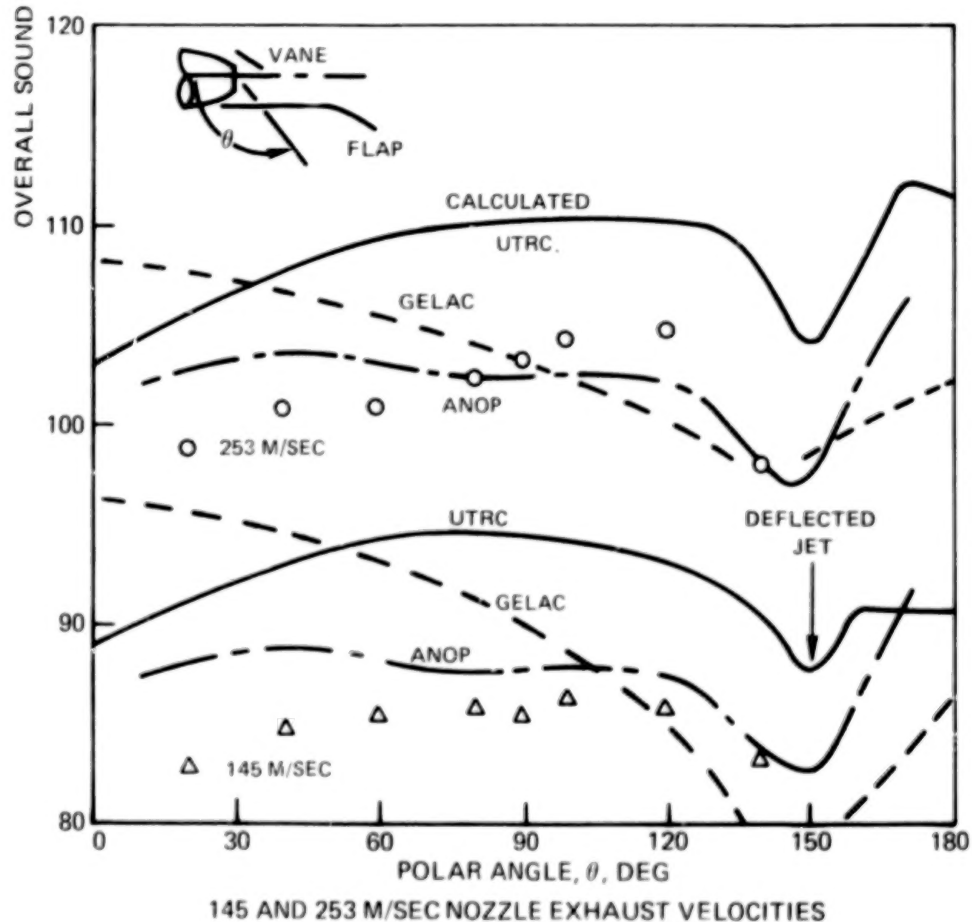
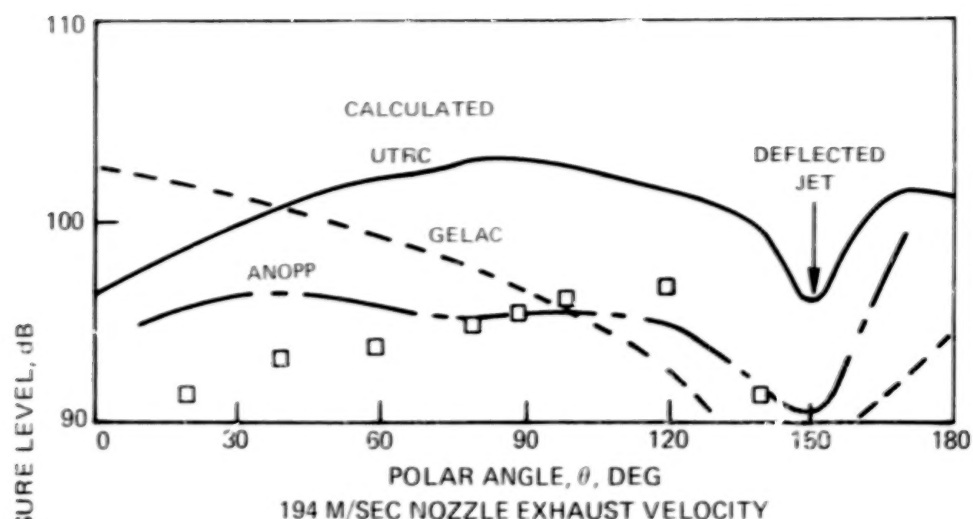


FIGURE 23. — CALCULATED AND MEASURED OASPL DIRECTIVITY IN THE FLYOVER PLANE FOR USB WITH CIRCULAR NOZZLE AND VANE DEFLECTOR IN TAKEOFF CONFIGURATION

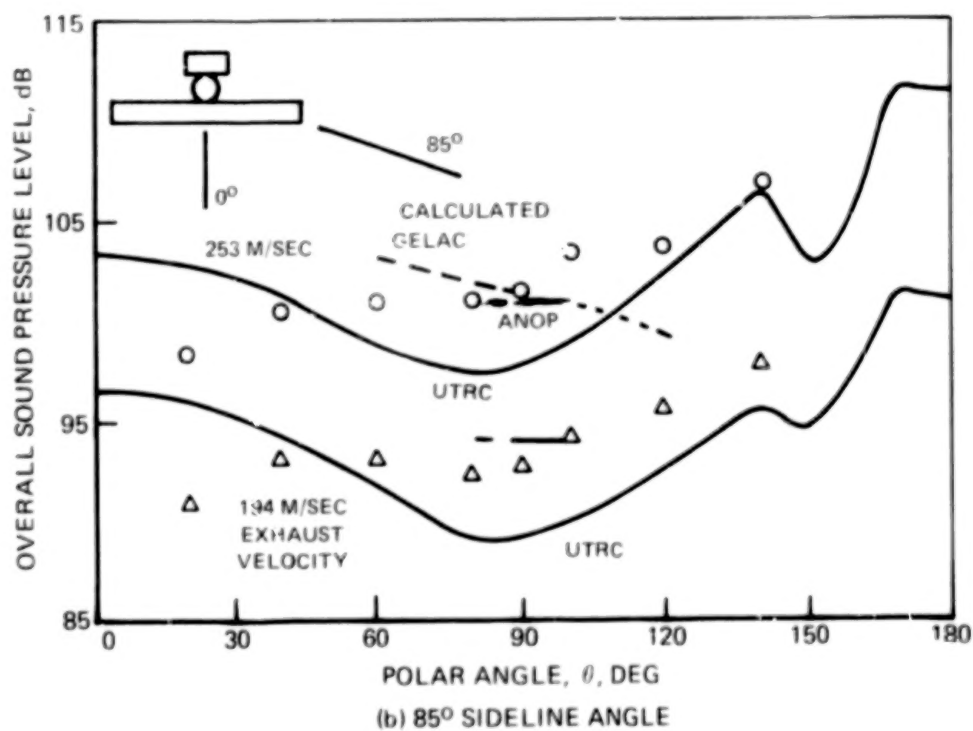
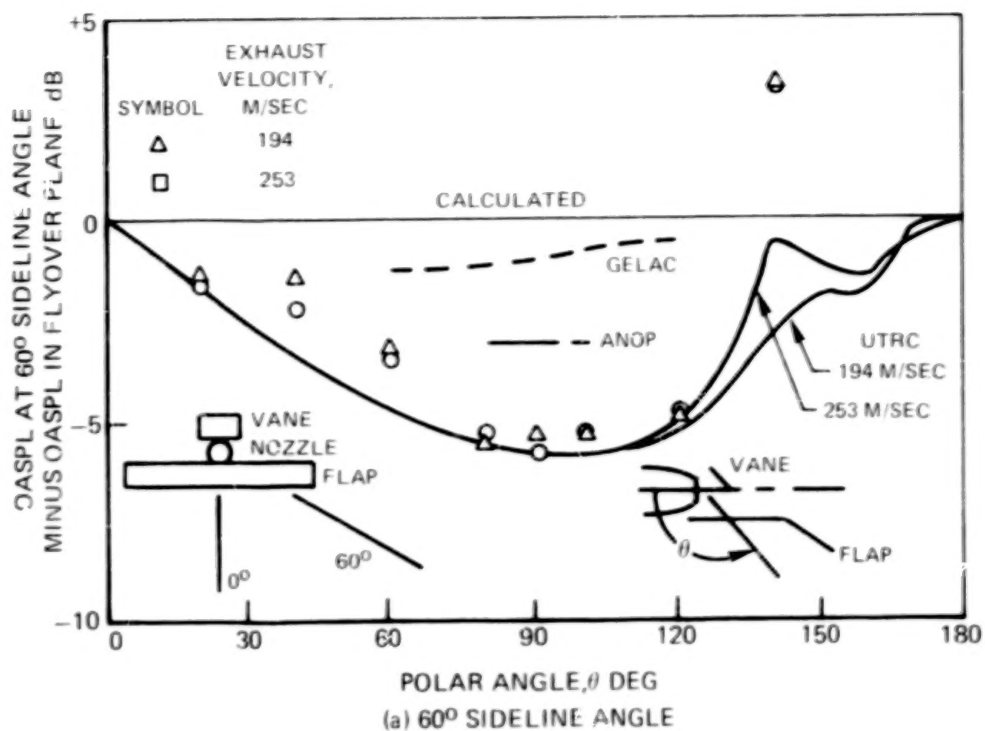
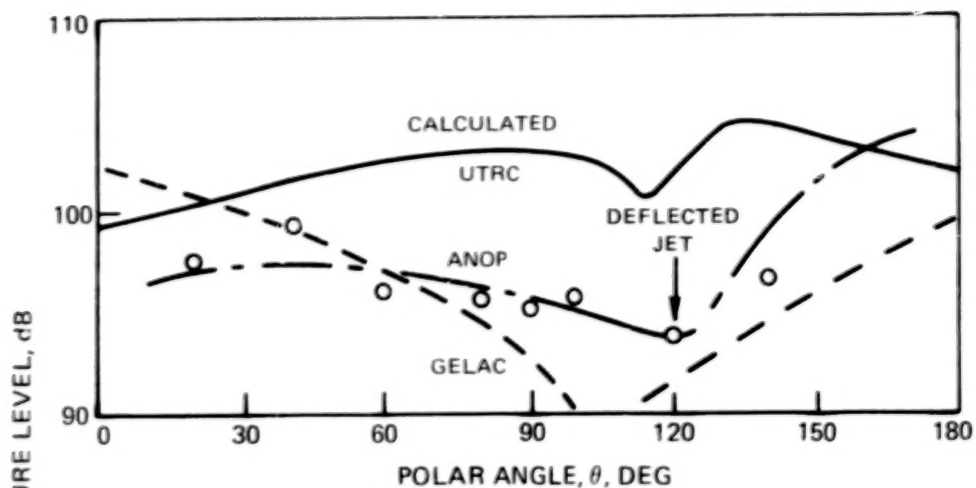
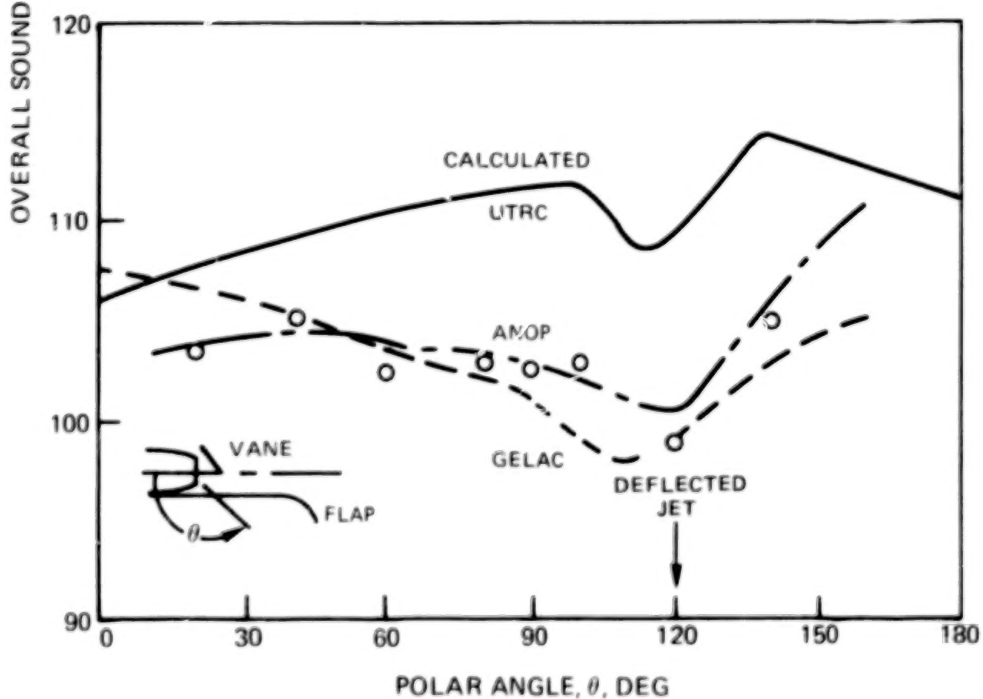


FIGURE 24.— EFFECT OF POLAR ANGLE ON CALCULATED AND MEASURED SIDELINE DIRECTIVITY FOR USB WITH CIRCULAR NOZZLE AND VANE DEFLECTOR IN TAKEOFF CONFIGURATION

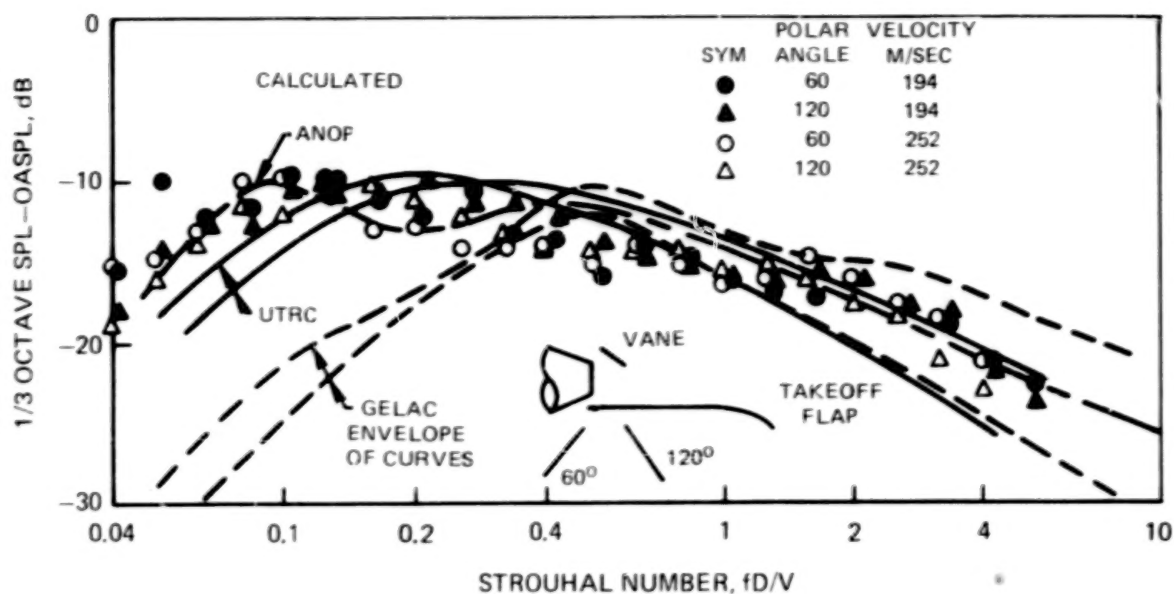


(a) 197 M/SEC NOZZLE EXHAUST VELOCITY

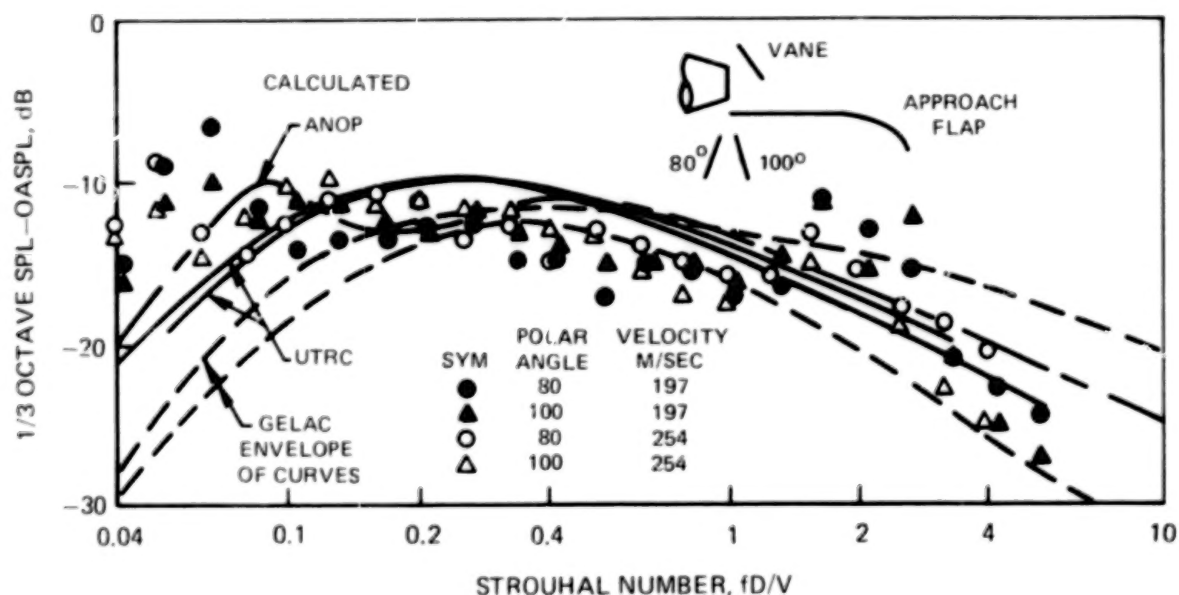


(b) 261 M/SEC NOZZLE EXHAUST VELOCITY

**FIGURE 25.—CALCULATED AND MEASURED OASPL DIRECTIVITY
IN THE FLYOVER PLANE FOR USB WITH CIRCULAR NOZZLE
AND VANE DEFLECTOR IN APPROACH CONFIGURATION**

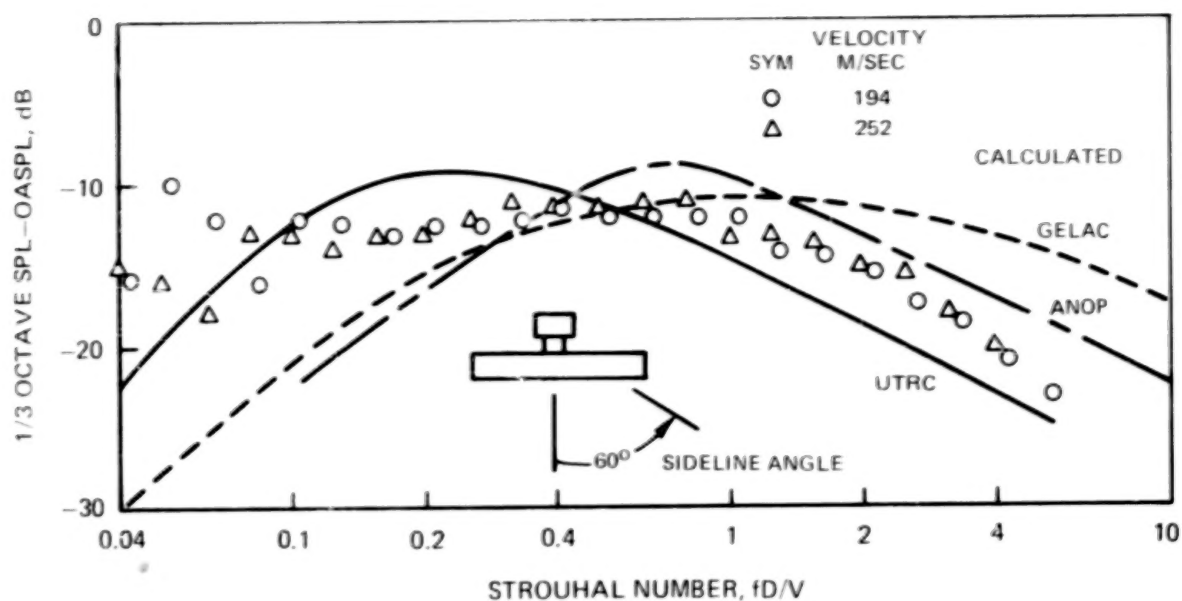


(a) TAKEOFF CONFIGURATION

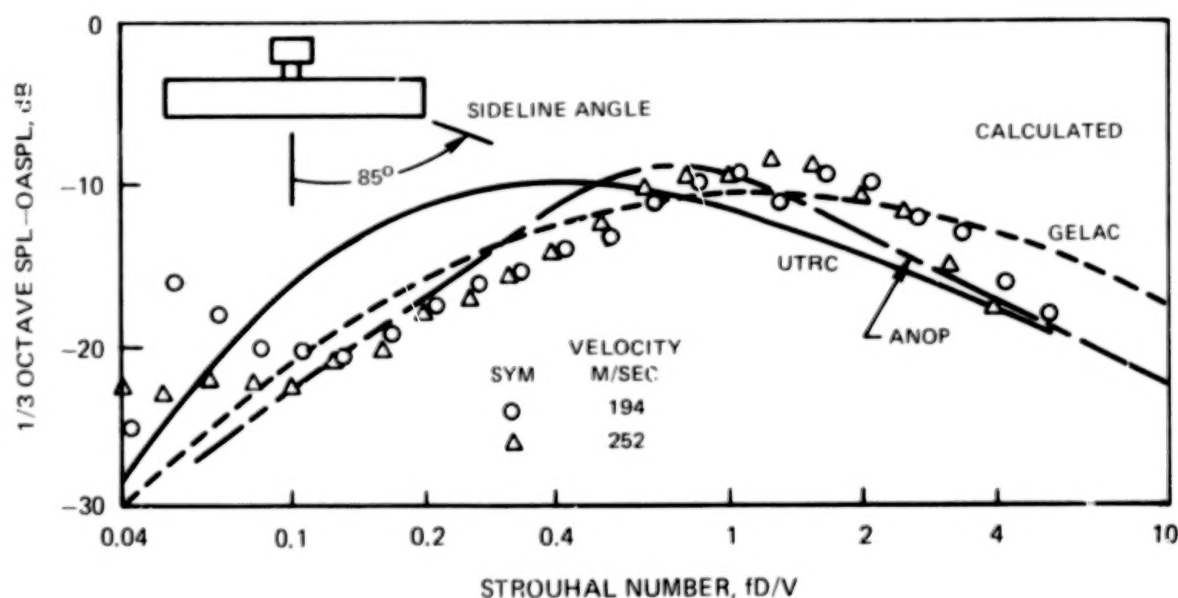


(b) APPROACH CONFIGURATION

FIGURE 26. -EFFECT OF POLAR ANGLE AND EXHAUST VELOCITY ON CALCULATED AND MEASURED NORMALIZED 1/3 OCTAVE SPECTRA IN FLYOVER PLANE FOR USB WITH CIRCULAR NOZZLE AND VANE DEFLECTOR IN TAKEOFF AND APPROACH CONFIGURATIONS



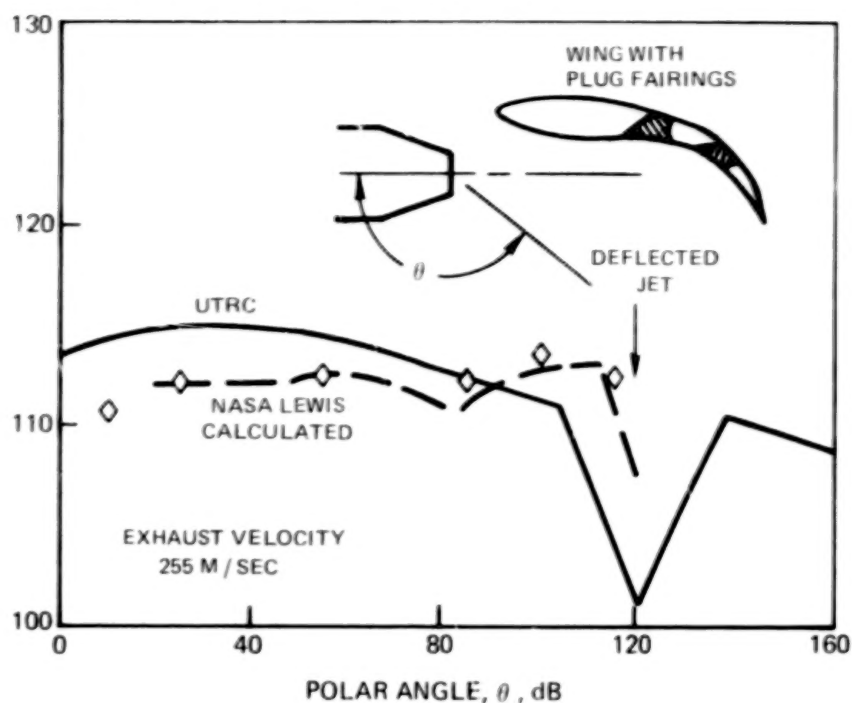
(a) 60° SIDELINE ANGLE



(b) 85° SIDELINE ANGLE

FIGURE 27.—EFFECT OF EXHAUST VELOCITY AND SIDELINE ANGLE ON CALCULATED AND MEASURED NORMALIZED 1/3 OCTAVE SPECTRA AT 90° POLAR ANGLE FOR USB WITH CIRCULAR NOZZLE AND VANE DEFLECTOR IN TAKEOFF CONFIGURATION

OVERALL SOUND PRESSURE LEVEL, dB



OVERALL SOUND PRESSURE LEVEL, dB

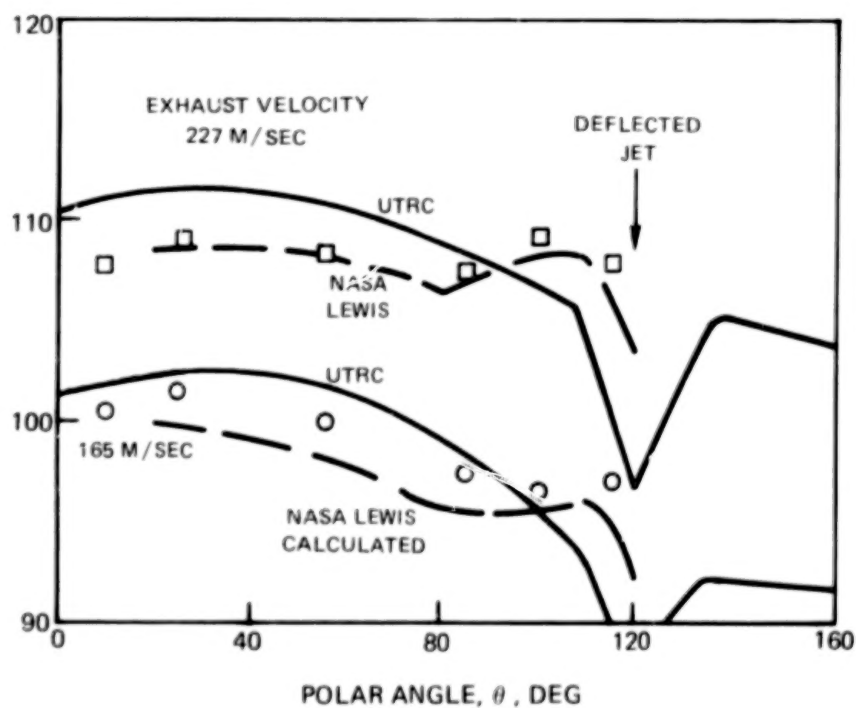


FIGURE 28. — CALCULATED AND MEASURED OASPL DIRECTIVITIES IN THE FLYOVER PLANE FOR LARGE DOUBLE SLOTTED WING WITH PLUG FAIRINGS IN SLOTS

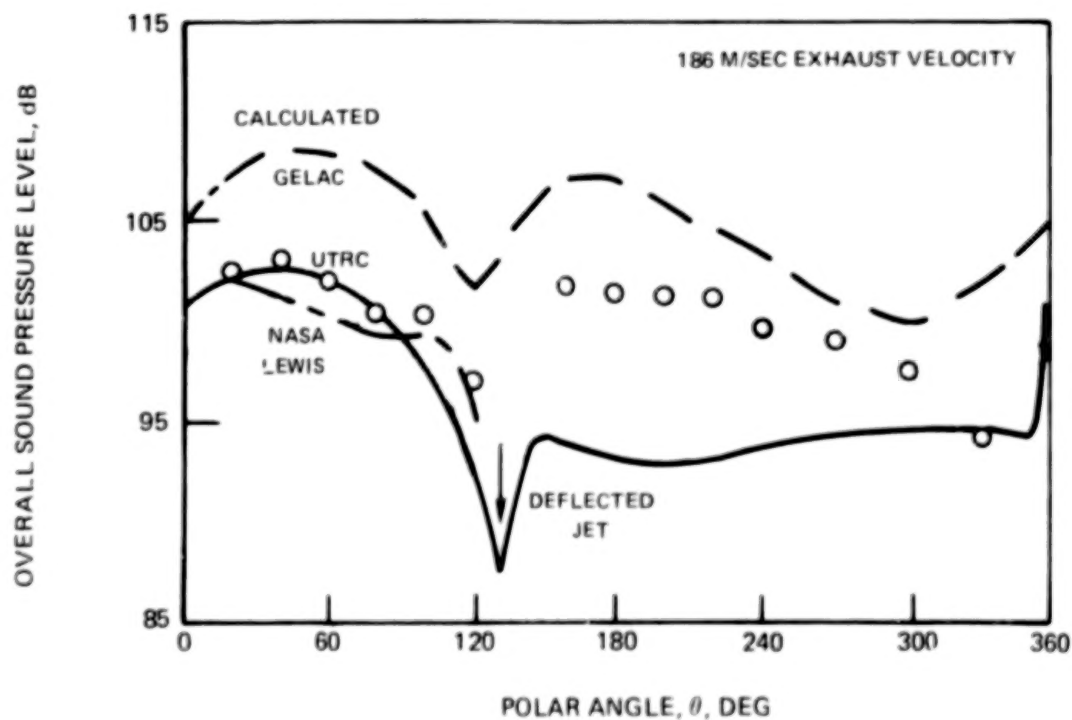
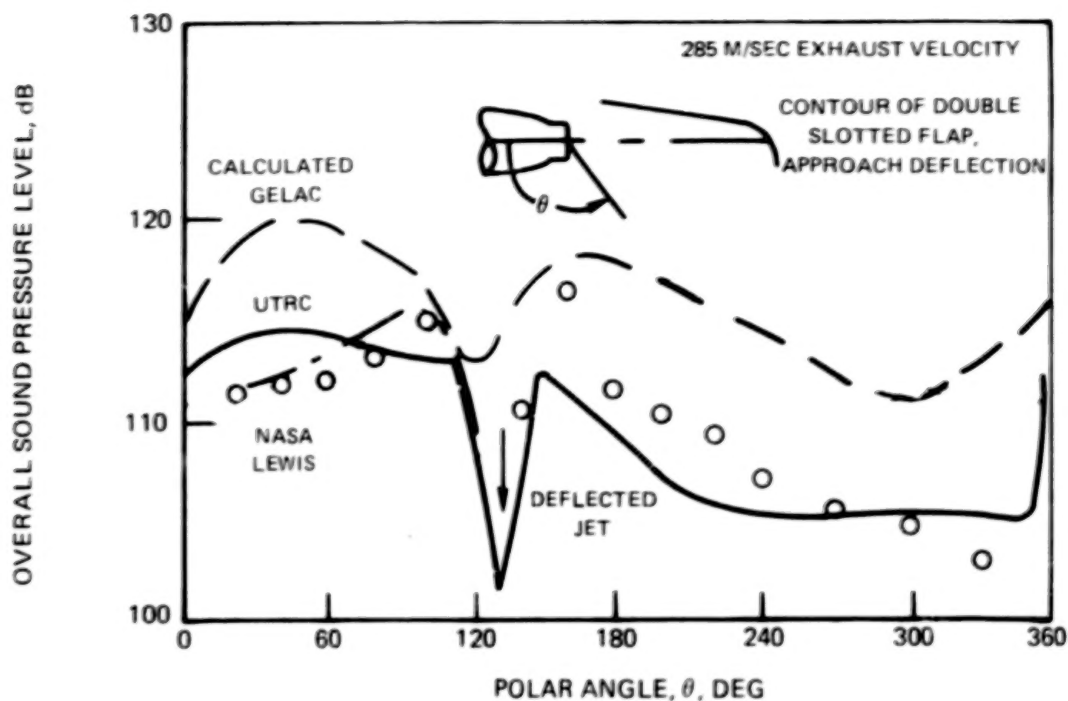
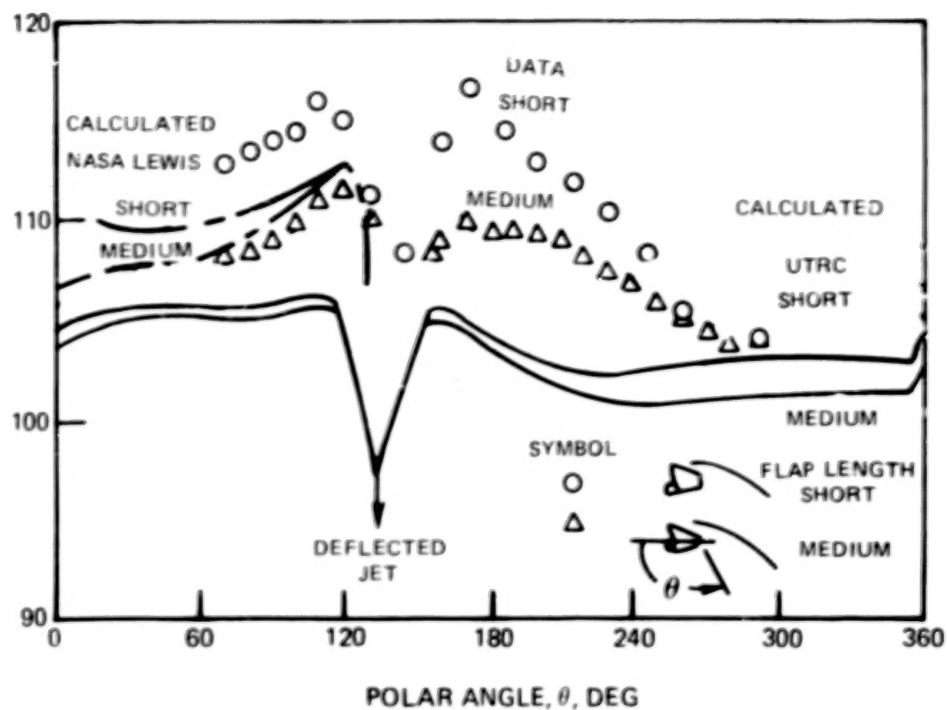


FIGURE 29. — CALCULATED AND MEASURED OASPL DIRECTIVITY IN FLYOVER PLANE FOR UTW MODEL SLOTLESS WING HAVING CONTOUR OF DOUBLE SLOTTED FLAP

OVERALL SOUND PRESSURE LEVEL, dB



OVERALL SOUND PRESSURE LEVEL, dB

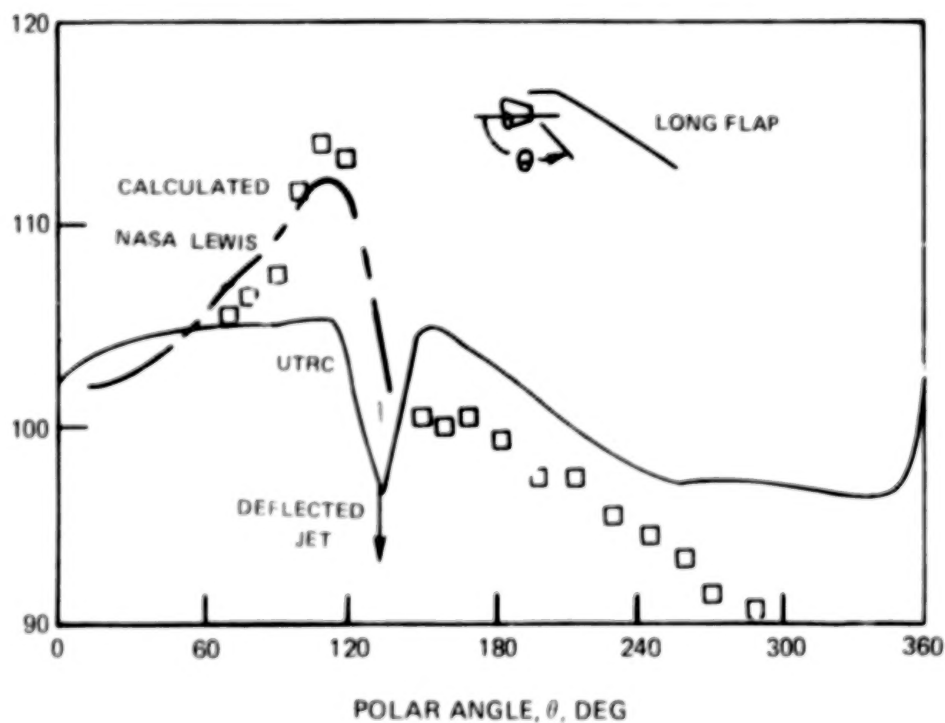
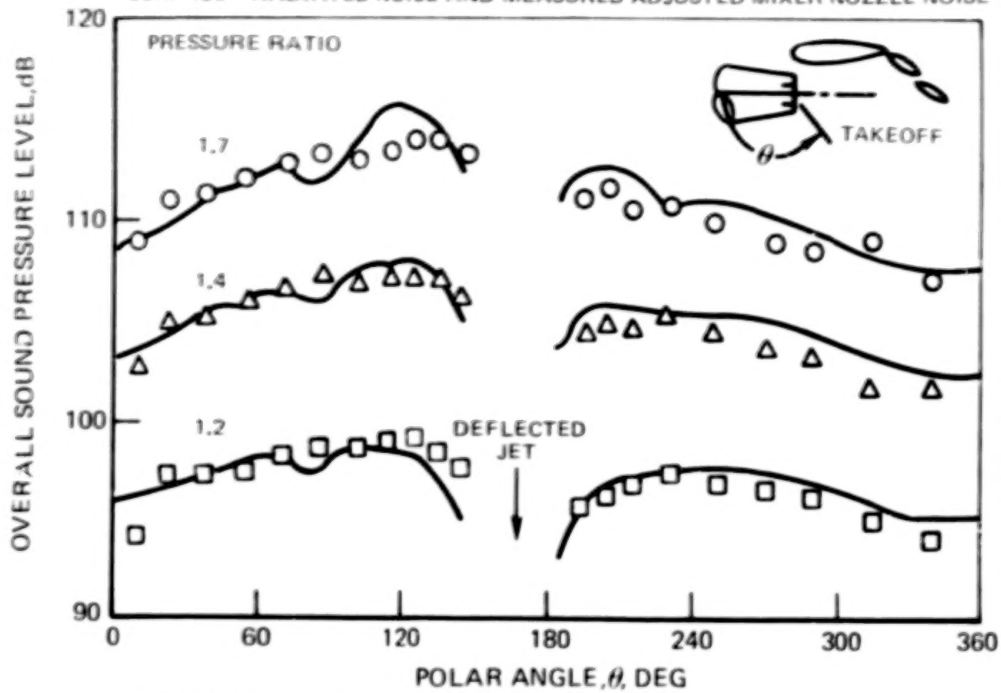
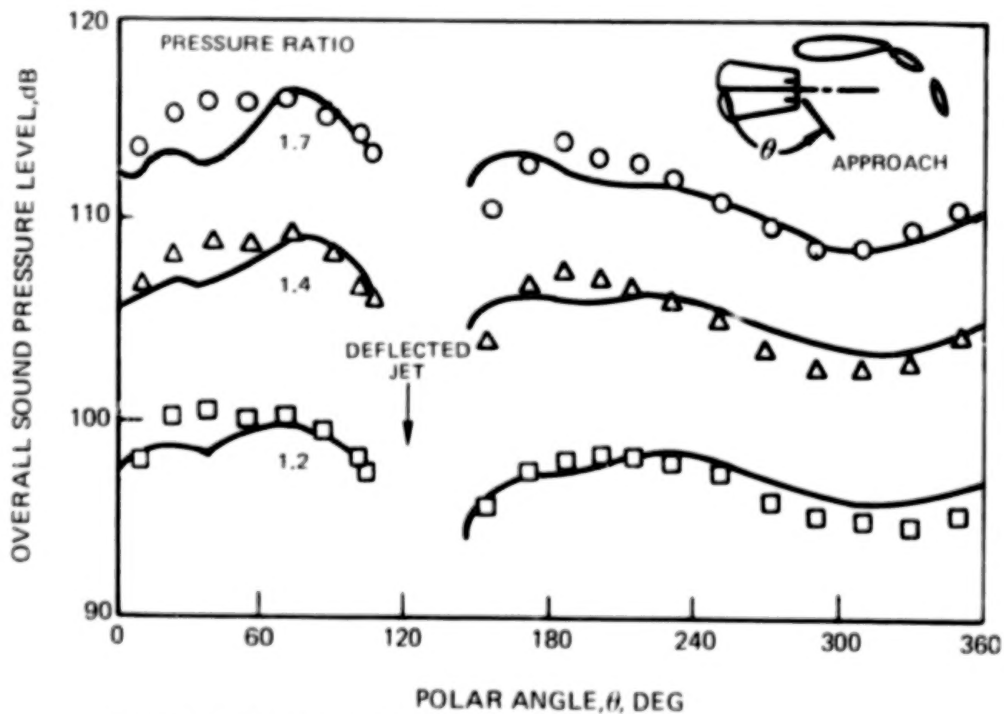


FIGURE 30. -CALCULATED AND MEASURED OASPL DIRECTIVITY IN FLYOVER PLANE FOR 45° DEFLECTION UTW SLOTLESS WING AT THREE FLAP LENGTHS AND 270 M/SEC EXHAUST VELOCITY

SYMBOLS ARE EBF DATA POINTS. LINES ARE THE SUM OF CALCULATED SURFACE - RADIATED NOISE AND MEASURED ADJUSTED MIXER NOZZLE NOISE

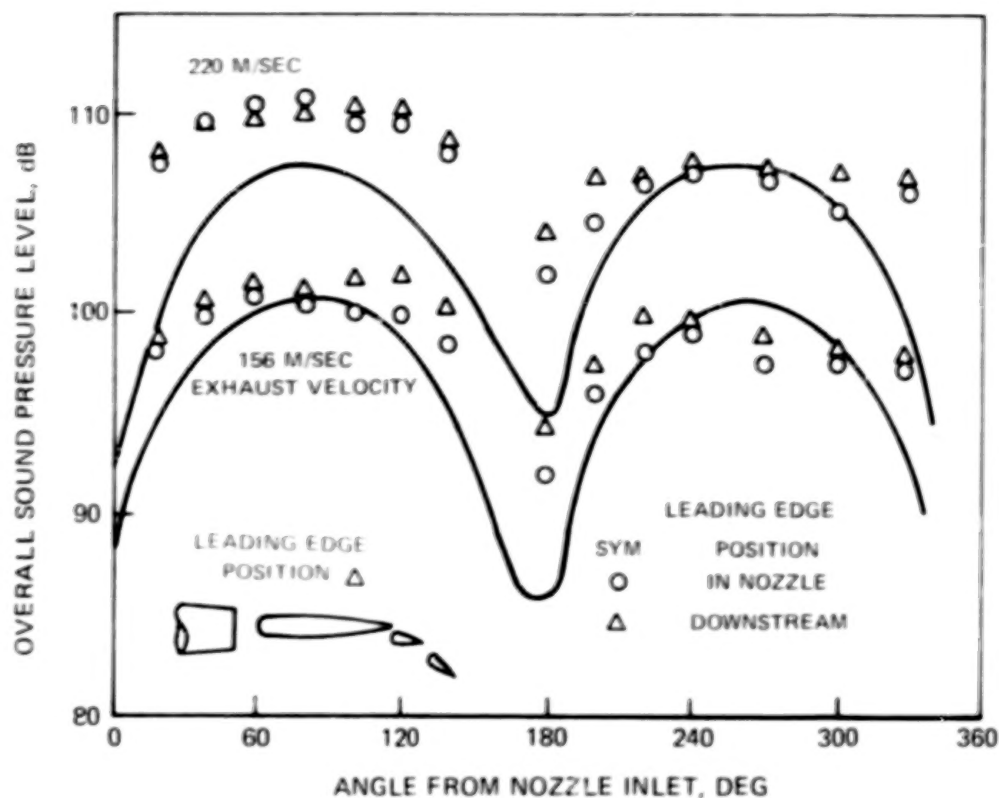


(a) TAKEOFF FLAP CONFIGURATION

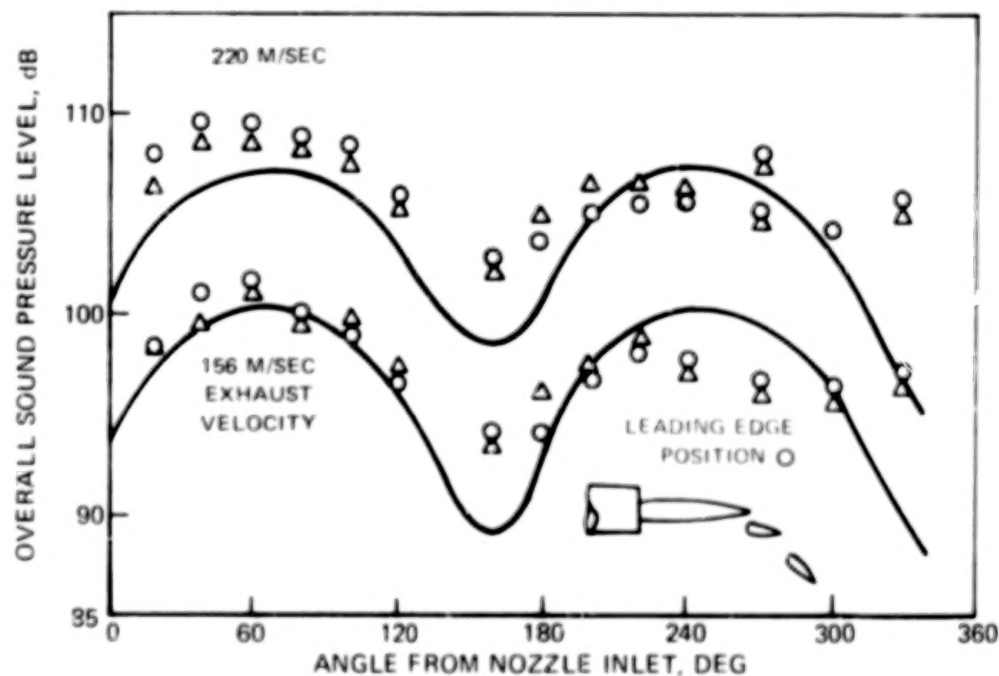


(b) APPROACH FLAP CONFIGURATION

FIGURE 31 - COMPARISON OF CALCULATED AND MEASURED OASPL DIRECTIVITY FOR LARGE-SCALE UTW MIXER NOZZLE

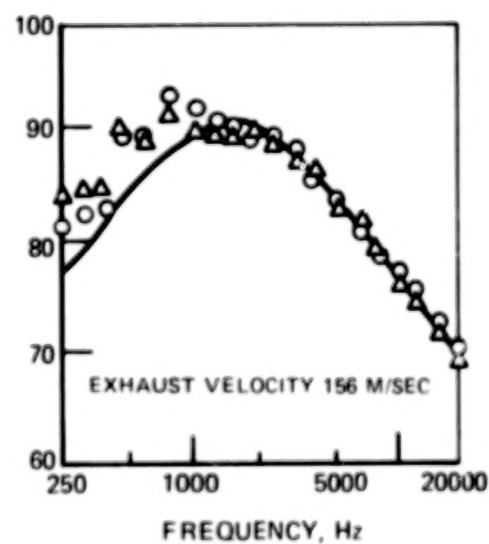
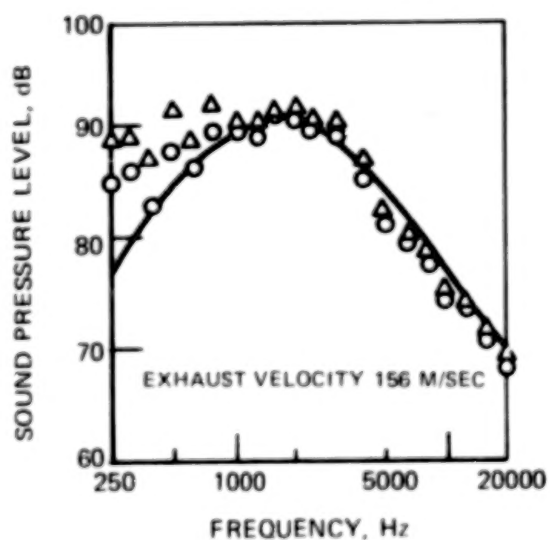
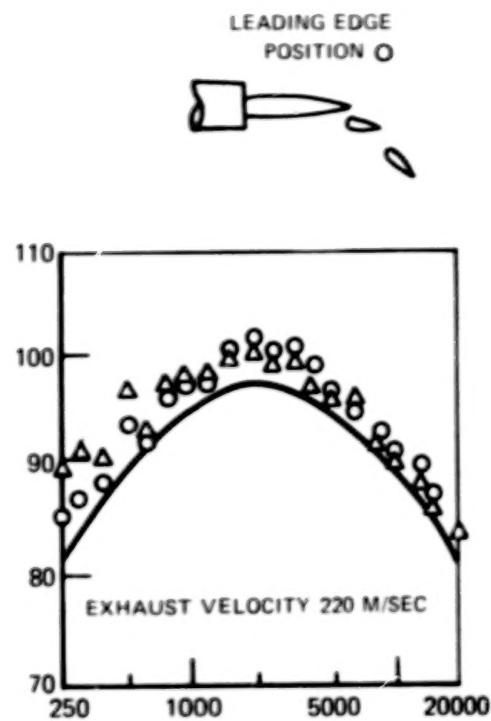
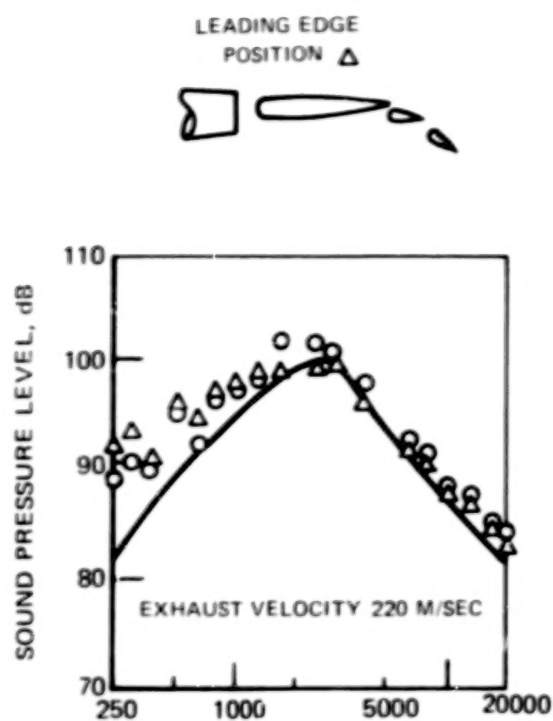


(a) TAKEOFF FLAP DEFLECTION



(b) APPROACH FLAP DEFLECTION

FIGURE 32. — COMPARISON OF CALCULATED AND MEASURED OASPL DIRECTIVITY FOR ENGINE-IN-FRONT-OF-WING CONFIGURATION DATA DECREASED 3dB FOR COMPARISON WITH FREE-FIELD PREDICTIONS



(a) TAKEOFF FLAP DEFLECTION,
100° MICROPHONE ANGLE

(b) APPROACH FLAP DEFLECTION,
80° MICROPHONE ANGLE

FIGURE 33. — COMPARISON OF CALCULATED AND MEASURED SPECTRA FOR
ENGINE-IN-FRONT-OF-WING CONFIGURATION. DATA DECREASED 3 dB
FOR COMPARISON WITH FREE-FIELD PREDICTIONS

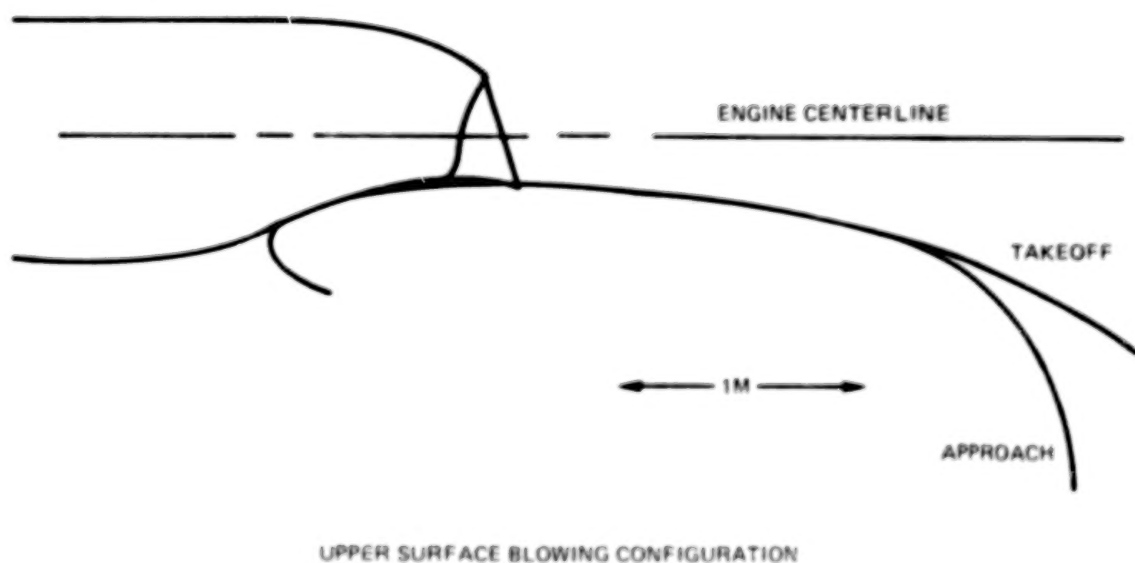
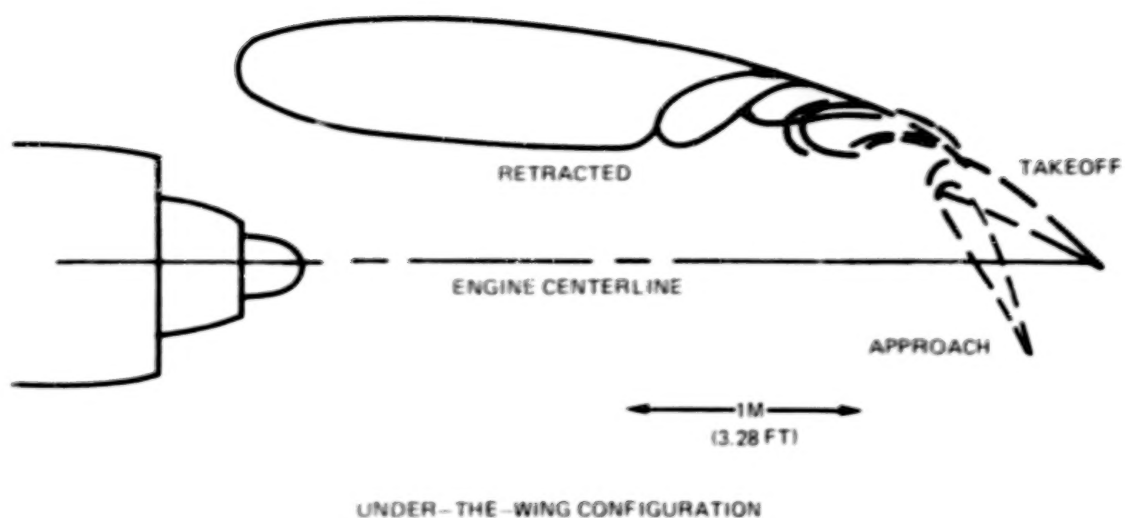


FIGURE 34. – SKETCH OF FULL SCALE OCSEE ENGINE EXHAUST NOZZLE AND EXTERNALLY BLOWN FLAP CONFIGURATIONS

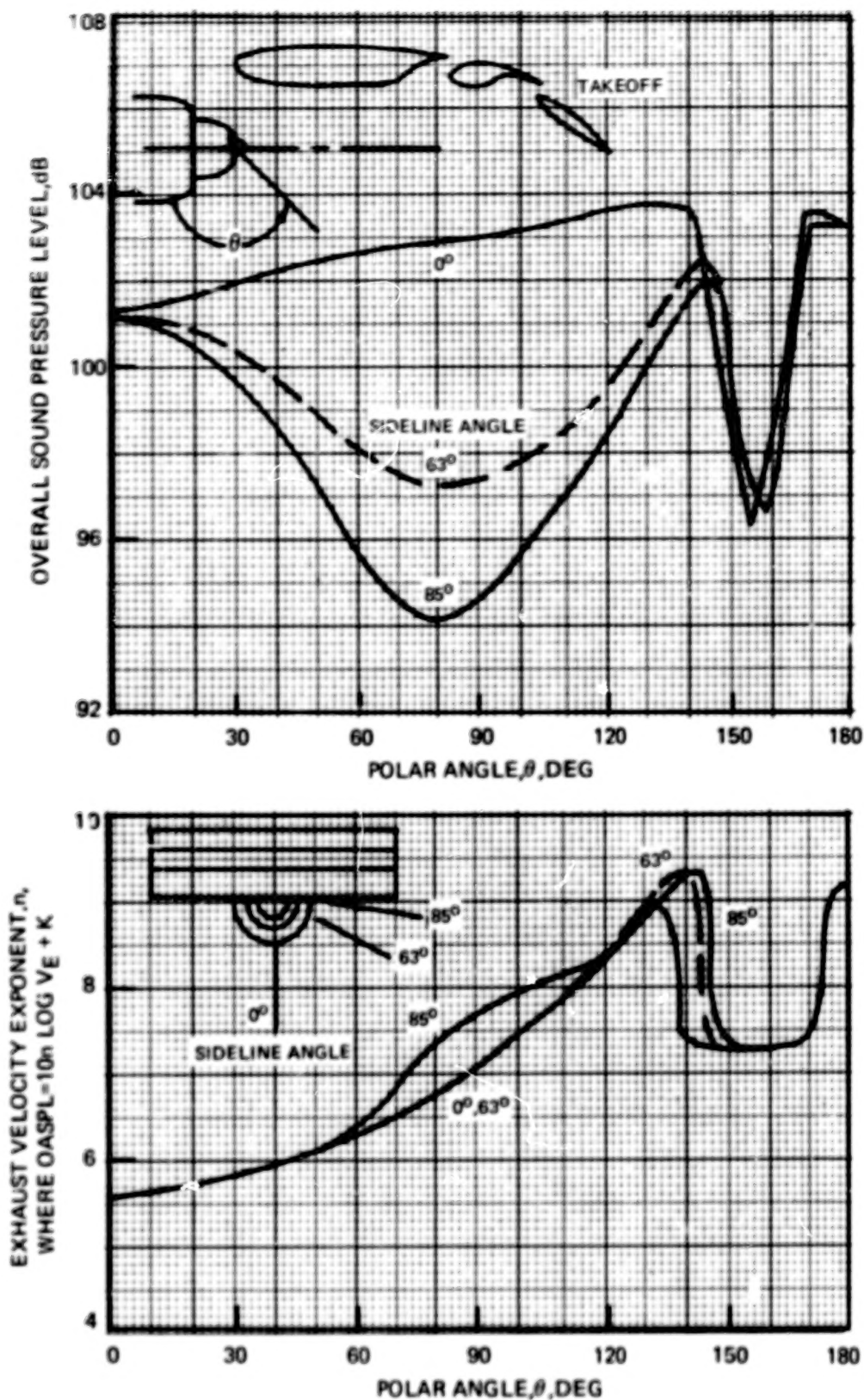


FIGURE 35.—CALCULATED FREE FIELD DIRECTIVITY OF FULL SCALE QCSEE UTW TAKEOFF CONFIGURATION AT 100 M RADIUS AND 215 M/SEC EXHAUST VELOCITY BY UTRC PREDICTION METHOD

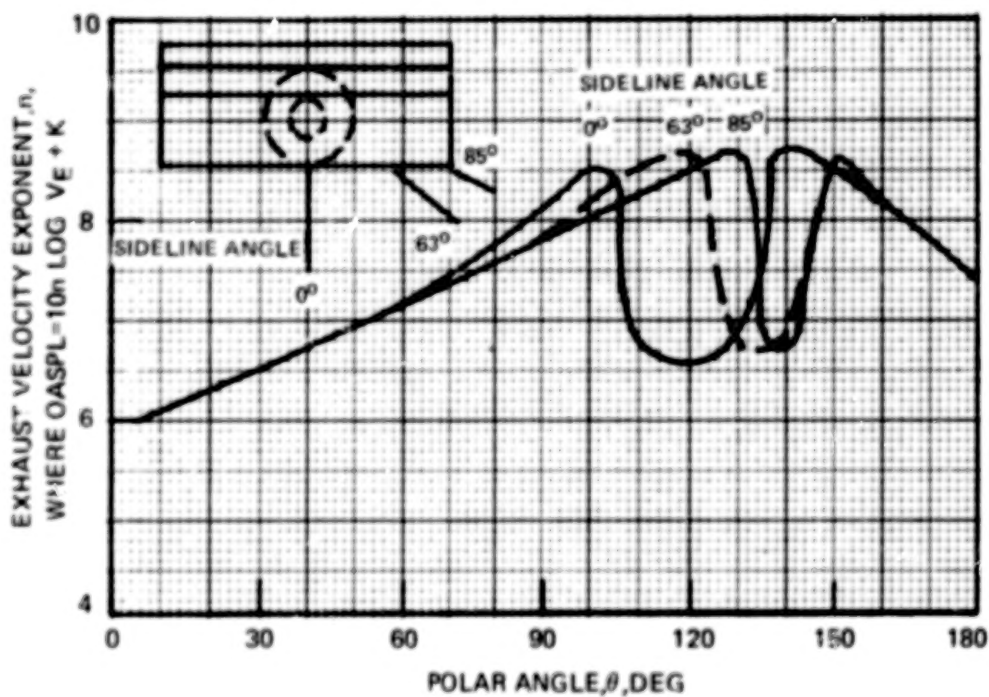
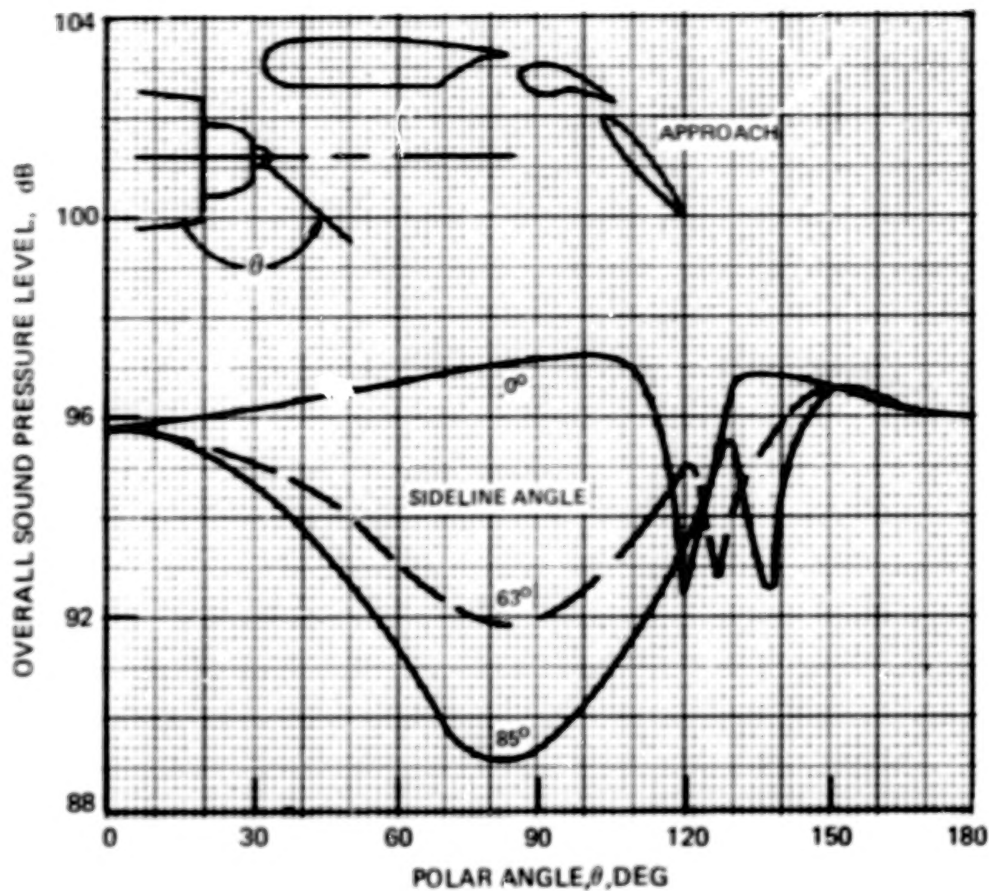


FIGURE 36. - CALCULATED FREE FIELD DIRECTIVITY OF FULL SCALE QCSEE UTW APPROACH CONFIGURATION AT 100M RADIUS AND 161 M/SEC EXHAUST VELOCITY BY UTRC PREDICTION METHOD

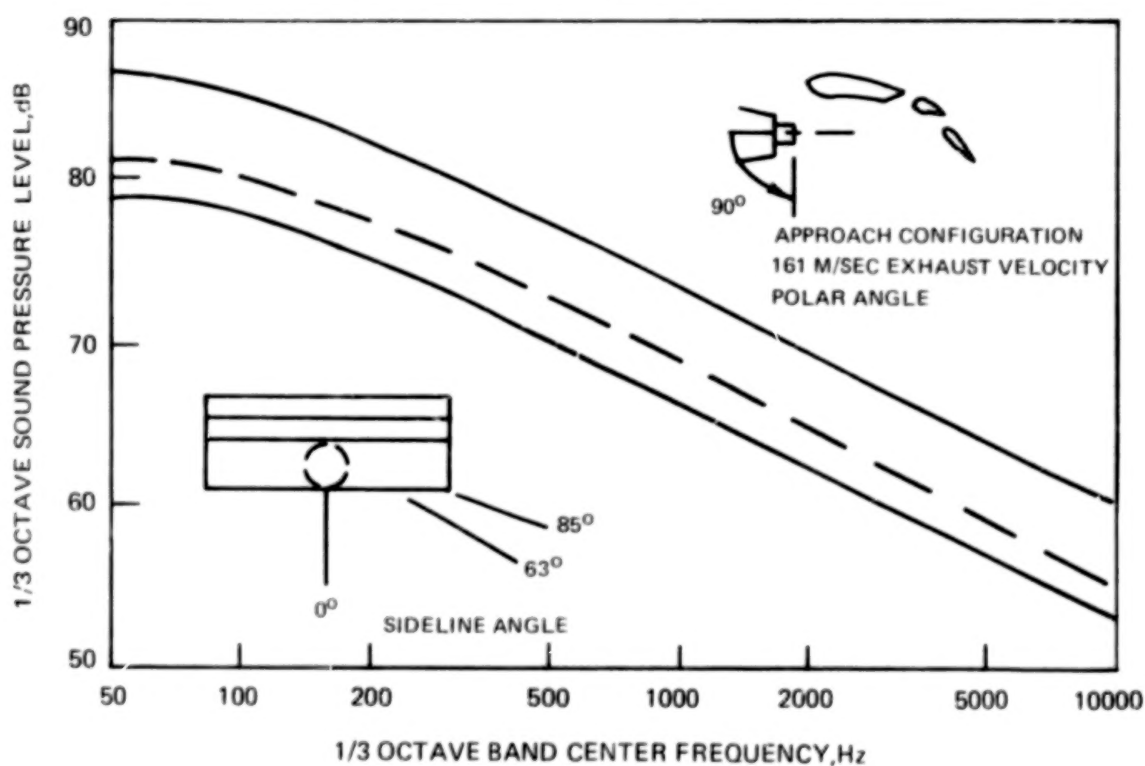
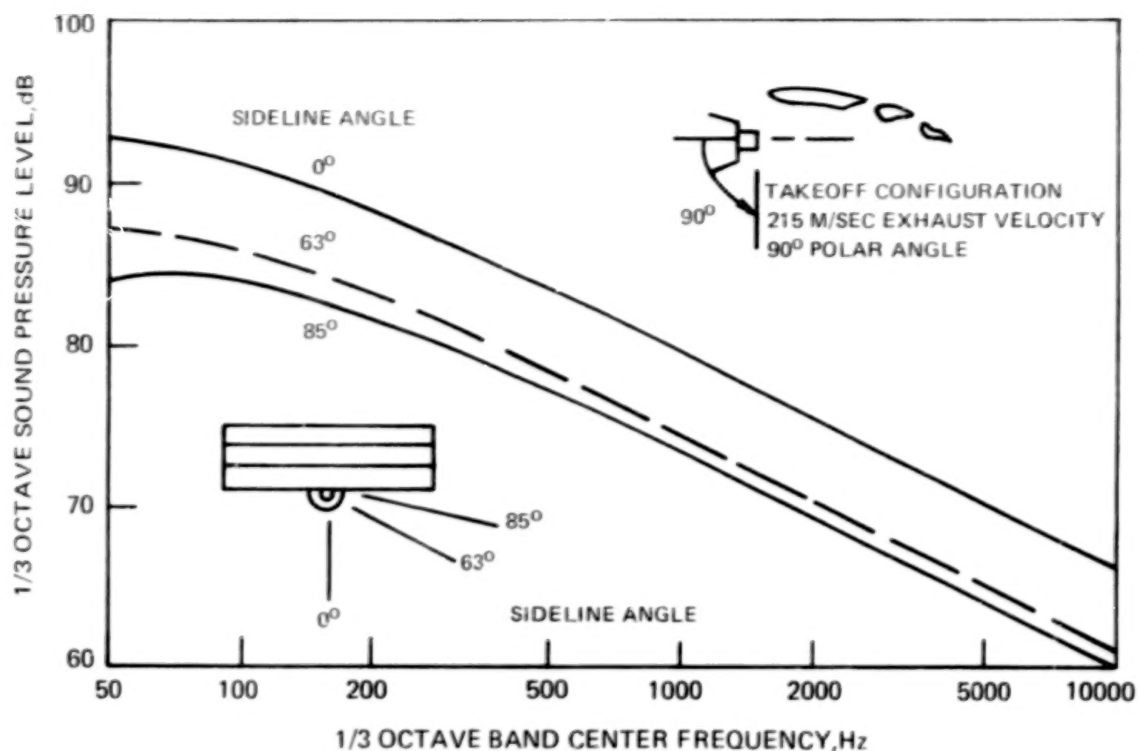


FIGURE 37. -CALCULATED 1/3 OCTAVE SPECTRA AT 90° POLAR ANGLE FOR FULL SCALE QCSEE UTW IN TAKEOFF AND APPROACH CONFIGURATIONS AT 100M RADIUS BY UTRC PREDICTION METHOD

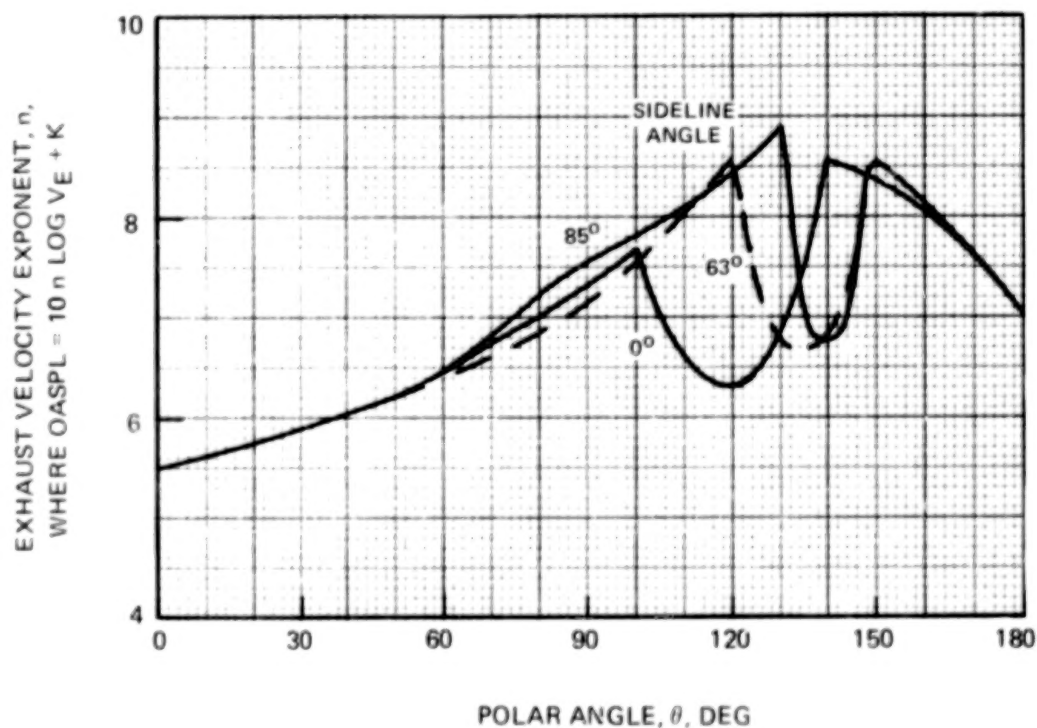
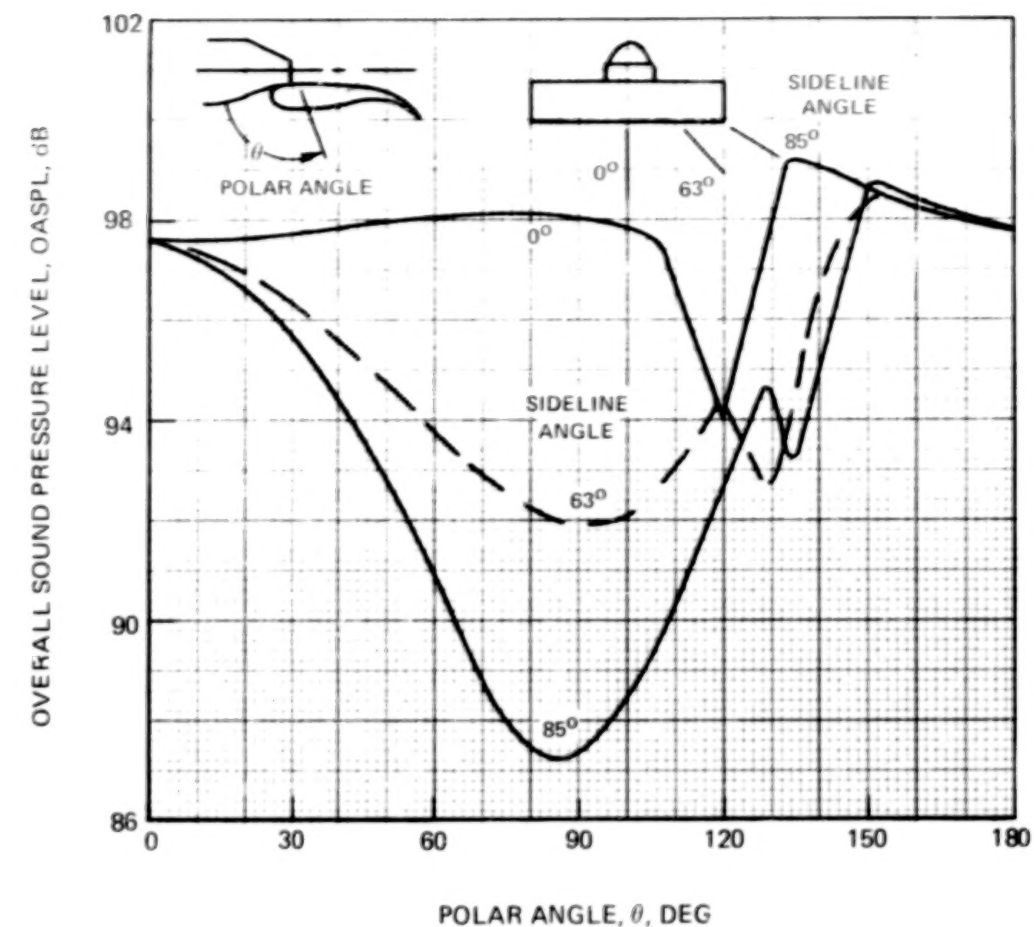


FIGURE 38. — CALCULATED FREE FIELD DIRECTIVITY OF FULL SCALE QCSEE USB APPROACH CONFIGURATION AT 100 M RADIUS AND 190 M/SEC EXHAUST VELOCITY BY UTRC PREDICTION METHOD

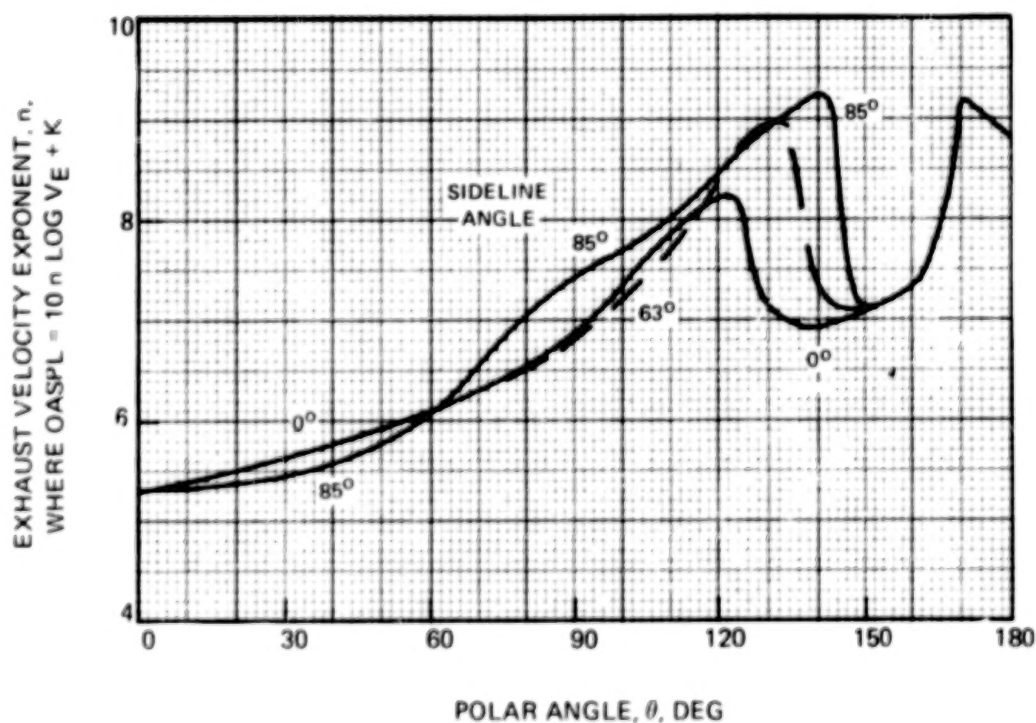
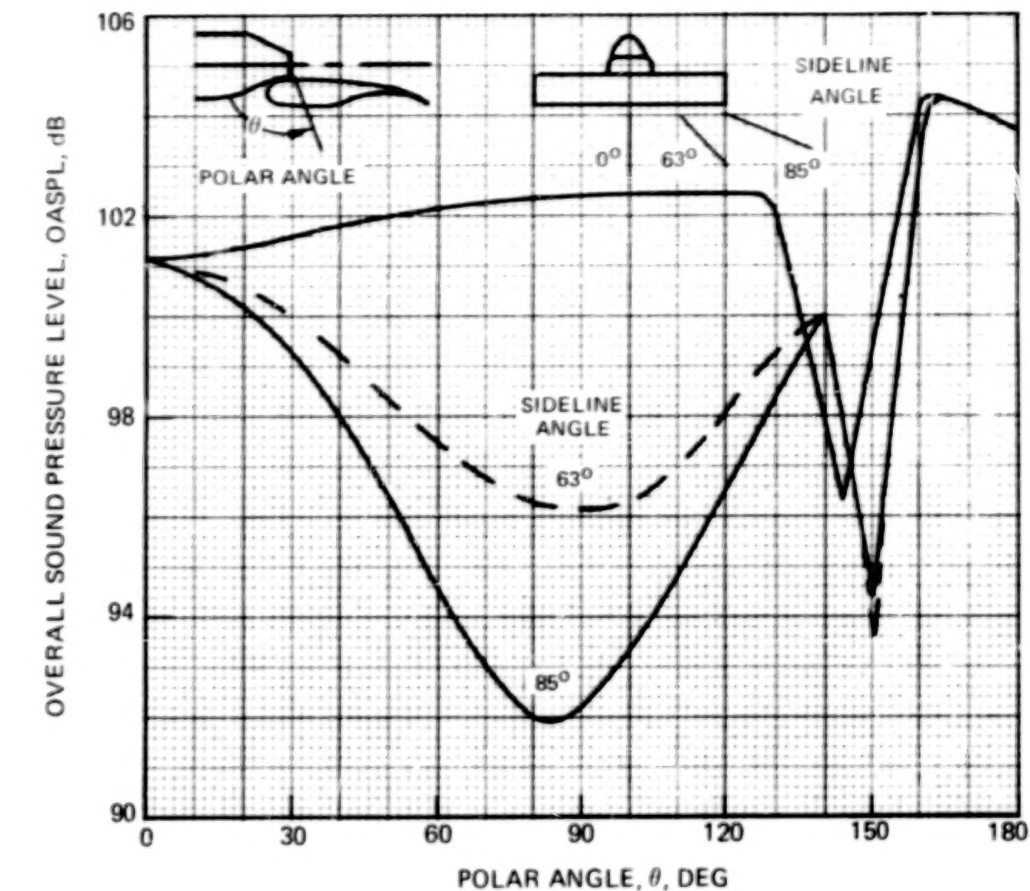


FIGURE 39. — CALCULATED FREE FIELD DIRECTIVITY OF FULL SCALE QCSEE US_B TAKEOFF CONFIGURATION AT 100 M RADIUS AND 220 M/SEC EXHAUST VELOCITY BY UTRC PREDICTION METHOD

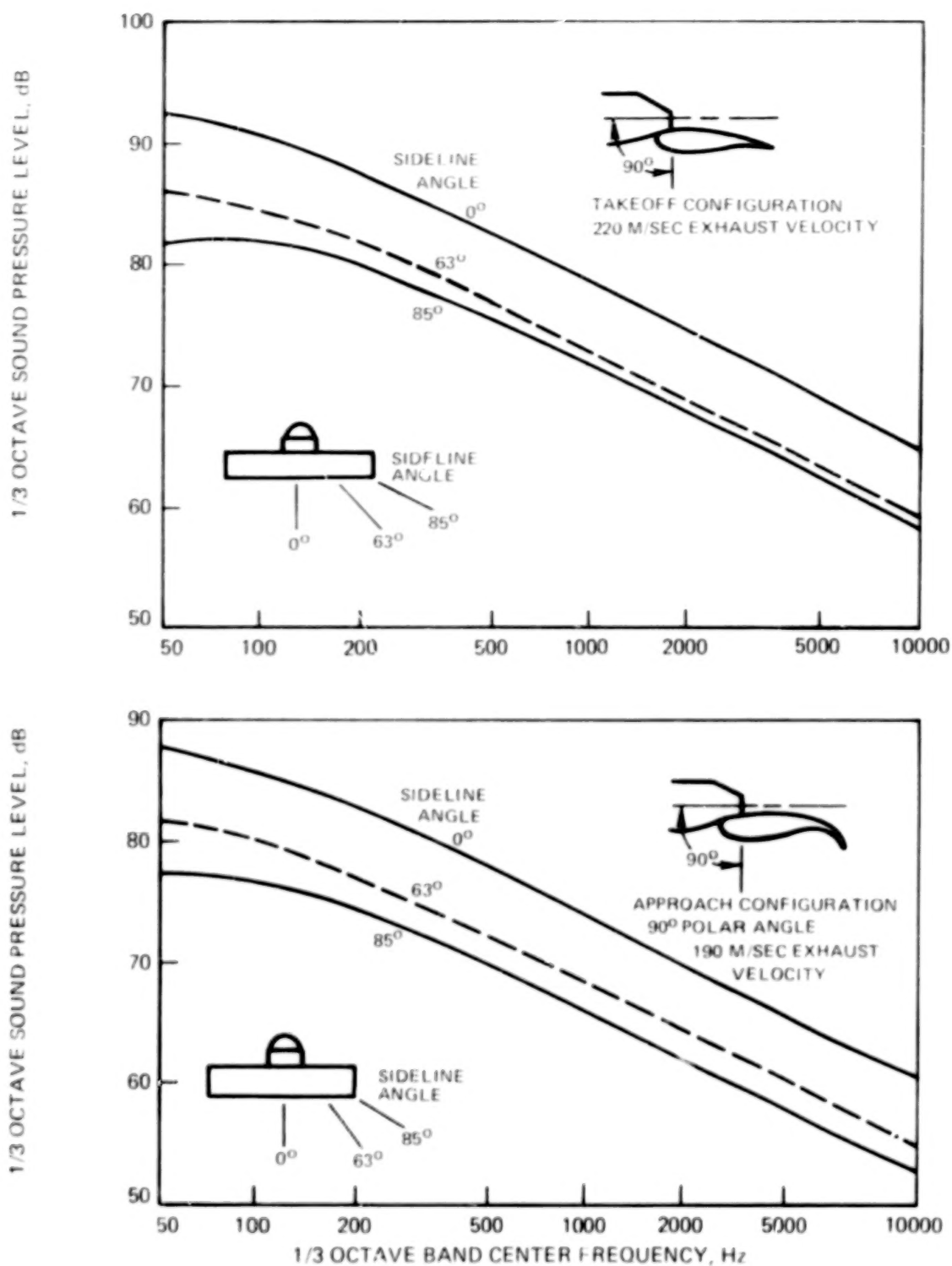


FIGURE 40.— CALCULATED 1/3 OCTAVE SPECTRA AT 90° POLAR ANGLE FOR FULL SCALE QCSEE USB IN TAKEOFF AND APPROACH CONFIGURATIONS AT 100 M RADIUS BY UTRC PREDICTION METHOD

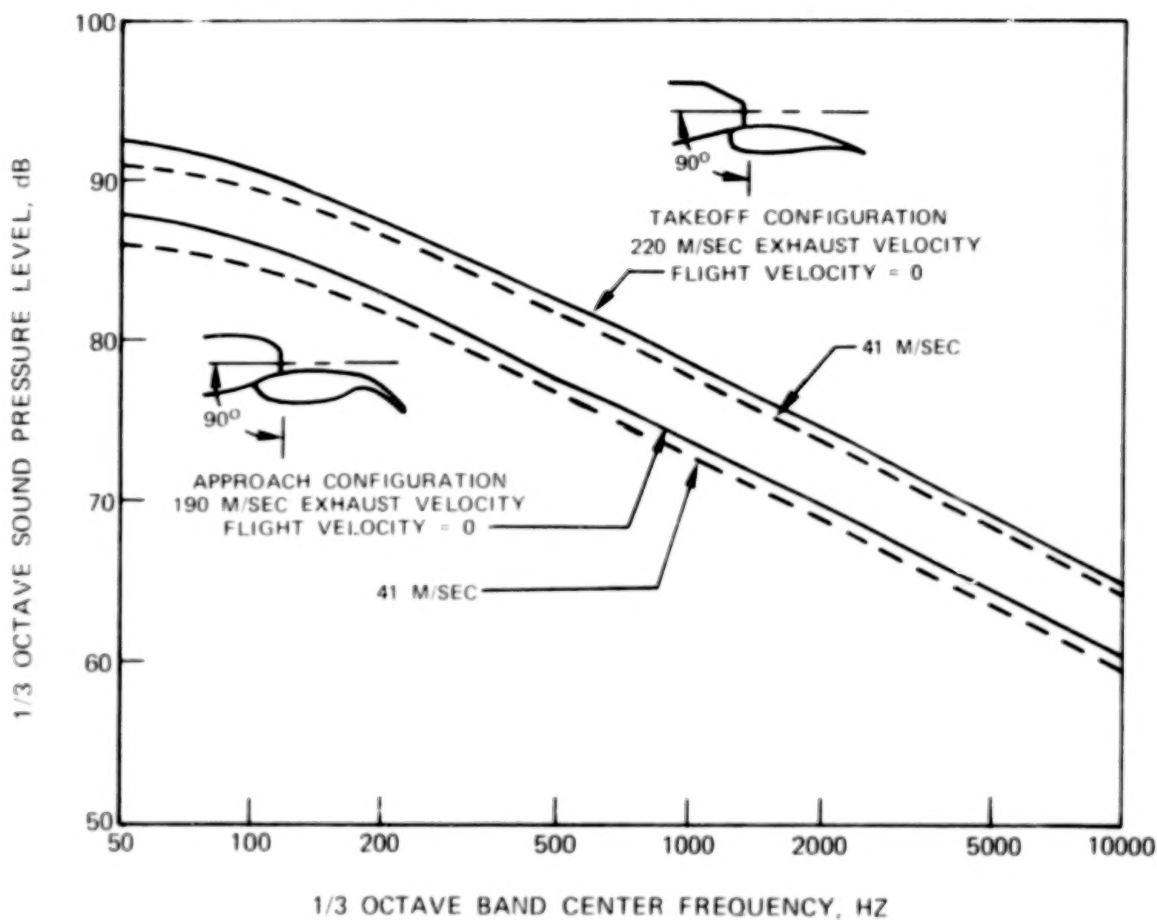


FIGURE 41. - CALCULATED EFFECT OF 41 M/SEC (80 KNOT) FLIGHT VELOCITY ON FLYOVER SPECTRUM AT OVERHEAD POSITION AND 100 M ALTITUDE FOR QCSEE USB CONFIGURATIONS BY UTRC PREDICTION METHOD

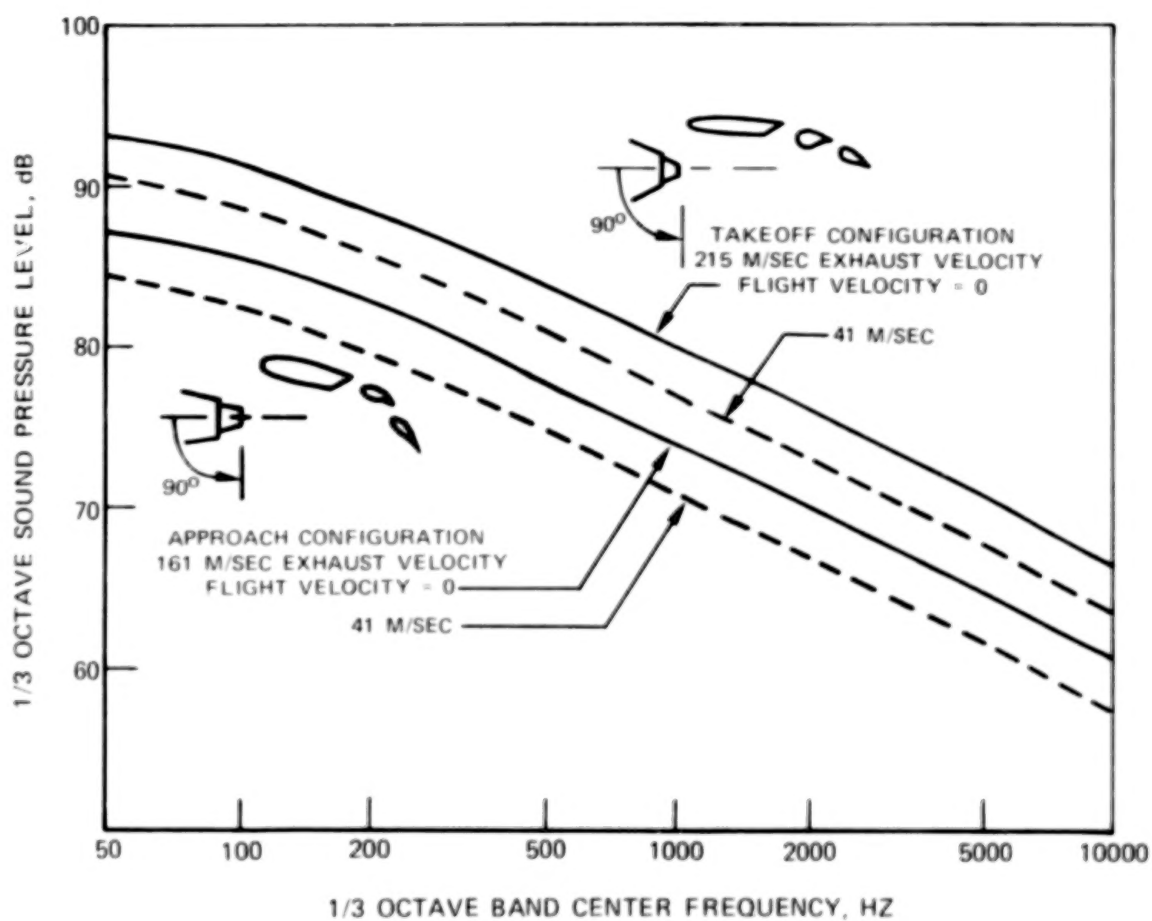
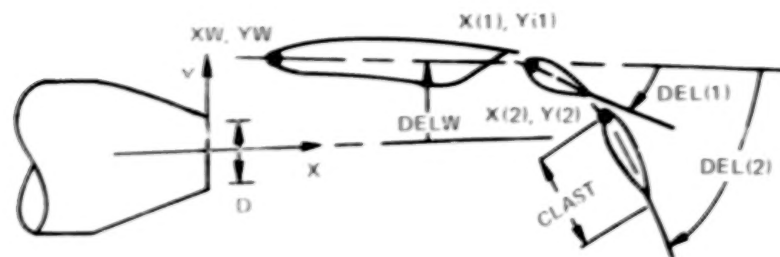
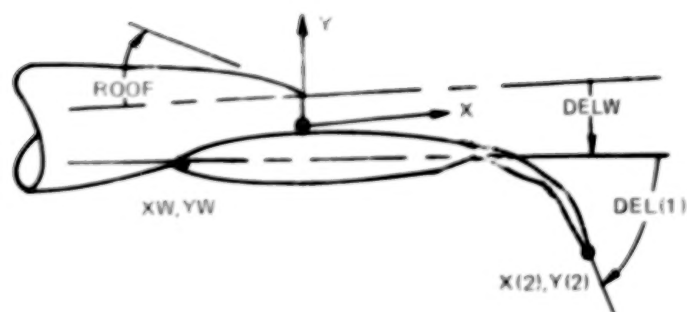


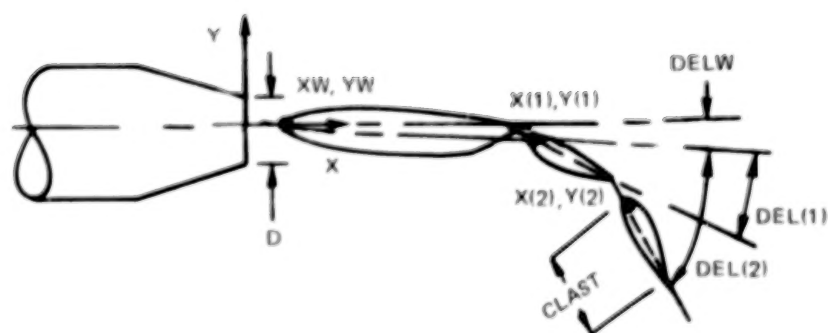
FIGURE 42. —CALCULATED EFFECT OF 41 M/SEC (80 KNOT) FLIGHT VELOCITY ON FLYOVER SPECTRUM AT OVERHEAD POSITION AND 100 M ALTITUDE FOR QCSEE UTW CONFIGURATIONS BY UTRC PREDICTION METHOD



UNDER THE WING, CONFIG - 1



UPPER SURFACE BLOWING, CONFIG - 2



ENGINE IN FRONT OF THE WING, CONFIG - 3

FIGURE 43. - GEOMETRIC INPUT FOR EXTERNALLY BLOWN FLAP CONFIGURATIONS

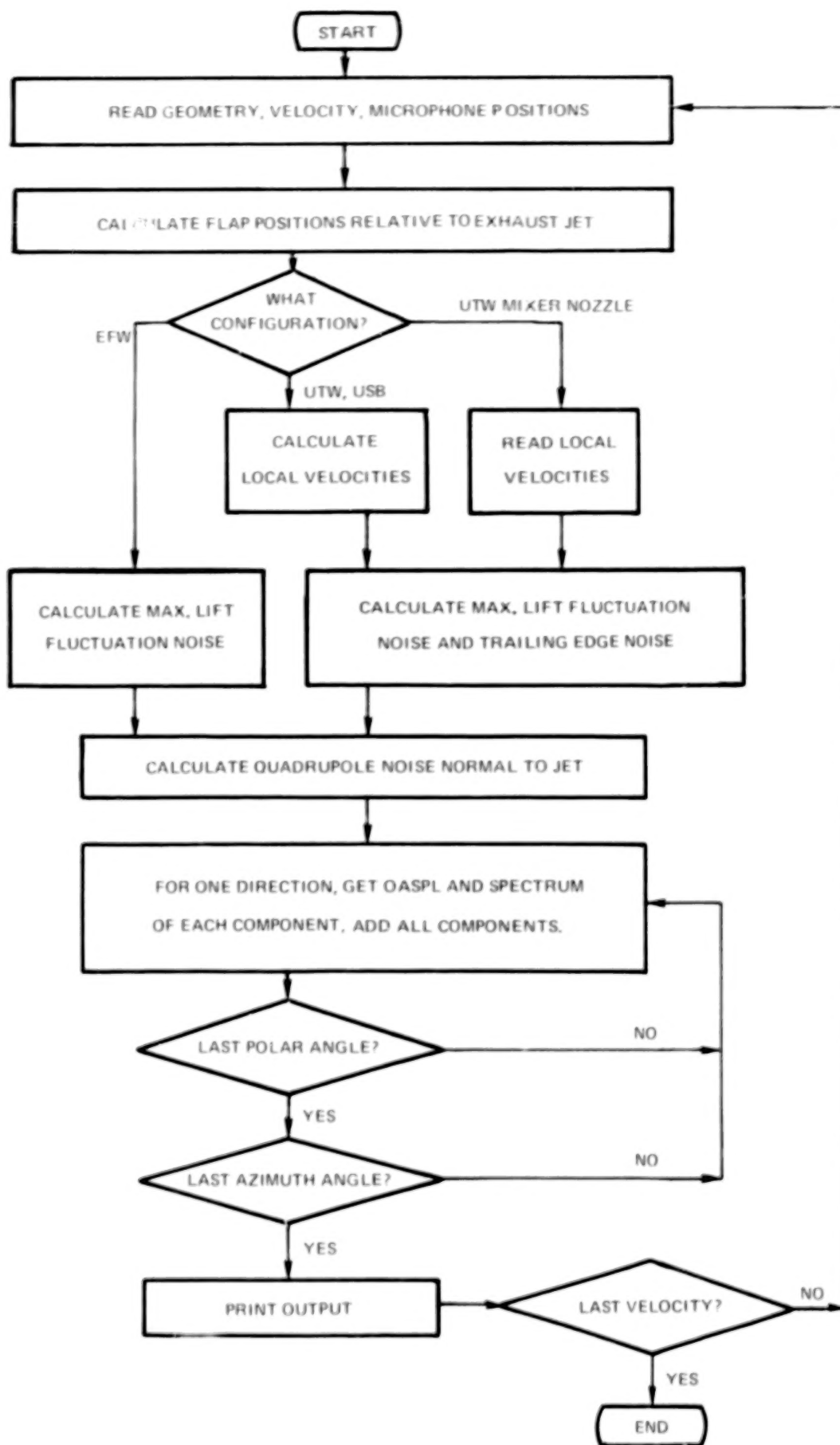


FIGURE 44. -FLOW CHART FOR EBF NOISE PREDICTION COMPUTER PROGRAM

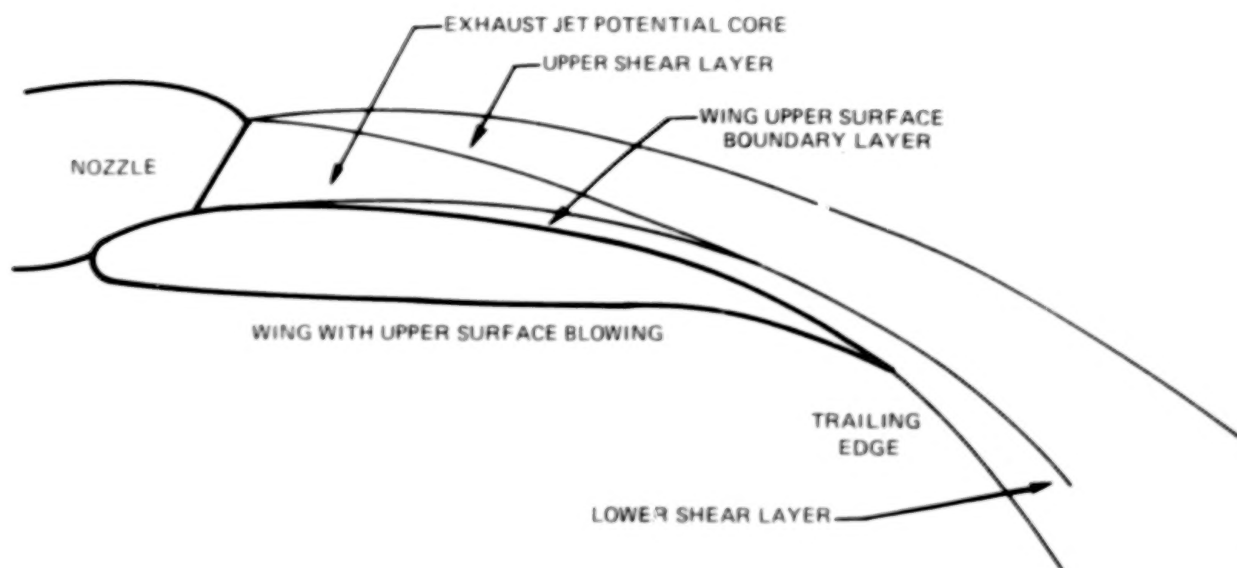


FIGURE 45. SKETCH OF EXHAUST JET FLOW REGIONS FOR UPPER SURFACE BLOWING EXTERNALLY BLOWN FLAP

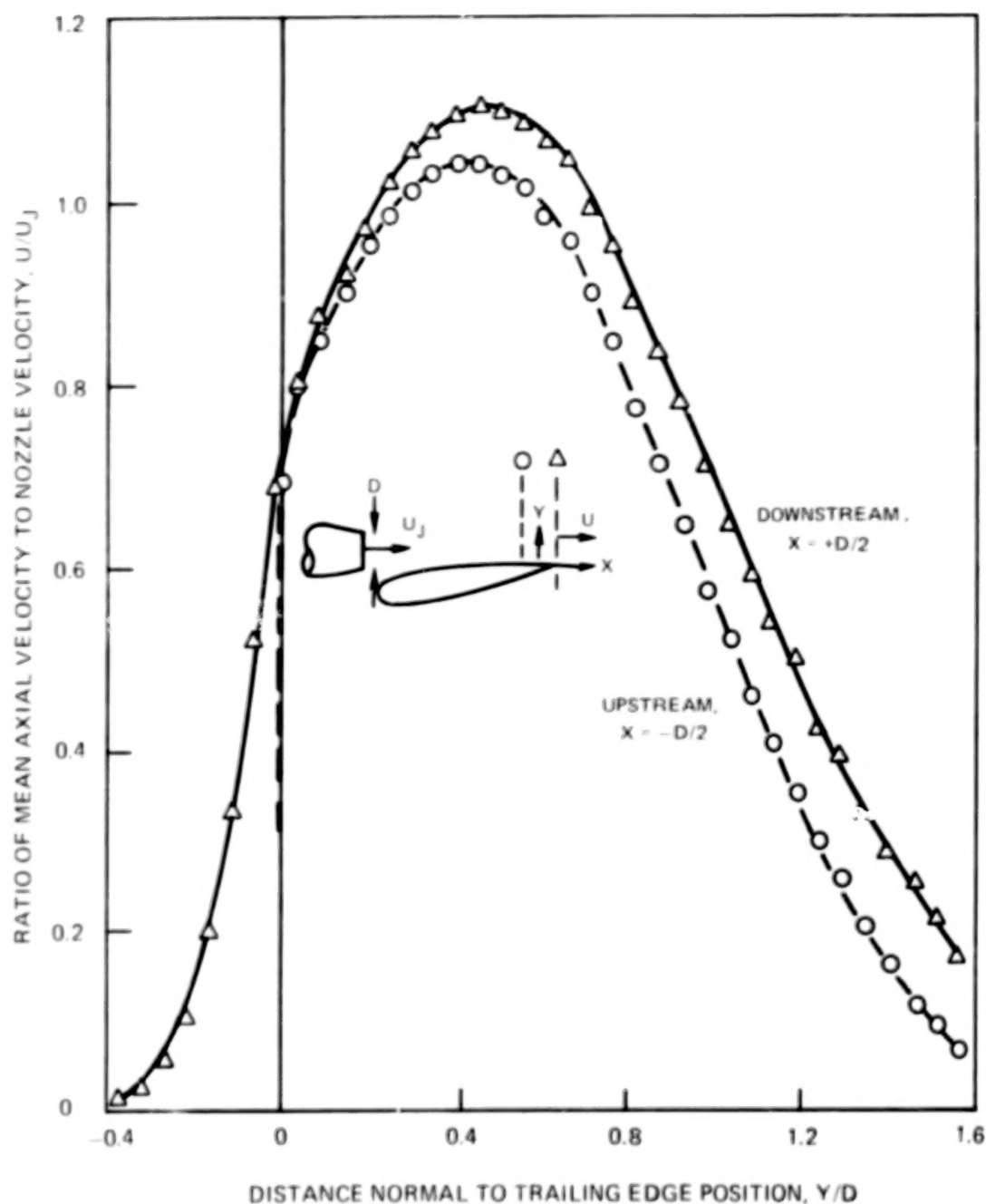


FIGURE 46. — MEAN VELOCITY PROFILES UPSTREAM AND DOWNSTREAM OF UPPER SURFACE BLOWING MODEL TRAILING EDGE. SPANWISE CENTERLINE, 100 M/SEC NOZZLE VELOCITY

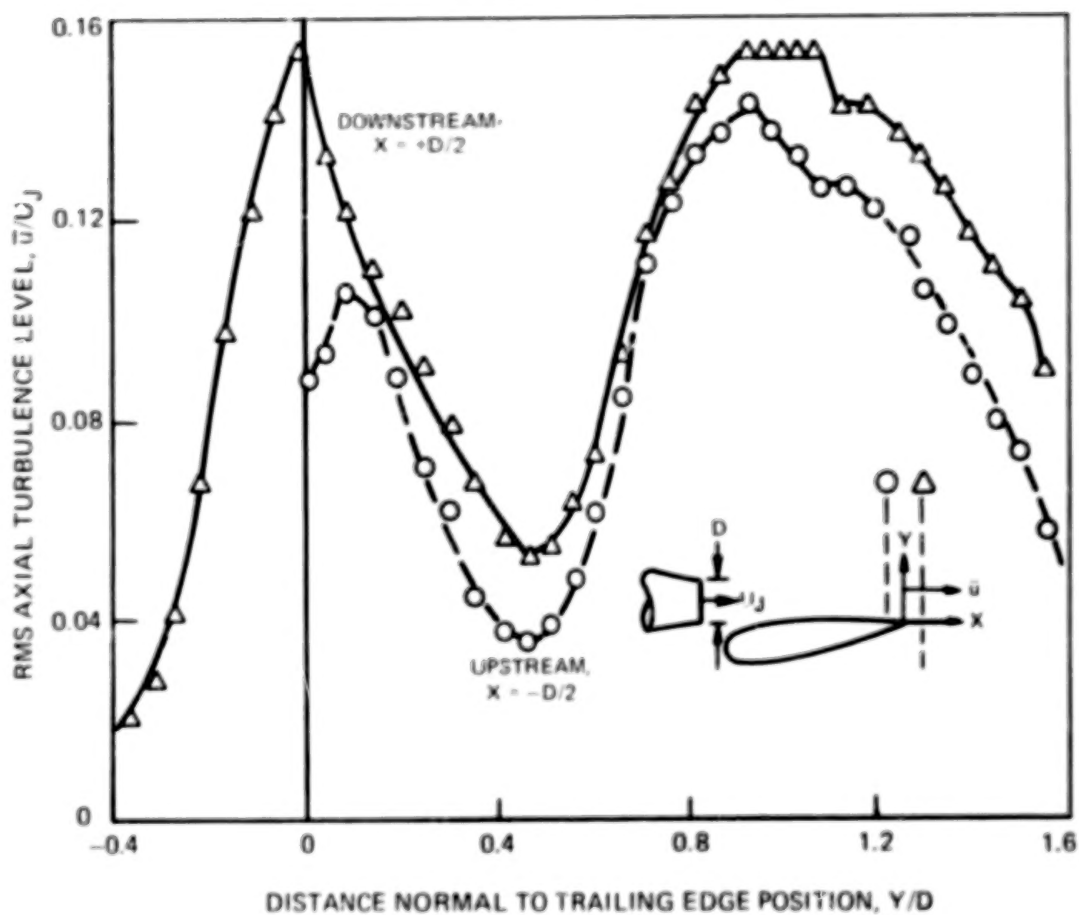


FIGURE 47—AXIAL TURBULENCE VELOCITY PROFILES UPSTREAM AND DOWNSTREAM OF UPPER SURFACE BLOWING MODEL TRAILING EDGE. SPANWISE CENTERLINE, 100 M/SEC NOZZLE VELOCITY

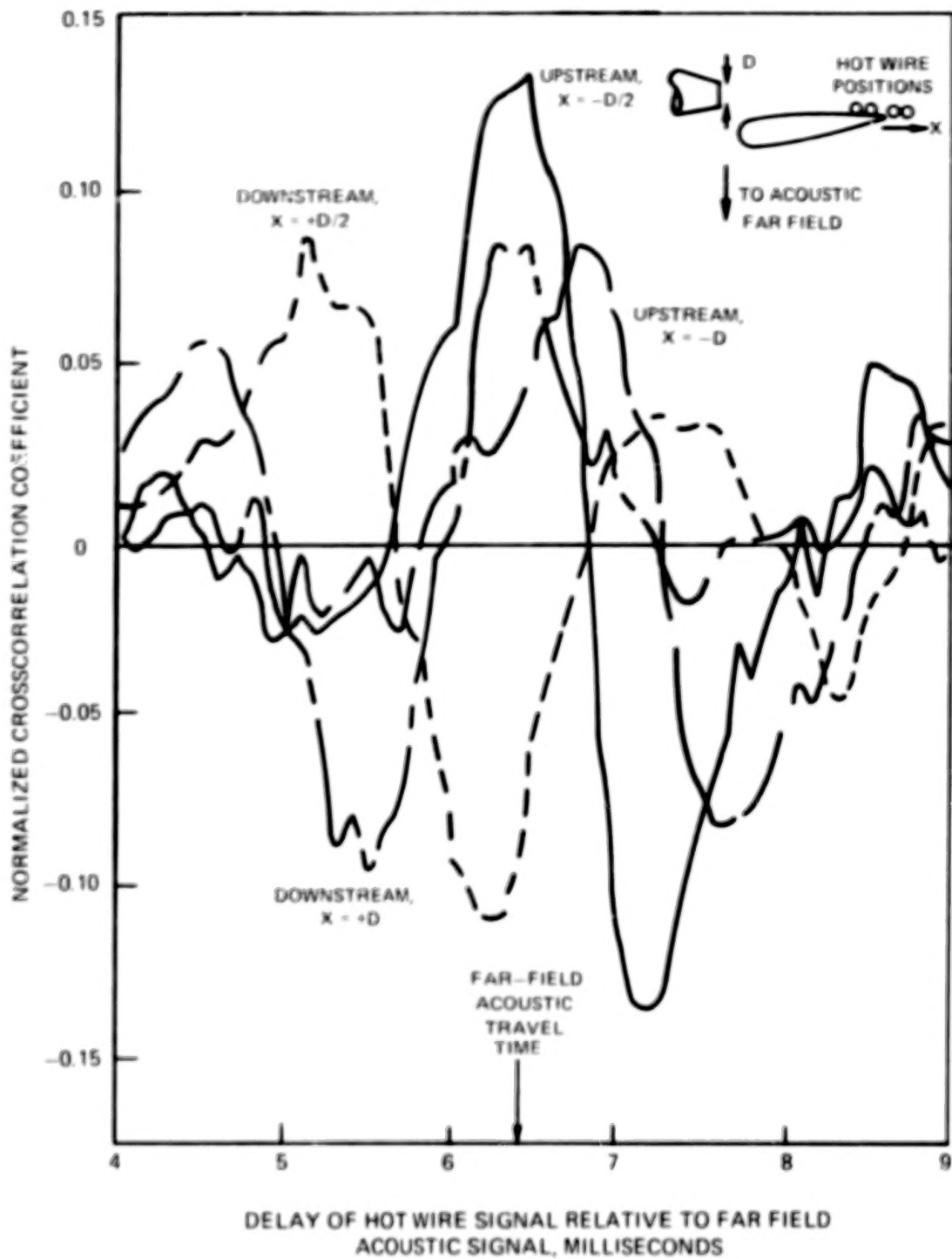


FIGURE 48. — CROSSCORRELATIONS BETWEEN LOWER SHEAR REGION VELOCITIES AND ACOUSTIC FAR FIELD

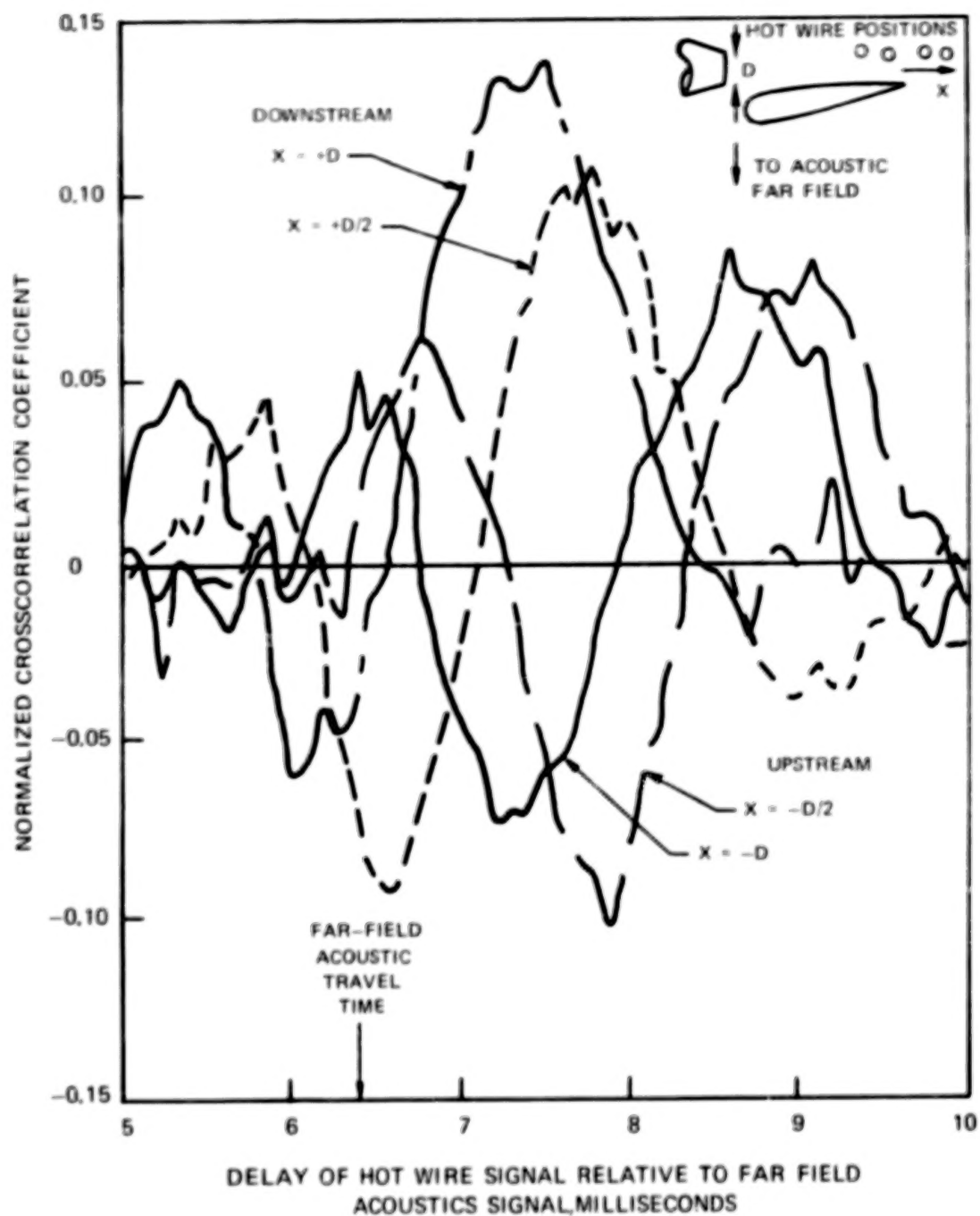
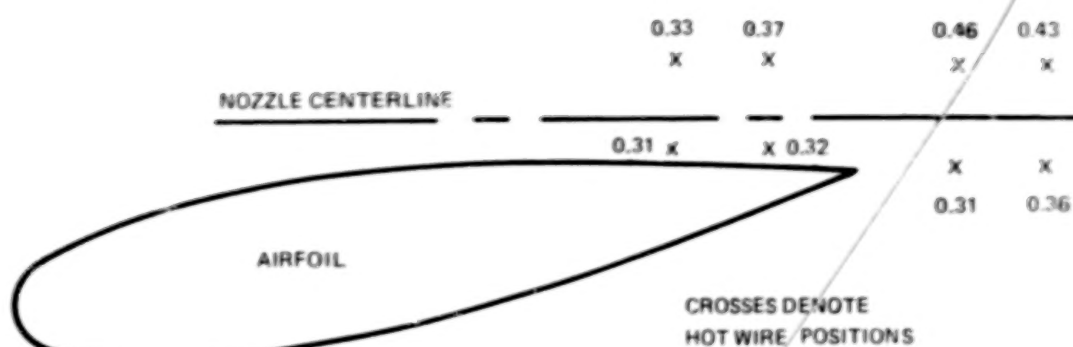
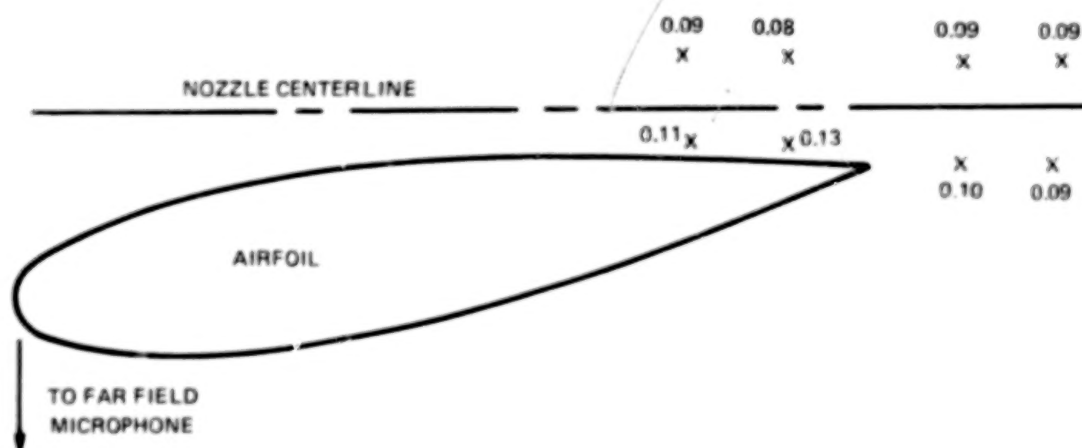


FIGURE 49. -CROSSCORRELATIONS BETWEEN UPPER SHEAR REGION VELOCITIES AND ACOUSTIC FAR FIELD



(a) RATIOS OF AXIAL INTEGRAL SCALE LENGTH TO NOZZLE DIAMETER



(b) MAXIMUM NORMALIZED CROSSCORRELATION COEFFICIENTS BETWEEN EXHAUST JET VELOCITY FLUCTUATIONS AND FAR FIELD NOISE

FIGURE 50. —SPATIAL DISTRIBUTION OF INTEGRAL SCALE LENGTH, AND CORRELATION BETWEEN LOCAL VELOCITY AND FAR FIELD NOISE, NEAR UPPER SURFACE BLOWING MODEL TRAILING EDGE. SPANWISE CENTERLINE, 100 M/SEC NOZZLE VELOCITY

1 Report No. NASA CR-2954	2 Government Accession No.	3 Recipient's Catalog No.	
4 Title and Subtitle A METHOD FOR CALCULATING EXTERNALLY BLOWN FLAP NOISE		5 Report Date March 1978	
		6 Performing Organization Code	
7 Author(s) Martin R. Fink		8 Performing Organization Report No. R77-911739-17	
		10 Work Unit No.	
9 Performing Organization Name and Address United Technologies Research Center Silver Lane East Hartford, Connecticut 06108		11 Contract or Grant No. NAS3-17863	
		13 Type of Report and Period Covered Contractor Report	
12 Sponsoring Agency Name and Address National Aeronautics and Space Administration Washington, D.C. 20546		14 Sponsoring Agency Code	
15 Supplementary Notes Final report. Project Manager, William A. Olsen, V/STOL and Noise Division, NASA Lewis Research Center, Cleveland, Ohio 44135.			
16 Abstract <p>A method is described for calculating externally blown flap noise as a sum of several simple basic noise components. These components are (1) compact lift dipoles associated with the wing and flaps, (2) trailing edge noise associated with the last trailing edge, and (3) quadrupole noise associated with the undeflected exhaust jet, deflection by a flap surface or nozzle deflecting surface, and the free jet located downstream of the trailing edge. These noise components are combined to allow prediction of directivity and spectra for under-the-wing (UTW) slotted flaps with conventional or mixer nozzles, UTW slotless flaps, upper-surface-blowing (USB) slotless flaps, and engine-in-front-of-the-wing slotted flaps. The development of this method as part of a four-year effort under this Contract is described. A digital computer program listing is given for this calculation method. Directivities and spectra calculated by this method, the current NASA ANOP method, and a method developed by Lockheed-Georgia Co. are compared with free-field data for UTW and USB configurations recently tested by NASA Lewis Research Center. These data had not been part of the data base used in development of these three methods. The UTRC method best predicted the details of the measured noise emission, but the ANOP method best estimated the noise levels directly below these configurations.</p>			
17 Key Words (Suggested by Author(s)) Noise, Aerodynamic noise, STOL aircraft noise, EBF noise, High-lift system noise, Aircraft noise		18 Distribution Statement Unclassified - unlimited STAR Category 71	
19 Security Classif. (of this report) Unclassified	20 Security Classif. (of this page) Unclassified	21 No. of Pages 128	22 Price* A07

90

50

END

DEC 12 1978